Using Genome-Wide CRISPR/Cas9 Screens to Identify Novel Therapeutic Targets in Small Cell Lung Cancer

Justin Norton

A dissertation

submitted in partial fulfillment of the

requirements for the degree of

Doctor of Philosophy

University of Washington

2020

Reading Committee:

David MacPherson, Chair

Jonathan Cooper

Andrew Oberst

Program Authorized to Offer Degree:

Molecular and Cellular Biology

University of Washington

Abstract

Using Genome-Wide CRISPR/Cas9 Screens to Identify Novel Therapeutic Targets in Small Cell Lung Cancer

Justin Norton

Chair of the Supervisory Committee:

David MacPherson, Associate Member

Division of Human Biology, Fred Hutchinson Cancer Research Center

Small Cell Lung Cancer (SCLC) is a highly aggressive and metastatic form of lung cancer and is one of the most lethal sold tumor malignancies. The classical subtype of SCLC is noted for its neuroendocrine differentiation features. Standard treatment options have not improved in decades and SCLC tumors develop near universal rates of resistance to chemotherapy. This project aimed to elucidate novel therapies to SCLC using genome-wide CRISPR/Cas9 inactivation screens of genetically simplified murine small cell lines developed in our lab. These screens identified genes and pathways in which their functional depletion causes decreased viability in SCLC cells. A number of these identified vulnerabilities are targeted by small molecules, which include known SCLC-specific vulnerabilities like CHEK1 and BCL2L1. Here we show novel SCLC vulnerabilities, specifically focusing on NEDD8 and the neddylation pathway. Perturbation of this pathway causes SCLC death in vitro. Additionally, the SCLC patient

derived xenografts models LX108 and RU280 show strong sensitivity to the neddylation inhibitor MLN4924 in vivo. Neddylation inhibition causes reduced expression levels of the neuroendocrine proteins INSM1, ASCL1, and POU3F2 and FOXA2. Genetic perturbation of neddylation pathway members or treatment with MLN4924 leads to a downregulation of the neuroendocrine signature in SCLC cells. A genome-wide CRISPR/Cas9 suppressor screen identified the mTOR and NF-κB pathways as potential mechanisms of resistance to the effects of neddylation inhibition in SCLC. This work identifies neddylation as a novel potential therapeutic target for the treatment of SCLC.

Table of Contents

A version of portions for Chapters 1, 2 and 5, 6 are being prepared for peer review:

Using Genome-Wide CRISPR/Cas9 Screens to Identify Novel Therapeutic Targets in Small Cell Lung Cancer

Justin P. Norton, Arnaud Augert, Emily C. Eastwood, and David P. MacPherson

Chapter 1 – Using Genome-Wide CRISPR/Cas9 Screens to Identify Novel Therapeutic Targets in Small Cell Lung Cancer

1.1: Introduction

Introduction to Small Cell Lung Cancer

Small cell lung cancer (SCLC) is a highly metastatic and aggressive neuroendocrine tumor of the lung which accounts for roughly 15% of all lung cancers (Bunn et al., 2016), (Byers and Rudin, 2015), (Rudin et al., 2019), (Poirier et al., 2020). SCLC patients almost universally have histories of long-term smoking (Bunn et al., 2016). SCLC is often initially highly responsive to a chemotherapy doublet of a platinum and etoposide (Rossi et al., 2012), but this is typically followed by rapid reemergence of chemoresistant tumors. The 5-year survival rate is only 5-6% (Pietanza et al., 2015) making it one of the deadliest cancers in the country. Recent FDA approval for the addition of immune checkpoint inhibitors to chemotherapy regimens (Horn et al., 2018), (Pacheco and Bunn, 2019), (Paz-Ares et al., 2019) resulted in the first major change in SCLC standard of care in decades, but have only modestly improved outcomes. SCLC is driven by the inactivation of the tumor suppressors TP53 and RB1 in almost all cases

and does not exhibit frequent mutations in “druggable” oncogenic targets common in other lung cancers (Rudin et al., 2012), (Peifer et al., 2012), (George et al., 2015). SCLC also exhibits inactivating mutations in chromatin regulators such as KMT2D and CREBBP (Augert et al., 2017), (Jia et al., 2018) as well as amplifications of MYC, MYCL, and MYCN (Peifer et al., 2012), (Sos et al., 2012). Targeted therapies directed towards any SCLC subset harboring specific gene alterations have thus far proved elusive.

Neuroendocrine Features of SCLC

SCLC is a tumor type featuring neuroendocrine characteristics and is thought to derive predominantly from pulmonary neuroendocrine cells (PNEC) located in central lung airways, as Rb/p53 deletion in these rare PNEC cells develop SCLC in mice (Sutherland and Berns, 2010), (Calbo et al., 2005) (Sutherland et al., 2011). In addition to the Rb/p53 (RP) genetically engineered mice model (GEMM) commonly used in SCLC studies, recent advancements have lead to the increased availability of patient derived xenograft (PDX) models for SCLC. PDX models can be generated from patient tumor biopsy samples or from the isolation of circulating tumor cells from patient blood samples (Daniel et al., 2009), (Hodgkinson et al., 2014). The prevalence of PDX SCLC samples, which better recapitulate the tumor characteristics and chemotherapeutic response of patient tumors, has furthered our understanding of SCLC. Transcriptional analyses of human SCLC samples have been used to stratify SCLC into subtypes based on activity of key transcription factors (Wooten et al., 2019), (Rudin et al., 2019). ASCL1 is a master regulator of pulmonary neuroendocrine cells and deletion of ASCL1

prevents the NE cell population in the lung from forming (Borges et al., 1997), (Ito et al., 2000). ASCL1 is also necessary for SCLC development, as deletion of ASCL1 completely abrogates SCLC appearance in mouse models (Borromeo et al., 2016). The majority of SCLC tumors are of the ASCL1-high (SCLC-A), classical NE subtype while ASCL1-low subtypes express lineage transcription factors including NEUROD1 (SCLC-N), POU2F3 (SCLC-P), or YAP1 (SCLC-Y) (Rudin et al., 2019).

Another transcription factor important for pulmonary neuroendocrine cells is INSM1, a transcription factor known to promote neuroendocrine differentiation in the lung (Lan and Breslin, 2009), (Fujino et al., 2015). The lungs of embryonic mice lacking INSM1 fail to properly develop differentiated neuroendocrine cells despite an observed initial expression of ASCL1 (Jia et al., 2015). Further, both SCLC-A and SCLC-N subtypes express high levels of INSM1 (Rudin et al., 2019), and INSM1 can regulate the expression of the NE genes ASCL1 and POU3F2 (Fujino et al., 2015). Transcriptional profiling of high-grade NE SCLC has elucidated a set of the most highly differentially expressed genes in comparison to non-malignant control adrenal cortex samples (Zhang et al., 2018). ASCL1 and INSM1 are prominent in this list of NE signature genes. H3K27Ac ChIP-seq identified INSM1 and ALSCL1 as SCLC super-enhancer-associated genes in two ASCL1-high cell lines but not in a NEUORD1-high cell line (Christensen et al., 2014). Suppression of INSM1 slows growth in one of these same cell lines (Fujino et al., 2015). Transcription factor genes like INSM1 and ASCL1 that associate with super-enhancers are potential proto-oncogenes, and their inhibition may preclude SCLC tumor development (Christensen et al., 2014). Though we currently lack

a reported INSM1 GEMM model of SCLC, current studies suggest a role for INSM1 in promoting the growth of SCLC tumors and as a transcriptional regulator in SCLC. The highly expressed NE transcription factors ASCL1 and INSM1 are potentially attractive therapeutic targets for SCLC but remain directly "undruggable." Recent work has connected the inhibition of LSD1 and KDM5A genes with suppression of neuroendocrine genes through activation of the NOTCH pathway (Augert et al., 2019), (Oser et al., 2019). Targeting genes and pathways that reduce the expression of ASCL1, INSM1, and the overall NE signature of SCLC, remain attractive clinical targets for therapy.

Introduction of CRISPR/Cas9 Screens and Neddylation as a Target Pathway

For this study, we set out to identify new "druggable" targets for SCLC by using CRISPR inactivation screens to elucidate genes and pathways that are essential for SCLC cell proliferation and viability. Recently, the increased availability and efficacy of whole-genome CRISPR libraries have allowed for functional screening of an expansive variety of cell types. Libraries incorporating a lentiviral delivery system (Sanjana et al., 2014) have made possible the screening of difficult to transfect cell types, including suspension cells like SCLC. In this study we highlight how our genome-wide CRISPR screen identified potential novel therapeutic targets for SCLC, most notably the neddylation pathway as a SCLC-specific target. Neddylation is a post-translational modification involving the covalent addition of the ubiquitin-like NEDD8 (neuronal precursor cell-expressed developmentally down-regulated protein 8) molecule to lysine residues (Kamitani et al., 1997), (Xirodimas, 2008). Neddylation functions to regulate

substrate proteins in their stability, degradation, localization, and confirmation (Zhao et al., 2014). One critical function of the neddylation pathway is the regulation of protein ubiquitination, especially those targeted by cullin-RING ligase (CRL) complexes as cullin proteins require neddylation to function (Pan et al., 2004), (Petroski and Deshaies, 2005), (Chiba and Tanaka, 2004). The disruption of CRL-directed degradation has been connected to aberrant levels of cell cycle regulators and pro-apoptotic proteins including p21, p27, WEE1, and CDT1 (Soucy et al., 2009), many of which have critical roles in cancer. Chapters 1 and 2 detail our identification of the neddylation pathway as a SCLC target and interrogates how SCLC is sensitive to a small molecule inhibitor of neddylation. Chapter 3 will discuss recent reports of SCLC CRISPR screens and contrast their findings to our screen results. Chapter 3 will also examine additional SCLC genes and pathways from our screen that may be of therapeutic value. Lastly, Chapter 4 provides a look at how future work will be directed.

Chapter 1.2: Results

Genome Scale CRISPR Inactivation Screen of Murine SCLC Cell Lines

To identify potential therapeutic targets for the treatment of small cell lung cancer, we performed a series of genome scale CRISPR/Cas9 screens. We employed a panel of 5 cell lines that were derived from a genetically engineered autochthonous SCLC mouse model in which *Trp53* and *Rb1* deletion results in tumors with molecular and histological features resembling human SCLC. To compare to a non-neuroendocrine cell population, we generated and performed similar screens on mouse embryonic

fibroblasts (MEFs) from the embryos of *Trp53*$^{lox/lox}$ mice (Augert et al 2020, in submission). We infected cells with the GeCKO v2 pooled lentiviral sgRNA library (Sanjana et al., 2014) containing 130,209 sgRNAs targeting 20,611 genes, with most genes harboring 6 distinct sgRNAs per gene (Fig. 1A). Screening of each MEF isolate and mSCLC cell line was conducted at a multiplicity of infection of less than 1 by identifying the virus amounts needed to achieve a 30% transduction rate. Cells were spinfected with enough pooled library lentivirus to ensure 500-fold coverage of transduced cells. Immediately after selection we collected a full representative P0 for sequencing. Cell lines were passaged until reaching 12 population doublings (P12) at 500-fold coverage. At the P12 screen endpoint, cells were collected for sequencing. Genomic DNA was isolated from pellets followed by library construction prior to sequencing. We employed MAGeCK analysis (Li et al., 2014), (Li et al., 2015) to identify genes that become significantly enriched or depleted in the P12 samples when compared to the P0 set. Volcano plots for the mSCLC (Fig. 1B) and MEF (Fig. 1C) data sets show a large number of common depleted genes, likely representing essential genes in most cell types. To further identify mSCLC-specific enriched and depleted genes, we calculated CRISPR scores (Wang et al., 2015), which average the fold change in frequency relative to the P0 for all sgRNAs targeting a given gene. A heat map of CRISPR scores (Fig. 1D) reveals different dependencies between mSCLC cells and MEFs.

Our screen detected sgRNAs preferentially enriched in mSCLC but not MEFs, corresponding to candidate SCLC tumor suppressor genes, and also detected sgRNAs

that were depleted preferentially in mSCLC samples, indicating candidate oncogenes and potential therapeutic targets. Some tumor suppressors, such as Pten, were enriched in both mSCLC and MEF sample sets. In our mSCLC cells, we found sgRNAs targeting the pro-apoptotic Bcl2l11 (BIM) and the histone methyltransferase Crebbp to be enriched suggestive of SCLC-specific tumor suppressor function. Indeed, we recently validated Crebbp as a SCLC tumor suppressor (Jia et al., 2018). However, our main goal from the inactivation screens was to identify therapeutically targetable genes necessary for SCLC growth and survival. sgRNAs targeting orthologs of known SCLC dependencies (BCL2L1, ATR, CHEK1, MYCL) were significantly depleted in mSCLC cells but not in MEFs. ATR (Doerr et al., 2017), CHEK1 (Sen et al., 2017b) MYCL (Kim et al., 2016) and BCL2 family members (Rudin, 2012), (Gandhi et al., 2011) are all genes for which pharmacologic inhibition or genetic deletion impairs SCLC growth and/or viability. In addition to identifying known SCLC dependencies, we also found novel dependencies. sgRNAs targeting genes in the heme synthesis pathway, including Cpox, Hmbs, and Fech were significantly depleted in mSCLC cells. Also, members of the purine synthesis pathway, including Pfas, Paics and Adsl were identified as essential in mSCLC and may be therapeutically targetable. We were particularly interested in “druggable” dependencies and found that sgRNAs targeting the methyltransferase Prmt5 and its binding partner Wdr77 were depleted in the mSCLC cells. Moreover, sgRNAs targeting numerous members of the neddylation machinery, including Nedd8, Rbx1, and Cul2 significantly became depleted in mSCLC cells.

To validate screen hits, we performed proliferation assays using a two-vector system in an mSCLC cell line (G6263) used in our screen. The mSCLC cell line was infected with a constitutively active U6-promoted sgRNA vector as well as a doxycycline-inducible Cas9 vector. Ten-day proliferation (Fig. S1A) assays were performed on individual sgRNA for genes within our identified pathways of interest. We show reduced viability of the tested guides, including for Nedd8, Rbx1, Cul2, Insm1, Ascl1, Rpia, Bcl2l1, and Cpox, in comparison to control guides, identified for their neutral activity within our screen results.

Murine SCLC Lines and a Subset of PDX SCLC Models Display Sensitivity to Pharmacological Neddylation Inhibition

The neddylation pathway was of particular interest owing to the availability of a small molecule inhibitor of the neddylation pathway in advanced clinical trials for other indications (Soucy et al., 2009), (Bhatia et al., 2016), (Shah et al., 2016), (Lockhart et al., 2019). MLN4924 is an ATP competitive inhibitor of the neddylation activation enzyme (NAE1), which prevents the downstream neddylation of the E3 ligase and ultimately prevents degradation of the target protein substrate (Soucy et al., 2009), (Brownell et al., 2010), (Liao et al., 2011). To determine whether pharmacologic inhibition recapitulates effects of neddylation pathway gene deletion, we tested this inhibitor on mSCLC cell lines and MEF isolates employed in our screens. Dose response curves (Fig. 2A) performed on two murine SCLC lines, two MEF isolates, and

two murine non-small cell lung cancer lines (NSCLC) indicate that the mSCLC lines are indeed more sensitive to neddylation inhibition than MEFs or mouse NSCLC cells. IC50 plots (Fig. 2B) indicate an IC50 range of 0.4-1.2 uM for the mSCLC lines screened compared to 3-5 uM for the MEFs and 10-15 uM for the mNSCLC lines tested. Western blotting analysis (Fig. 2C) of tested cell lines treated with MLN4924 for 48 hours confirms target engagement of the drug, as shown by loss of the neddylated-cullin band.

To better determine the therapeutic potential of the neddylation inhibition in SCLC, we tested MLN4924 sensitivity across a panel of SCLC PDX models that we briefly cultured ex vivo (Augert et al., 2019) (Fig. 2D). ASCL1-high models LX108, RU280, and FHSC04 were more sensitive to MLN4924 than the ASCL1-low, NEUROD1 high models LX33B and FHSC39. Moreover, two SCLC-A subtype models, LX108 and RU280 exhibited IC50 values of 25 and 15 nM, which were orders of magnitude lower than other models (Fig. 2E). Western blotting analysis of four of the PDX models cultured ex vivo show a reduction of neddylated-cullins at a 10 nM dose of MLN4924 at 48 hours (Fig. 2F).

In Vivo MLN4924 Treatment of PDX SCLC Models Dramatically Slows Growth

We next determined whether ex vivo sensitivity of RU280 and LX180 to MLN4924 correlated to in vivo sensitivity. Approximately 1 million cells were injected into the flanks of NOD-SCID-gamma (NSG) mice and allowed to grow to a tumor volume of 150-

200 mm^3. Mice were then randomized to either 60 mg/kg of MLN4924 or the (2-Hydroxypropyl)-B-cyclodextrin (HPBCD) vehicle control given once daily by subcutaneous injection. Treatments continued for 15 days with daily measurements for weight and tumor volume before resecting the tumors for histological and molecular analysis. Both the LX108 (Fig. 3A) and RU280 (Fig. 3C) PDX models exhibit significant decrease in tumor growth when treated with MLN4924. In contrast, the FHSC39 PDX model (Fig. 2D-E) showed limited sensitivity to the treatment in vivo (Fig S2A). To elucidate effects of treatment on proliferation and apoptosis we performed immunohistochemical staining for phospho Ser10 histone H3 (PH3) and TUNEL analyses on fixed tumor samples from the treated LX108 and RU280 cohorts. LX108 (Fig. 3B) and RU280 (Fig. 3D) show a significant decrease in the number of PH3-positive mitotic cells with MLN4924 treatment (Quantified in Fig. 3E). TUNEL staining revealed a significant increase in apoptosis with MLN4924 in both LX108 and RU280 (Quantified in Fig. 3F). Thus, monotherapy with a neddylation inhibitor in a subset of PDX models causes tumor growth inhibition associated with reduced proliferation and increased apoptosis.

Transcriptional Analysis of MLN4924 Treatment

To interrogate molecular pathways associated with responsiveness to MLN4924 in SCLC, we employed RNA-seq analyses. We used EdgeR (Robinson et al., 2010) to identify differentially expressed genes in PDX tumors treated for 15 days with vehicle or MLN4924. Volcano plots showing MLN4924 dependent genes in the exceptionally responsive RU280 and LX108 models revealed striking downregulation of

neuroendocrine genes such as INSM1, ASCL1, FOXA2 and POU3F2 upon inhibition of the neddylation pathway (Fig. 4A-B). We also observed upregulation of NRF2 target genes, including NQO1, GCLC, GCLM, and OSGIN1. Analysis of the less sensitive FHSC39 PDX model showed no significant decrease in the same neuroendocrine genes (Fig. S3A) but did show upregulation of NRF2 targets. Of note, FHSC39 is a variant subtype model (SCLC-N) that expresses NEUROD1, lower protein levels of INSM1, and lacks ASCL1. We identified a sizeable number of common genes in LX108 and RU280 that were significantly downregulated or upregulated in the treated samples. Included in the common downregulated genes (Fig. 4C) are INSM1, ASCL1, FOXA2 and POU3F2. Using a list of identified SCLC-specific ASCL1 direct targets (Borromeo et al., 2016) we performed gene set enrichment analysis (GSEA). Both LX108 and RU280 show significant enrichment in the downregulation of ASCL1 targets when treated with MLN4924 (Fig. 4D). Conversely, the FHSC39 model lacked the significant enrichment in ASCL1 targets seen in the sensitive models (Fig S3C). Compared to the LX108 and RU280 models, FHSC39 features lower initial expression levels of the ASCL1 target genes. Included in the common significantly upregulated genes (Fig. 4E) are NQO1 and other NRF2 targets. While GSEA on LX108 and RU280 show significant enrichment in NRF2 targets upon MLN4924 treatment (Fig. 4F), and interestingly similar enrichment is seen in FHSC39 (Fig. S3D). Whether FHSC39 is insensitive to increased NRF2 levels is unclear. The functional relevance of heightened NRF2 activity is under further interrogation. Zhang et al. recently identified a SCLC associated neuroendocrine signature gene set (Zhang et al., 2018), and upon treatment of MLN4924 the LX108 and RU280 PDX models transcriptionally downregulate many of these neuroendocrine

signature genes. A heat map (Fig. 4G) of row Z-scores for the transcript FPKMs for treated LX108 and RU280 PDX models for the expressed NE signature genes depicts this broad downregulation. Conversely, treated FHSC39 tumors (Fig. S3E) do not show a meaningful downregulation pattern in expressed NE signature genes. Pathway enrichment analysis on the common significant downregulated genes in LX108 and RU280 show significant enrichment in pathways for dopaminergic neurogenesis (Fig S3E). Common upregulated genes are enriched in pathways for benzo(a)pyrene metabolism, glutathione metabolism, proteasome degradation, and NRF2 transcription and signaling. While all three treated models show upregulation for NRF2 transcription, the downregulation of neuroendocrine signature genes was exclusive to the sensitive models.

Perturbation of Neddylation Pathway Disregulates Neuroendocrine Signature

After identifying reduced expression of neuroendocrine genes in upon MLN4924 treatment, we next examined protein levels. Treatment of both LX108 and RU280 for 48 hours with 100 nM of MLN4924 reduced protein expression levels of INSM1, FOXA2, and ASCL1 (Fig. 5A). We also observed increased protein levels for NRF2 and P21, which are known targets of ubiquitin-mediated degradation known to increase upon MLN4924 treatment in other systems (Soucy et al., 2009), but their expression increase showed no direct correlation with sensitivity (Fig. S4A). In contrast, LX108 and RU280 were the only models to show downregulation in protein levels for each of the neuroendocrine regulators INSM1, ASCL1, FOXA2, and POU3F2. Western blot analysis of RU280 cells treated with MLN4924 confirmed reduction of neddylated-cullins

protein levels and increased levels of free NEDD8 (Fig S4B). We next wanted to determine if this NE signature change would be observed in other models of SCLC. We returned to our mSCLC lines used in our initial screen. Western blot analysis of the mouse G6263 and G6337 mSCLC cell lines treated with MLN4924 lead to decreased levels of NE lineage genes (Fig. S4C) similar to treated human LX108 and RU280 PDX ex vivo cells. Additionally, we profiled the treated tumors from the in vivo LX108 PDX model and observed a similar NE downregulation by western blot (Fig. S4D), mirroring the RNA-seq results.

To interrogate the genetic consequences of neddylation inhibition, we next used lentiviral vectors to inducibly knockdown neddylation pathway members NEDD8 and RBX1 with shRNA in RU280 ex vivo cells. Doxycycline was supplemented to cells every 48 hours and cells collected at time points of 72 and 96 hours to validate knockdown by western blot analysis (Fig. 5B). Knockdown of NEDD8 and RBX1 replicated the effects of pharmacologic inhibition of neddylation in leading to neuroendocrine gene downregulation. We also found strong reduction in proliferation with NEDD8 and with RBX1 knockdown compared with the GFP controls (Fig. 5C-E). We next examined the functional importance of reductions in INSM1 upon neddylation inhibition. We again used the inducible hairpin system to knock down levels of INSM1 (Fig. 5F) in RU280 ex vivo cells. Knockdown of INSM1 reduced proliferation compared to the off-dox control over 10 days (Fig. 5G). We similarly targeted FOXA2 for knockdown and validated the hairpin by western blot (Fig S5A). Interestingly, ASCL1 levels are reduced with the knockdown of INSM1 or FOXA2, indicating INSM1 and FOXA2 maintain some

transcriptional control of ASCL1. Next we overexpressed INSM1 in the sensitive RU280 ex vivo model to test if this confers resistance to effects of pharmacological inhibition of neddylation. Constitutive overexpression of INSM1 was validated by western blot (Fig. 5H). RU280 cells overexpressing INSM1 exhibit a 2-fold increase in IC50 for MLN4924 compared to an empty vector control (Fig. 5I). Overexpression of FOXA2 resulted in a similar increase in resistance to INSM1 (Fig S5B-E). We looked at proliferation of RU280 cells when overexpressing INSM1 and discovered significant increase in cell viability when grown in the presence of 25 nM MLN4924 over 7 days (Fig. 5J) when compared to control cells. Overexpression of FOXA2 showed a similar proliferative increase to INSM1 (Fig S5B). Interestingly, overexpression of INSM1 and FOXA2 in RU280 cultured in normal growth media showed an increased proliferation rate (Fig. S5C), possibly indicating that restoration of NE expression can overcome strong cell cycle changes induced by MLN4924 and observed in our PH3 IHC samples.

Suppressor Screen in Sensitive SCLC PDX Connects the NF-κB and mTOR Pathways with MLN4924 Resistance

To gain insights into the mechanism underlying sensitivity to neddylation inhibition in SCLC, we performed a genetic suppressor screen using the RU280 PDX ex vivo model. We infected with the GeCKO v2 human CRISPR inactivation library and passaged the cells under DMSO or with MLN4924 (25 nM) (Fig. 6A). After library infection of RU280 cells at an MOI of 0.3, cells were selected for 3 days with puromycin. After selection, 65 million cells were collected for an initial time point (P0), 65 million were left untreated (DMSO) and passaged for 12 population doublings (P12), and 65 million were treated

with 25 nM of MLN4924 and passaged until the DMSO arm reached completion (21 days). To identify genes that when inactivated confer resistance to MLN4924; we quantified the average CRISPR Score for each gene across three replicates for both our DMSO and MLN4924 treated samples. Plotting the CRISPR Scores in the DMSO P12 vs MLN4924 conditions (Fig. 6B), a number of pathways were found enriched specifically in the MLN4924 condition. The COPS9 signalosome promotes neddylation turnover, and COPS1 (GPS1), COPS2, COPS3, COPS4, COPS5, COPS6, COPS7A, and COPS8 were all highly enriched compared to the DMSO replicates. Many components of the NF-κB pathway, including the ligand TLR2, adaptor proteins MYD88 and TIRAP, TAK1 (MAP3K7) and the IKK complex kinases were highly enriched in the MLN4924-treated replicates. Also enriched in the MLN4924 replicates are sgRNAs targeting the mTOR pathway genes mTOR, RHEB, RPTOR, and members of the GATOR2 complex. However, deletion of mTOR pathway genes was slightly deleterious in the DMSO replicates. A heat map of CRISPR scores (Fig. 6C) identified in the suppressor screen organizes the results by pathways and similar functions. In addition to the COPS9 signalosome, NF-κB and mTOR pathways, the known neddylation substrate NRF2, cell cycle genes CDKN1A and CDKN1B, and several epigenetic regulators like CREBBP and KDM3B score highly in our suppressor screen (Figure 6C). To provide confirmation that our suppressor screen induced resistance to the MLN4924 treatment, we tested each of the polyclonal replicates from the screen for their sensitivity to the inhibitor (Fig. S6B). Each of the replicates increased their quantified IC50 to beyond the 25 nM screen dosage, indicating the replicates' increased resistance to MLN4924.

Pharmacological Inhibition of mTOR and NF-κB Pathways Abrogates the Effects of Neddylation Pathway Perturbation

We then tested pharmacologic inhibitors of the mTOR and NF-κB pathway for their ability to replicate the effects of genetic inactivation observed in our suppressor screen. Treatment of RU280 with the mTOR inhibitor Everolimus at 1 nM or the IKK complex inhibitor IKK-16 at 500 nM reduced the effectiveness of MLN4924 (Saran et al., 2015), (Prescott and Cook, 2018). RU280 cells co-treated with the mTOR inhibitor have a 5X increase in the MLN4924 IC50, while the NF-κB inhibitor affected an 11X increase in the IC50 (Fig. 7A). We next examined protein levels of a neuroendocrine lineage gene upon co-treatment and observed an increase an INSM1 expression levels by western blot (Fig 7B). Considering the prevalence of NF-κB genes in our suppressor screen results, we then examined effects of MLN4924 on NF-κB pathway activation. Western blot analysis of RU280 cells treated for 48 hours with MLN4924 (Fig. 7C) showed strong increases in the phosphorylation levels of both IKKalpha/beta and p65, indicating pronounced changes in the NF-κB pathway. We identified an enriched sgRNA from our screen results for the CHUK gene, which encodes the kinase IKKalpha, and produced knockout cells in RU280. After confirmation of protein loss by western blot (Fig. S7A) we then observed dramatic reductions of phosphorylated-p65 levels when IKKalpha knockout cells were treated with 25 nM MLN4924 (Fig. S7B). Co-treatment of MLN4924 and either the mTOR or NF-κB inhibitors reduced the phosphorylated-p65 protein levels we observed in MLN4924 treated cells (Fig. 7D). Similar to the MLN4924 resistance effects gained by treatment of IKK-16, knockout IKKalpha cells show an increase in IC50 for the neddylation inhibitor (Fig. S7C).

1.3: Discussion

CRISPR/Cas9 Screens Identifies the Neddylation Pathway as a Therapeutic Target

The therapeutic options for SCLC remain limited, resulting in incredibly low survival rates. We theorized that a whole-genome inactivation screen in a panel of Rb/p53 mouse cell lines could provide an unbiased and comprehensive search for vulnerabilities of SCLC. Genes identified as SCLC-specific vulnerabilities could then be queried for existing inhibitors with potential for translational results. Highly significant in our depleted sgRNA list were the guides for Nedd8, Rbx1, and Cul2 genes, leading us to investigate neddylation inhibition as a novel therapeutic strategy for SCLC. Of note, previous inactivation screens in SCLC did not uncover and expound on the neddylation pathway. This report shows that the pharmacological and genetic inhibition of neddylation can suppress the growth of the SCLC.

Neddylation is a ubiquitination-like posttranslational modification pathway that adds the NEDD8 molecule to targets (Kamitani et al., 1997) (See Figure A). This reversible conjugation of NEDD8 to target proteins involves a three-step series of reactions beginning with the ATP-dependent activation of the NEDD8 precursor by the NEDD8-activing enzyme (NAE1) homodimer (Walden et al., 2003). NAE is a heterodimer constituted by the two proteins of UBA3 and NAE1, equivalent to the E1 enzyme in the ubiquitin enzyme cascade (Walden et al., 2003), (Chen et al., 2000). Our results showed that knockdown of NEDD8 in a SCLC PDX model and thus inhibition of the E1 activation step lead to a dramatic reduction in proliferation. After E1, the NEDD8

molecule is passed to one of two E2 enzymes in the neddylation pathway, UBE2M and UBE2F (Gong and Yeh, 1999). We were encouraged to see that both NAE1 and the E2 enzyme UBE2M are strongly significant in our RU280 CRISPR inactivation screen and we hypothesize that their inactivation would result in a similar growth reduction in SCLC. Additionally, UBE2F sgRNAs do not become significantly depleted, supporting UBE2M as the predominant E2 enzyme relevant in SCLC. This finding also allows us to concentrate on pathway members that preferentially use UBE2M, which could aide in our continuing attempts in identifying relevant substrates in SCLC.

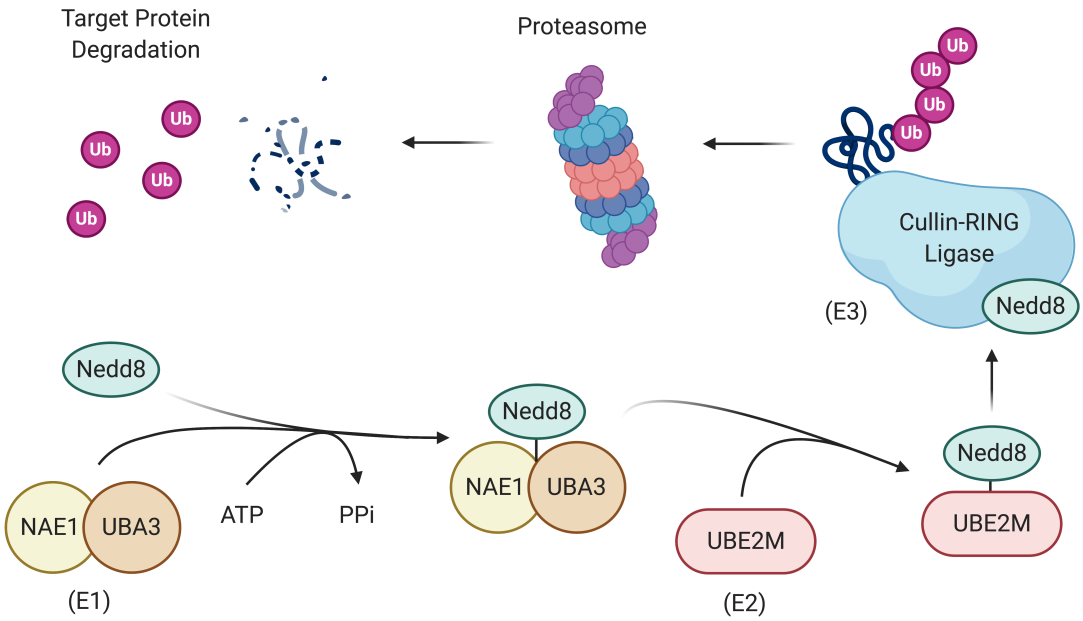

Figure A: Neddylation Pathway

After the E2 portion of the cascade, the neddylation pathway features RING E3 ligases which bind both the NEDD8-activated E2 enzyme as well as their own substrate (Huang et al., 2009). RBX1, the E3 enzyme that we identified in our inactivation screen, is one of two RING E3 ligases involved in neddylation. RBX1 also functions as an E3 ubiquitin ligase for neddylation-activated cullin RING ligase (CRL) complexes (Huang et al., 2009). The CRL complexes feature an array of adaptor proteins, receptor proteins, and substrates (Kamura et al., 1999). Due to this complexity, we have been unable to identify a specific CRL complex with target protein that is solely responsible for our observed phenotypes despite the initial identification of Cul2 in our mSCLC screen. Our knockdown studies of cullin family members showed modest (See Additional Fig. S8A-D), but weaker growth inhibition compared with NEDD8 or RBX1 knockdowns in the RU280 PDX model. We hypothesize that inherent redundancy in the CRL complexes prevent complete recapitulation of the inhibition provided by NEDD8 and RBX1 perturbation. However, due to RBX1 inactivation's strong phenotype, and the lack of SAG (RBX2) in our screen results, we theorize that RBX1 is the main E3 contributor, and thus limited our search to the CRL1-4 complexes that feature RBX1 (Chen et al., 2015b). Despite our inability to genetically discern the importance of specific CRL complex function in SCLC through our proliferation assays, we were able to phenocopy our genetic inactivation results of NEDD8 and RBX1 with a novel small molecule inhibitor of the pathway. Chapter 2.1 will further examine the role of CRLs in SCLC.

The selective inhibitor of the neddylation pathway, MLN4924, works by preventing the initial step of NEDD8-mediated cascade (Soucy et al., 2009). This small molecule,

which is structurally similar to AMP, binds to the active site of NAE and forms a stable adduct which competitively inhibits ATP binding and ceases further NAE function (Brownell et al., 2010). MLN4924 has been tested in numerous tumor types, slowing proliferation in both cells lines and in vivo PDX models (Tong et al., 2017), (Lin et al., 2010), (Milhollen et al., 2011), (Wei et al., 2012), (Milhollen et al., 2010), (Swords et al., 2010). Our tests found mSCLC cell lines more sensitive to MLN4924 treatment than either mNSCLC cell lines or MEF isolates, which indicated a SCLC-specific sensitivity to the inhibition of neddylation. We also identified several SCLC PDX models that exceptionally responded to MLN4924 both in vitro and in vivo, which promoted the targeting of the neddylation pathway as a therapeutic option for a subset of SCLC. We report that MLN4924 monotherapy in the flank tumors of mice leads to dramatic increases in apoptosis plus decreases in proliferating cell numbers. Though the specific mechanisms in which MLN4924 promotes these phenotypes are still being uncovered, our findings suggest that the neddylation pathway inhibition could be a clinically viable SCLC treatment.

MLN4924 Downregulates the Neuroendocrine Signature in SCLC

SCLC is a tumor type notable for its neuroendocrine characteristics and high expression levels of key NE transcription factors (Wooten et al., 2019), (Rudin et al., 2019). Our transcriptional profiling of treated PDX models identified a pronounced neuroendocrine gene downregulation in two of the three models we assayed. We noticed that the models with decreased NE gene transcripts aligned with the two most sensitive models (LX108 and RU280) from our IC50 assays. Conversely, the model (FHSC39) that did

not change NE transcript levels was resistant to the effects of MLN4924. Recent transcriptional analyses of SCLC tumors have promoted the development of a classification system based on the expression of driver transcription factors like ASCL1, NEUROD1, POU2F3, and YAP1 (Rudin et al., 2019). Our findings suggest that the subtype classification of the sample often predicts sensitivity to MLN4924. The SCLC-A subtype typically expresses high levels of ASCL1, INSM1 and other NE genes, and our two sensitive PDX models do classify as SCLC-A. Alternatively, the SCLC-N subtype expresses NEUROD1 and variable levels of INSM1 (Rudin et al., 2019), and is the subtype of our resistant FHSC39 PDX model. It's possible that the transcriptional profile induced by expression of NEUROD1 promotes resistance to MLN4924. Unfortunately, subtype alone does not fully subdivide our tested models into either exceptional responders or those completely resistant. The resistance that less sensitive SCLC-A models display to MLN4924 may be in part due to an individual tumor's ability to withstand the consequences of NE downregulation. Further studies could look to identify mechanisms that sensitize moderately resistant models to MLN4924.

Recent studies have looked into the functional roles of NE genes in the development and progression of SCLC (Borromeo et al., 2016), (Fujino et al., 2015), (Christensen et al., 2014). These studies have highlighted how the genetic inhibition of NE genes like ASCL1 and INSM1 can either preclude SCLC tumorigenesis or inhibit tumor cell proliferation. Our genetic studies showed similar effects in the stalling of proliferation upon loss of INSM1. However, MLN4924 treatment not only downregulated INSM1 expression, but also many other NE transcription factors like ASCL1 and FOXA2.

Transcriptional profiling of high-grade SCLC resulted in a list of NE signature genes (Zhang et al., 2018) which best represent the classical SCLC-A subtype. Dramatically, MLN4924 leads to the transcriptional repression of most of these NE signature genes, but this is only observed in our sensitive models. The broad NE signature downregulation imposed by MLN4924 treatment may provide a stronger phenotype than a theoretical direct pharmacological inhibitor of a NE gene like ASCL1 and INSM1. Repression of the NE signature is likely a clinically relevant approach as we know from recent reports that NE gene downregulation with inhibitors of LSD1 and KDM5A has shown promise in SCLC tumor models (Augert et al., 2019), (Oser et al., 2019).

Even with our striking results observed from the MLN4924-induced perturbation of NE signature genes, we are still left with many pressing questions. Treated PDX tumors showed decisive apoptotic and proliferative effects. Our cell-based NE restoration studies also displayed a capability to overcome MLN4924 growth phenotypes. However, it is still unclear if and how the broad NE signature downregulation is fully responsible for the phenotypes observed with MLN4924 treatment. Clarity for this question may come from determining the precise protein identities that connect aberrant neddylation to NE repression. We propose that a still to be resolved neddylation substrate(s) regulates the degradation of a target protein, which can repress the NE transcriptional signature. Determination of these relevant substrates and target proteins could facilitate novel therapies, as avoiding targeting of irrelevant neddylation substrates is clinically beneficial.

Note: Pathways identified in the MLN4924 suppression screen and their roles in neddylation inhibition are discussed in Chapter 2. Future directions are discussed in Chapter 4.

1.4: Materials and Methods

Genetically Engineered Mice Models of SCLC and Cell Line Generation

We thank Anton Berns for the $Trp53^{lox/lox}$ and Tyler Jacks for the $Rb1^{lox/lox}$ strains. We obtained Adenovirus containing a CGRP-promoted Cre (Ad5-CGRP-Cre) from the University of Iowa Vector Core. The CGRP promoter specifically drives Cre recombinase in neuroendocrine cells. Intratracheal infection of Ad-CGRP-Cre was performed on adult $Trp53^{lox/lox}$; $Rb1^{lox/lox}$ mice at a titer of 1.25×10^9 pfu per mouse. Monitoring of mice continued each week after infection until mice showed noticeable signs of labored breathing. After euthanasia, tumor fragments were extracted to generate cell lines, snap frozen for molecular analysis, or fixed in NBF for histology and immunochemistry. All animal procedures were approved by the Institutional Animal Care and Use Committee (IACUC) at the Fred Hutchinson Cancer Research Center.

$Trp53^{lox/lox}$ MEF Generation

At 13.5 days post coitum, embryos from a $Trp53^{lox/lox}$ mouse were collected and moved to a sterile 10cm dish in a tissue culture hood. Individual embryos were cleaned with PBS before all maternal tissues, innards, and embryo heads were removed. After

shifting the embryo body to a clean dish, 1 milliliter of .05% trypsin in EDTA was added and the embryo body chopped with a sterilized razor blade. The resulting embryo mince was incubated for 1 hour at 37^{o}C. Fresh DMEM was added to the digested MEF cells and then moved to a fresh sterile 10 cm culture dish. Cells were cultured for 72-96 hours, splitting before reaching confluence, and frozen for liquid nitrogen stock. To deactivate p53 expression, Ad5-CMV-Cre was added to the media of cultured MEFs at a MOI of 100. The virus addition was repeated to ensure complete p53 loss.

Cell Culture

MEF and 293TN cells were both cultured in DMEM supplemented with Penicillin (100 units/mL), Streptomycin (100 ug/mL) (Pen/Strep 15140122, ThermoFisher Scientific) and 10% FBS (FB-01, Omega Scientific). Mouse SCLC and PDX ex vivo cell lines were grown in RPMI Complete media. The recipe was as follows: RPMI 1640 (11875-093, ThermoFisher Scientific), Penicillin (100 units/mL), Streptomycin (100 ug/mL), 15% FBS, 1 mM sodium pyruvate (11360070, ThermoFisher Scientific), 100 uM beta-mercaptoethanol (31350010, ThermoFisher Scientific), and 10 ug/mL Insulin, human recombinant zinc solution (12585014, ThermoFisher Scientific). Doxycycline (44577, Sigma) was used for inducible lentiviral systems at noted concentrations. All cells were incubated at 5% CO2 and 95% air.

Pooled Library DNA and Virus Creation

The DNA and viral productions of both the GeCKO v2 mouse (#1000000052, #1000000053, Addgene, a gift from Feng Zhang) and human (#1000000048, #1000000049, Addgene, a gift from Feng Zhang) libraries were performed as described previously (Sanjana et al., 2014).

CRISPR Library Titering

Titer of half libraries (for both mouse and human GeCKO v2) for SCLC cells was determined by spinfection of 3 million cells of individual cell lines in a well of a 12-well plate. Cells were supplemented with virus and 8 ug/mL of polybrene at a volume of 600 uL. Plates were centrifuged for 2 hours at 2000 rpm at 37 degrees. After spinfection cells wells were mixed with 900 uL of media and incubated overnight. Virus was removed the day after transduction. At 48 hours post transduction lines were treated with puromycin for 72 hours. Calculation of virus for desired .3 MOI was determined by comparing number of puromycin-surviving cells to the unselected control.

CRISPR Screening

For the p53-null MEF screen (Augert et al 2020, in submission), $2.5x10^8$ cells were transduced with the GeCKO v2 mouse pooled library at a MOI<1 to ensure a 30% successful transduction rate. After overnight virus addition, cells were selected with puromycin for 3 days. $6.6x10^7$ cells were collected for P0 and $6.6x10^7$ cells were

passaged until 12 population doublings were reached, maintaining 500-fold coverage of all guides. A P12 pellet was collected. Three replicates were performed. For screening of mouse SCLC cell lines, $4x10^8$ cells were transduced with both halves of the GeCKO v2 mouse pooled library at a MOI<1 to ensure a 30% successful transduction rate. 3 million cells in a 600 uL volume were spinfected in the presence of polybrene and virus for 2 hours at 2000 rpm and 37^{o}C. After completion of the spin, each well was resuspended with 900 uL of fresh media and the cell-virus mixture left overnight. Virus was removed the next day and the wells pooled. The following day transduced cells were selected with puromycin for 3 days. $6.6x10^7$ million cells were collected for a P0 pellet sample and $6.6x10^7$ cells were passaged until 12 population doublings were reached, maintaining 500-fold coverage of all guides. A P12 pellet was collected. Five mouse SCLC lines were screened. For the RU280 PDX ex vivo resistance screen, transduction of RU280 cells was performed similar to the mouse SCLC screen. We used the GeCKO v2 human pooled library for this screen. After selection with puromycin, $6.6x10^7$ cells were collected for a P0 pellet, $6.6x10^7$ cells were cultured with DMSO as an untreated control, and $6.6x10^7$ cells were cultured with a final MLN4924 concentration of 25 nM. DMSO control cells were passaged until 12 population doublings were achieved, maintaining 500-fold coverage of guides. MLN4924-treated cells were repassaged every 3-4 days with fresh MLN4924-supplemented media until the DMSO control cells reached endpoint. Pellets for the DMSO control (P12) and MLN4924-treated cells were collected for each of the three replicates.

Genomic DNA Extraction

To extract genomic DNA from frozen cell pellets we performed a previously described method (Chen et al., 2015a). 6 mL of NK Lysis Buffer (50 mM EDTA, 1% SDS, 50 mM Tris, pH 8.0) was added to each pellet in a 15 mL conical. 30 uL of 20 mg/mL Proteinase K (19131, Qiagen) was added to each sample and incubated while rotating at 55^{o}C overnight, adding aliquots of Proteinase K if needed. 30 uL of 10 mg/mL of RNase A (19101, Qiagen) was added to the lysis, inverted 25 times to mix, and incubated at 37^{o}C for 30 minutes. Samples were placed on ice and 3.5 mL of 5 M ammonium acetate solution (AM9071, Invitrogen) was added. Samples were vortexed for 30 seconds and then centrifuged for 10 min at 4000g at 4^{o}C. Supernatant of spun samples was transferred to a new 15 mL conical tube. Precipitation of DNA was achieved by adding 6 mL of isopropanol to samples and inverting tubes to mix. Tubes were centrifuged and the supernatant discarded. DNA was washed by two rounds of 70% ethanol additions and followed by 5 min of centrifugation. DNA pellets were air-dried for 10 minutes and resuspended in 500 uL of TE buffer. Concentration of samples was determined by spectrophotometry (NanoDrop).

Library Generation and CRISPR Screen Analysis

To prepare libraries for sequencing, 430 ug of extracted genomic DNA per sample (see section above) was amplified and prepared for sequencing using Phusion Flash High Fidelity Master Mix (F548L, ThermoFisher) according to a previously described protocol (Chen et al., 2015a). A two-step PCR reaction was employed to first amplify the sgRNA

cassette and maintain library complexity (12 cycles) and a second PCR reaction was performed to add barcodes and Illumina adapters (16 cycles). Reactions were pooled after each PCR. Following the second PCR, reaction products were run on a 2.5% agarose gel and the DNA purified using a gel extraction kit (PureLink Gel Extraction Kit, K210012, Invitrogen). Once purified, the concentration of individual libraries was quantified using the Kapa Biosystems Library Quantification Kit (KK4824, Roche) according to kit instructions. Libraries were sequenced using an Illumina HiSeq 2500. The sequencing results were analyzed using the MAGeCK-VISPR pipeline (Li et al., 2015). For CRISPR score analyses of aligned and normalized read counts, the following formula was used: CRISPR score = $\log_2$ (Initial sgRNA abundance / Final sgRNA abundance) (Wang et al., 2015).

Xenograft Models and Drug Treatment

Patient derived xenografts from SCLC circulating tumor cells were develop as previously described (Augert et al., 2019). Cells were re-injected as 100 uL aliquots of a 1:1 mixture of matrigel and disassociated cells into the flanks of NSG mice. Treatments of either MLN4924 or vehicle control were started at a flank tumor volume size of approximately 150-200 mm^3. Mice were administered MLN4924 or vehicle control at 60 mg/kg once daily for 15 days and individual flank tumors measured using calipers. At 15 days tumors were resected after euthanasia of the mice.

Plasmids

We cloned individual guide sgRNA vectors for screen validation using the lentiGuide-Puro (#52963, Addgene, a gift from Feng Zhang) vector in conjunction with Lenti-iCas9-neo (#85400, Addgene, a gift from Qin Yan). For knockouts of human IKKalpha and other validations of the RU280 resistance screen, we used the lentiCrisprV2 (#52961, Addgene, a gift from the Zhang lab). To induce knockdown of NEDD8, RBX1, INSM1, FOXA2, and ASCL1, CUL1, CUL2, CUL3, and CUL4 we used the EZ-Tet-pLKO series of plasmids (EZ-Tet-pLKO-Puro, #85966, Addgene, a gift from Cindy Miranti) (EZ-Tet-pLKO-Blast, #85973, Addgene, a gift from Cindy Miranti) (EZ-Tet-pLKO-Hygro, #85972, Addgene, a gift from Cindy Miranti). The FOXA2 cDNA was cloned from the EF1a_FOXA2_P2A_Hygro_Barcode plasmid (#120439, Addgene, a gift from Prashant Mali). The INSM1 cDNA was a gift from the Peter Nelson lab (RG215007, Origene). The POU3F2 cDNA was cloned from a designed plasmid (VectorBuilder). The ASCL1 lentiviral overexpression plasmid (phASCL1-N106, #31781, Addgene, a gift from Jerry Crabtree) was used as the base vector for the constitutive neuroendocrine overexpression constructs. The FOXA2, INSM1, and POU3F2 cDNAs were cloned into the phASCL1 vector backbone. To create the empty control (phEmpty), the ASCL1 cDNA was removed and the vector closed.

Lentiviral Infections

Individual CrisprV2 sgRNA, EZ Puro shRNA, and orf overexpression plasmids were infected using the spinfection protocol described above.

Drug Sensitivity, Cell Viability and Proliferation Assays

MLN4924 IC50 determination assays were conducted by seeding 17,000-20,000 cells (depending on basal proliferation rate) into an opaque-walled, clear-bottom 96-well culture plate in combination with increasing concentration of MLN4924. Total volume of cells, diluted MLN4924, and media totaled 100 uL. Each assay was done in triplicate with at least three independent replicates. At 72 hours, viability was assessed using CellTiter-Glo Luminescent Cell Viability Assay (Promega) following the manufacturer's protocol. The plate was mixed on a plate shaker and the luminescent signal read using a BioTek plate reader. For combined drug assays, 15 cm plates of RU280 were seeded for 24 hours with either 500 nM of IKK-16 or 1 nM of Everolimus. The MLN4924 IC50 assay was conducted as above with the addition of secondary drug. Proliferation assays were conducted by seeding 1750-2000 cells into an opaque-walled, clear-bottom 96-well tissue culture plate at a volume of 100 uL. Cells were seeded in replicate plates to account for each day of cell viability readings needed (Day 1, Day 4, Day 7 and if noted Day 10). For inducible lentiviral shRNA or sgRNA constructs, on doxycycline (On Dox) wells included 1 ug/mL of doxycycline upon seeding and was readministered to appropriate wells on even days of the assay. The collection of cell pellets for accompanying western, RNA, or histone analysis followed similar setups to above except seeded in single 15 cm dishes with scaled up cell numbers and volumes.

Immunohistochemistry

Fragments of dissected PDX tumors were fixed in neutral-buffer formalin for 48 hours and then stored in 70% ethanol. Tumors were embedded in paraffin blocks and sectioned at 4 um. Hematoxylin and eosin staining was completed using standard procedures. The primary antibody for anti-phospho-histone H3 (1:500; 06-570, EMD Millipore) was used for the immunohistochemical staining of slides. Briefly, slides were dewaxed in xylene, rehydrated through a decreasing gradient of ethanol in TBST. Antigen unmasking was performed in a microwave and slides allowed to cool. Prior to overnight antibody incubation, sections were blocked with a 5% goat serum solution (Jackson ImmunoReseaerch, 005-000-121) followed by blocking of endogenous peroxidases with a 3.5% H2O2 solution. A biotin-conjugated secondary antibody was used (Vector Laboratories, BA-1000) followed by the Vectastain ABC kit (Vector Laboratories, PK-4000). Finally, detection was performed (Vector Laboratories, SK-4100) and imaged using a Nikon E800 microscope. The POD in situ cell death detection kit (Roche, 11684817910) was used for the TUNEL assays.

RNA extraction, RNA-seq Libraries and Differential Expression Analysis

Extraction of RNA from tumor tissues was performed with TRIzol according to manufacturer's specifications. To generate RNA-seq libraries from 500 ng of total RNA, the Ultra RNA Library Prep Kit for Illumina (E7530L, New England BioLabs) was used according to manufacturer's instructions. Sequencing of 50-bp single ends was performed with an Illumina HiSeq 2500. Low quality reads were filtered and the

remaining reads mapped to the human genome using TopHat (Trapnell and Schatz, 2009). The FPKM values were quantified using Cuffdiff (Trapnell et al., 2013). The HTSeq Python package (Anders et al., 2015) was used to generate counts from the TopHat alignments. Differentially expressed genes upon MLN4924 treatment of PDX tumors were identified using the EdgeR software package (Robinson et al., 2010). The significance of differentially expressed genes was set at a false discovery rate (FDR) of 0.05.

Gene Set Enrichment and Pathway Analyses

Common significantly downregulated or upregulated genes from the LX108 and RU280 data sets were analyzed using the ENRICHR website application (amp.pharm.mssm.edu/Enrichr/). Gene Set Enrichment Analysis (GSEA) of differentially expressed genes from the LX108, RU280, and FHSC39 data sets was performed using the GenePattern site (www.genepattern.org).

Protein Extraction and Immunoblotting

Lysis from whole-cell extracts of cultured murine and human cell lines was prepared in diluted RIPA buffer (10X concentration, Cell Signaling, 9806). Phosphatase and Protease inhibitors were added to the RIPA buffer prior to extraction. Cells were disassociated by mechanical homogenization followed by repeated passaging through successive small gauge needles. Protein concentration was determined using Pierce BCA Protein Assay Kit (23227, ThermoFisher Scientific). Immunoblotting was

performed using standard protocols. The following antibodies were used in this study: anti-BETA ACTIN (Cell Signaling, 4970, 1:2000), anti-GAPDH (Santa Cruz, sc-32233, 1:2000), anti-NEDD8 (Cell Signaling, 2745, 1:1000), anti-RBX1 (Cell Signaling, 11922, 1:1000), anti-INSM1 (Santa Cruz, sc-271408, 1:1000), anti-MASH1 (ASCL1) (BD, 24B72D11.1, 1:1000), anti-FOXA2 (Cell Signaling, 8186, 1:1000), anti-BRN2 (Proteintech, 18998-1-AP, 1:1000), anti-H3 (Cell Signaling, 3638, 1:4000), anti-H3K27me1 (Abcam, ab194688, 1:2000), anti-H3K27me3 (Abcam, ab6002, 1:2000), anti-phosph-p65 Ser536 (Cell Signaling, 3033, 1:1000), anti-p65 (Cell Signaling, 8242, 1:1000), anti-Cul1 (Santa Cruz, sc-17775, 1:1000), anti-Cul2 (Santa Cruz, sc-166506, 1:1000), anti-Cul3 (Santa Cruz, sc-166110, 1:1000), anti-Cul4 (Santa Cruz, sc-377188, 1:1000), anti-CDT1 (Cell Signaling, 8064, 1:1000), anti-NRF2 (Cell Signaling, 12721, 1:1000), anti-p21 (Santa Cruz, sc-6246, 1:1000), anti-IKKalpha (Cell Signaling, 2682, 1:1000), anti-IKKbeta (Cell Signaling, 8943, 1:1000), anti-phospho-IKKalpha/beta Ser176/180 (Cell Signaling, 2697, 1:1000).

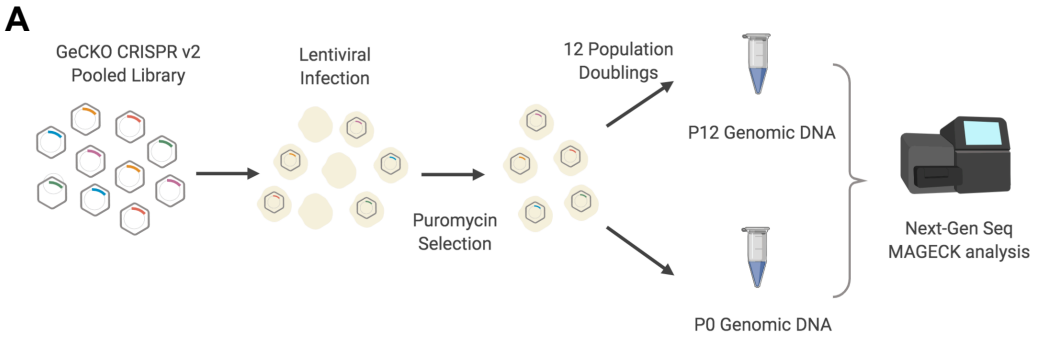
A
GeCKO CRISPR v2
Pooled Library
Lentiviral
Infection
Puromycin
Selection
12 Population
Doublings
P12 Genomic DNA
P0 Genomic DNA
Next-Gen Seq
MAGECK analysis

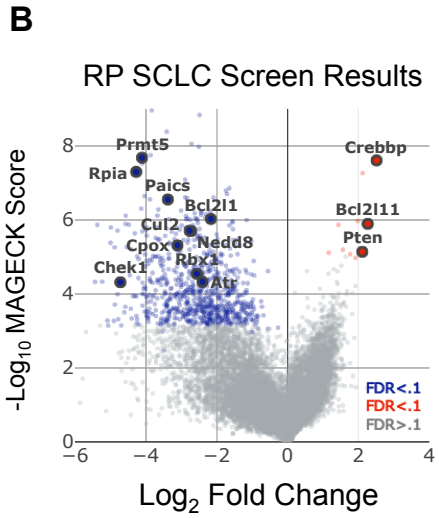
B
RP SCLC Screen Results
-Log10 MAGECK Score
Log2 Fold Change
Prmt5
Rpia
Paics
Bcl2l1
Cul2
Cpox
Nedd8
Rbx1
Chek1
Atr
Crebbp
Bcl2l11
Pten
FDR<.1
FDR<.1
FDR>.1

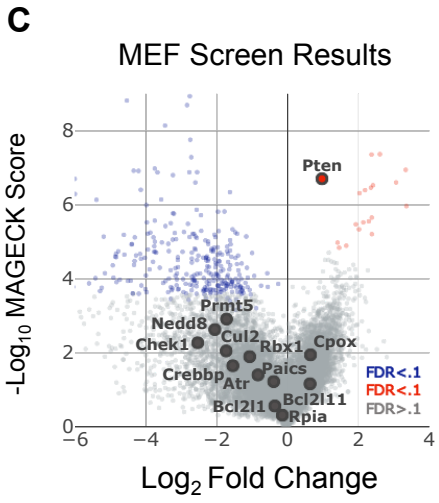
C
MEF Screen Results
-Log10 MAGECK Score
Log2 Fold Change
Pten
Prmt5
Nedd8
Cul2
Chek1
Rbx1
Cpox
Crebbp
Atr
Paics
Bcl2l1
Bcl2l11
Rpia
FDR<.1
FDR<.1
FDR>.1

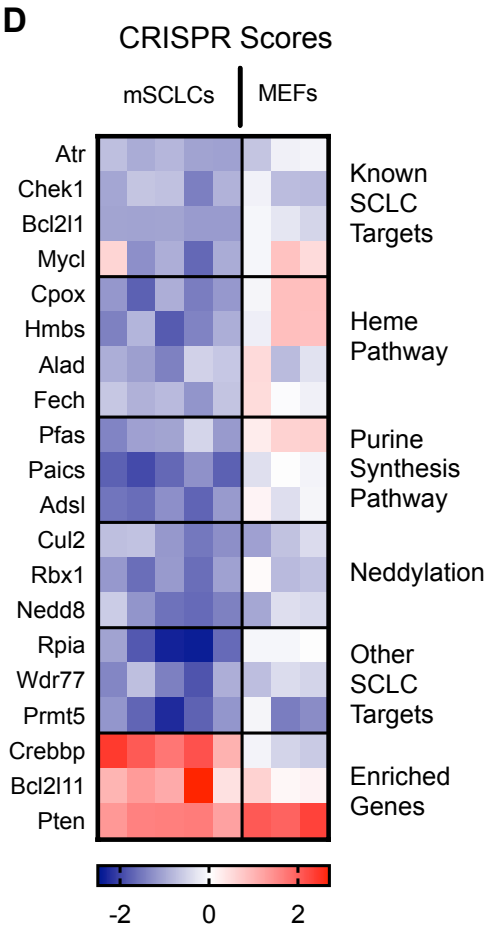
D
CRISPR Scores
mSCLCs
MEFs
Atr
Chek1
Bcl2l1
Mycl
Cpox
Hmbs
Alad
Fech
Pfas
Paics
Adsl
Cul2
Rbx1
Nedd8
Rpia
Wdr77
Prmt5
Crebbp
Bcl2l11
Pten
Known SCLC Targets
Heme Pathway
Purine Synthesis Pathway
Neddylation
Other SCLC Targets
Enriched Genes
-2
0
2

Figure 1

Whole genome CRISPR/Cas9 screen identifies potential therapeutic targets and pathways in SCLC:

A. Flowchart of the CRISPR/Cas9 inactivation screen conducted using the Gecko v2 lentiviral mouse library (130,209 total guides, 6 guides per gene). Cells were infected at approximately .3 MOI and to ensure 500 fold sequencing coverage.

B-C. Volcano plots of MAGECK analysis results from 5 screened mSCLC cell lines (**B**) and 3 screened p53-null MEF lines (**C**).

D. Heat map of the top depletion and enrichment CRISPR Scores of 5 mSCLC cell lines and 3 p53-null MEF lines.

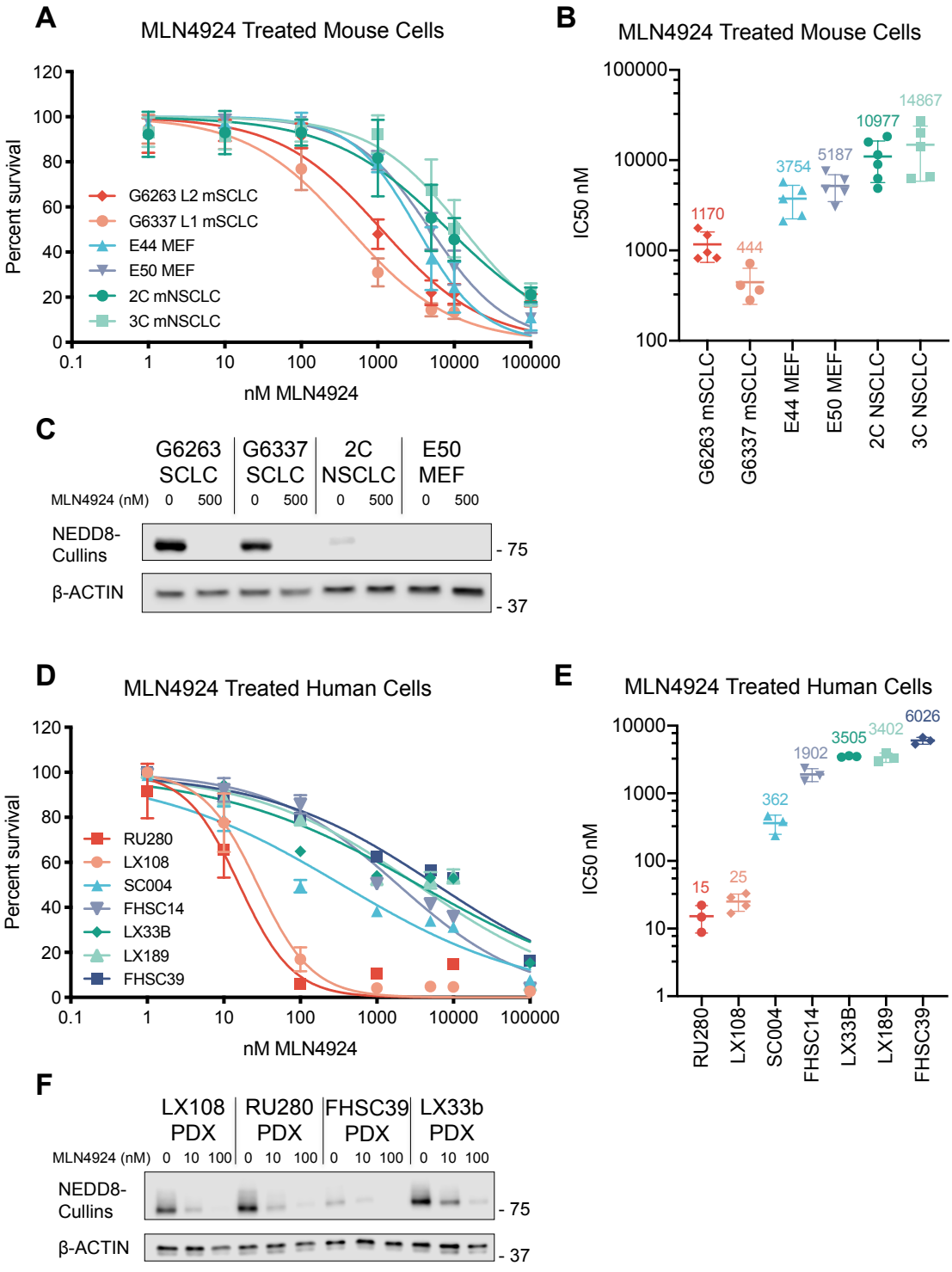
A
MLN4924 Treated Mouse Cells
Percent survival
nM MLN4924
G6263 L2 mSCLC
G6337 L1 mSCLC
E44 MEF
E50 MEF
2C mNSCLC
3C mNSCLC
B
MLN4924 Treated Mouse Cells
IC50 nM
1170
444
3754
5187
10977
14867
G6263 mSCLC
G6337 mSCLC
E44 MEF
E50 MEF
2C NSCLC
3C NSCLC
C
G6263 SCLC
G6337 SCLC
2C NSCLC
E50 MEF
MLN4924 (nM) 0 500 0 500 0 500 0 500
NEDD8-Cullins
β-ACTIN
- 75
- 37
D
MLN4924 Treated Human Cells
Percent survival
nM MLN4924
RU280
LX108
SC004
FHSC14
LX33B
LX189
FHSC39
E
MLN4924 Treated Human Cells
IC50 nM
15
25
362
1902
3505
3402
6026
RU280
LX108
SC004
FHSC14
LX33B
LX189
FHSC39
F
LX108 PDX
RU280 PDX
FHSC39 PDX
LX33b PDX
MLN4924 (nM) 0 10 100 0 10 100 0 10 100 0 10 100
NEDD8-Cullins
β-ACTIN
- 75
- 37

Figure 2

Treatment with the neddylation pathway inhibitor MLN4924 in murine SCLC cell lines and human PDX SCLC models:

A. Combined drug response curve for MLN4924 of murine $Rb^{lox/lox}$; $p53^{lox/lox}$ SCLC, $p53^{null}$ MEF, and $p53^{lox/lox}$; $KRAS^{K251D}$ NSCLC cell lines. Cell viability measured at 72 hours by CellTiter Glo.

B. Graph depicting experimental MLN4924 IC50 value replicates for mSCLC, MEF, and mNSCLC cell lines.

C. Western blot results for mSCLC, mNSCLC and MEF cell lines. Lines were collected after a 48 hour treatment of MLN4924 at two concentrations (0 nM and 500 nM).

D. Combined drug response curve for MLN4924 of human ex vivo PDX SCLC models. Cell viability measured at 72 hours by CellTiter Glo.

E. Graph depicting experimental MLN4924 IC50 value replicates for human PDX lines.

F. Western blot results for MLN4924-sensitive PDX models LX108 and RU280, and more resistant PDX models FHSC39 and LX33b. Lines were collected after a 48 hour treatment of MLN4924 at three concentrations (0 nM, 10 nM, 100 nM).

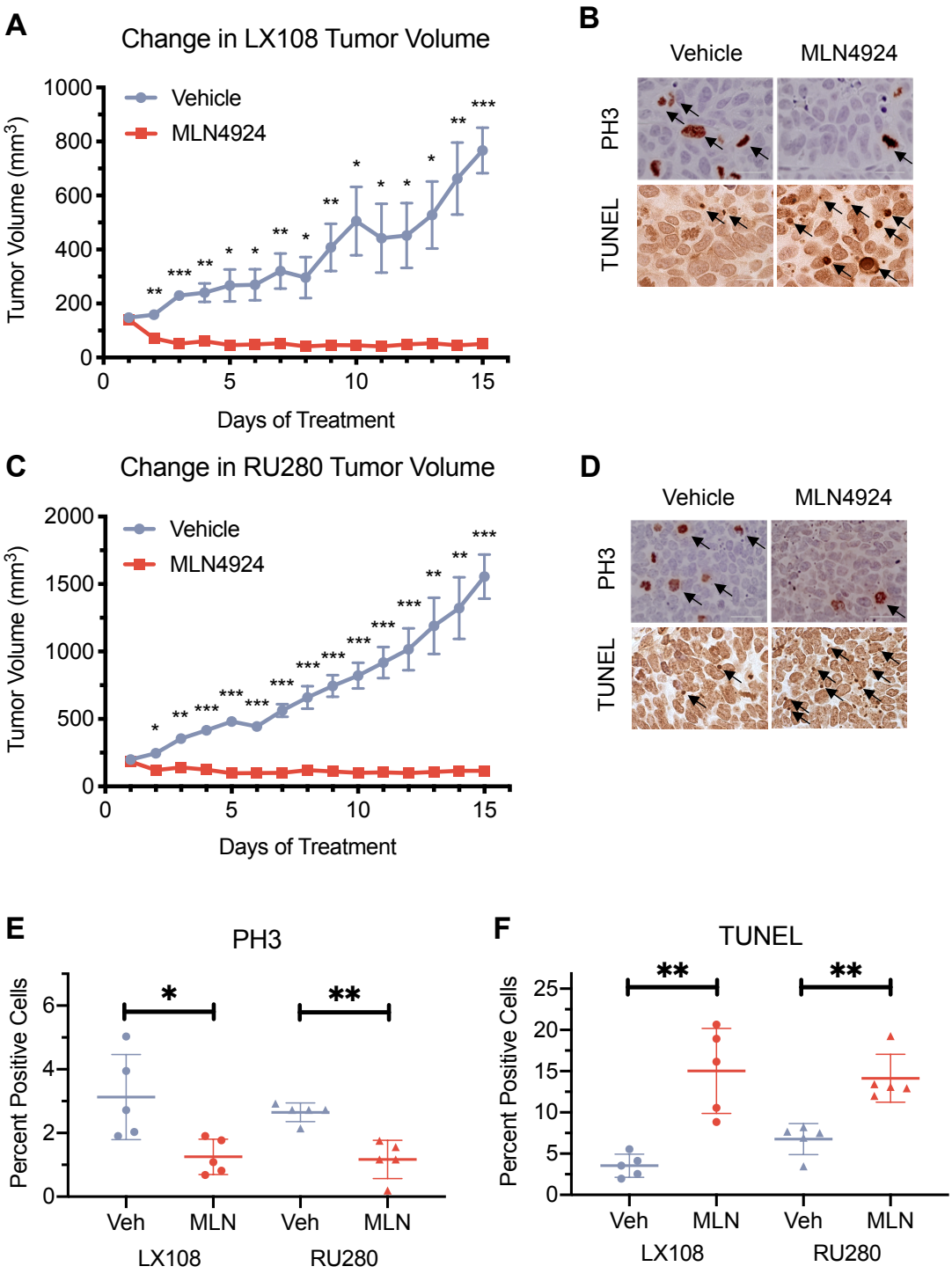
A
Change in LX108 Tumor Volume
Vehicle
MLN4924
Tumor Volume (mm3)
Days of Treatment
B
Vehicle
MLN4924
PH3
TUNEL
C
Change in RU280 Tumor Volume
Vehicle
MLN4924
Tumor Volume (mm3)
Days of Treatment
D
Vehicle
MLN4924
PH3
TUNEL
E
PH3
Percent Positive Cells
Veh
MLN
Veh
MLN
LX108
RU280
F
TUNEL
Percent Positive Cells
Veh
MLN
Veh
MLN
LX108
RU280

Figure 3

MLN4924 treatment of PDX models in vivo:

A. Tumor growth inhibition curves of 5 vehicle (HPBCD) and 5 MLN4924 (60 mg/kg, 7dpw) treated LX108 PDX flank tumors over 15 days. * Indicates $p < .05$, ** indicates $p < .01$, *** indicates $p < .001$.

B. Representative IHC images for PH3 and TUNEL in treated LX108 tumors. Scale bar, 100 um.

C. Tumor growth inhibition curves of 5 vehicle (HPBCD) and 5 MLN4924 (60 mg/kg, 7dpw) treated RU280 PDX flank tumors over 15 days. * Indicates $p < .05$, ** indicates $p < .01$, *** indicates $p < .001$.

D. Representative IHC images for PH3 and TUNEL in treated RU280 tumors. Scale bar, 100 um.

E. Quantification of 5 representative PH3 IHC field images for each of the 5 MLN4924 and 5 Vehicle treated LX108 or RU280 tumors.

F. Quantification of 5 representative TUNEL IHC field images for each of the 5 MLN4924 and 5 Vehicle treated LX108 or RU280 tumors. IHC Quantifications for **E, F:** * Indicates $p < .05$, ** indicates $p < .01$, *** indicates $p < .001$.

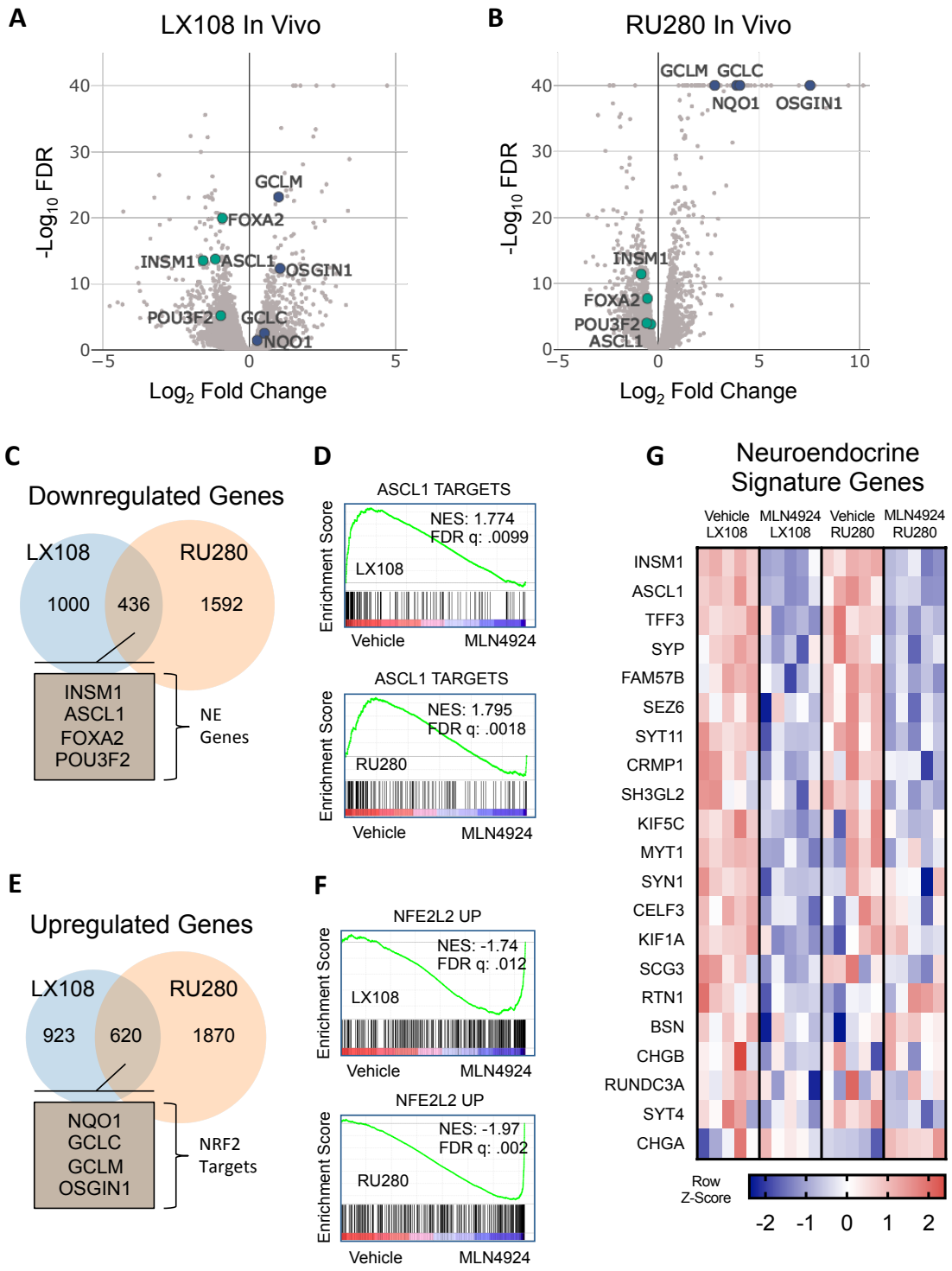
A
LX108 In Vivo
-Log10 FDR
Log2 Fold Change
GCLM
FOXA2
INSM1
ASCL1
OSGIN1
POU3F2
GCLC
NQO1
B
RU280 In Vivo
GCLM
GCLC
NQO1
OSGIN1
INSM1
FOXA2
POU3F2
ASCL1
C
Downregulated Genes
LX108
RU280
1000
436
1592
INSM1
ASCL1
FOXA2
POU3F2
NE Genes
D
ASCL1 TARGETS
NES: 1.774
FDR q: .0099
LX108
Enrichment Score
Vehicle
MLN4924
ASCL1 TARGETS
NES: 1.795
FDR q: .0018
RU280
E
Upregulated Genes
LX108
RU280
923
620
1870
NQO1
GCLC
GCLM
OSGIN1
NRF2 Targets
F
NFE2L2 UP
NES: -1.74
FDR q: .012
LX108
NFE2L2 UP
NES: -1.97
FDR q: .002
RU280
G
Neuroendocrine Signature Genes
Vehicle LX108
MLN4924 LX108
Vehicle RU280
MLN4924 RU280
INSM1
ASCL1
TFF3
SYP
FAM57B
SEZ6
SYT11
CRMP1
SH3GL2
KIF5C
MYT1
SYN1
CELF3
KIF1A
SCG3
RTN1
BSN
CHGB
RUNDC3A
SYT4
CHGA
Row Z-Score
-2
-1
0
1
2

Figure 4

Transcriptional analysis of MLN4924 treated tumors identify changes in neuroendocrine signature changes in SCLC:

A-B. Volcano plots of EdgeR analysis results from RNA-seq performed on 5 MLN4924 treated and 5 Vehicle treated LX108 **(A)** or RU280 **(B)** PDX SCLC tumors. Green markers indicate NE genes and blue dots indicate NRF2 targets.

C. Venn diagram of common significant downregulated genes (FDR <.05) through EdgeR analysis of MLN4924-sensitive LX108 and RU280 PDX models. Notable common genes in inset.

D. Gene set enrichment analysis plots for treated LX108 (top) and RU280 (bottom) tumors using list of identified direct targets of ASCL1 in SCLC.

E. Venn diagram of common significant upregulated genes (FDR <.05) through EdgeR analysis of MLN4924-sensitive LX108 and RU280 PDX models. Notable common genes in inset.

F. Gene set enrichment analysis plots for treated LX108 (top) and RU280 (bottom) tumors using list of NRF2 targets.

G. Heat map of expressed neuroendocrine signature genes of treated LX108 or RU280 in vivo PDX models compared to vehicle controls. Color indicates z-score for within each 5x5 comparison.

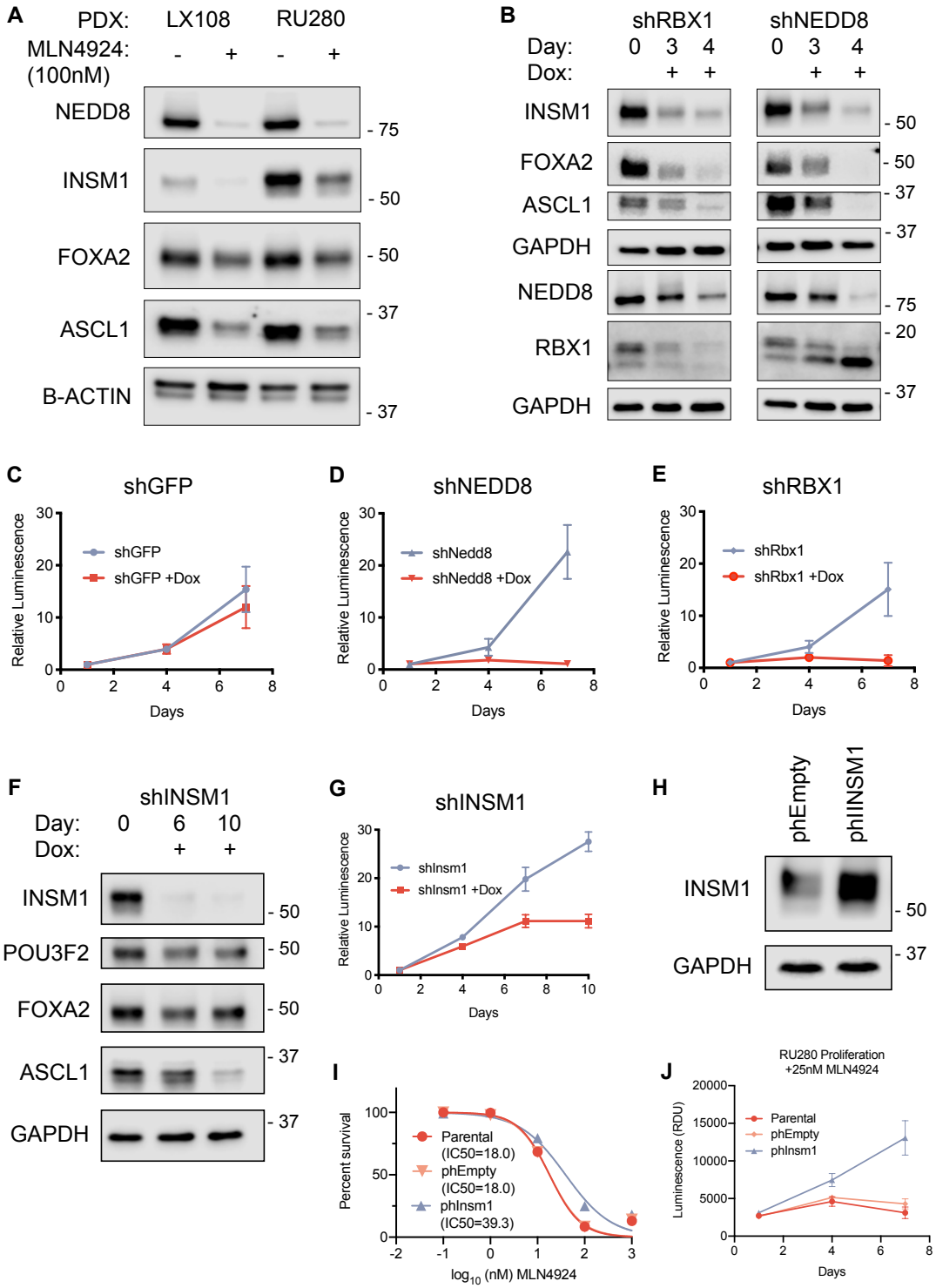
A
PDX:
LX108
RU280
MLN4924:
(100nM)
- + - +
NEDD8
INSM1
FOXA2
ASCL1
B-ACTIN
- 75
- 50
- 50
- 37
- 37
B
shRBX1
shNEDD8
Day:
Dox:
0 3 4
0 3 4
+ +
+ +
INSM1
FOXA2
ASCL1
GAPDH
NEDD8
RBX1
GAPDH
- 50
- 50
- 37
- 37
- 75
- 20
- 37
C
shGFP
Relative Luminescence
shGFP
shGFP +Dox
Days
D
shNEDD8
Relative Luminescence
shNedd8
shNedd8 +Dox
Days
E
shRBX1
Relative Luminescence
shRbx1
shRbx1 +Dox
Days
F
shINSM1
Day:
Dox:
0 6 10
+ +
INSM1
POU3F2
FOXA2
ASCL1
GAPDH
- 50
- 50
- 50
- 37
- 37
G
shINSM1
Relative Luminescence
shInsm1
shInsm1 +Dox
Days
H
phEmpty
phINSM1
INSM1
GAPDH
- 50
- 37
I
Percent survival
Parental
(IC50=18.0)
phEmpty
(IC50=18.0)
phInsm1
(IC50=39.3)
log10 (nM) MLN4924
J
RU280 Proliferation
+25nM MLN4924
Luminescence (RDU)
Parental
phEmpty
phInsm1
Days

Figure 5

Perturbation of the neddylation pathway disrupts the neuroendocrine signature in SCLC

A. Western blot of MLN4924 sensitive ex vivo PDX models LX108 and RU280. Cells were treated for 48 hours with 100 nM MLN4924 or DMSO.

B. Western blot of lentiviral infected inducible hairpins for RBX1 or NEDD8 in the PDX SCLC model RU280. Samples were supplemented with 1 ug/mL doxycycline and collected at day 0, 3, and 4.

C-E. Proliferation assay results comparing on-dox and off-dox RU280 shGFP (**C**), shNEDD8 (**D**), or shRBX1 (**E**) knockdown cell lines. Samples were assayed at day 1, 4, and 7 with readout determined by CellTiter Glo.

F. Western blot of lentiviral infected inducible hairpin for INSM1 in RU280. Samples were supplemented with 1 ug/mL doxycycline and collected at day 0, 6, and 10.

G. Proliferation assay results comparing on-dox and off-dox RU280 shINSM1 knockdown cells. Samples were assayed at day 1, 4, 7, and 10 with readout determined by CellTiter Glo.

H. Western blot of RU280 cells constitutively overexpressing INSM1 (phINSM1) or an empty vector control (phEmpty).

I. IC50 results of 72 hour treatment with MLN4924 in RU280 parental, empty vector, or INSM1 overexpression cells.

J. Proliferation results of RU280 overexpression lines. Proliferation results of overexpression lines cultured with 25 nM of MLN4924. Samples were assayed at day 1, 4, 7. Readout was measured by average luminescence value using CellTiterGlo.

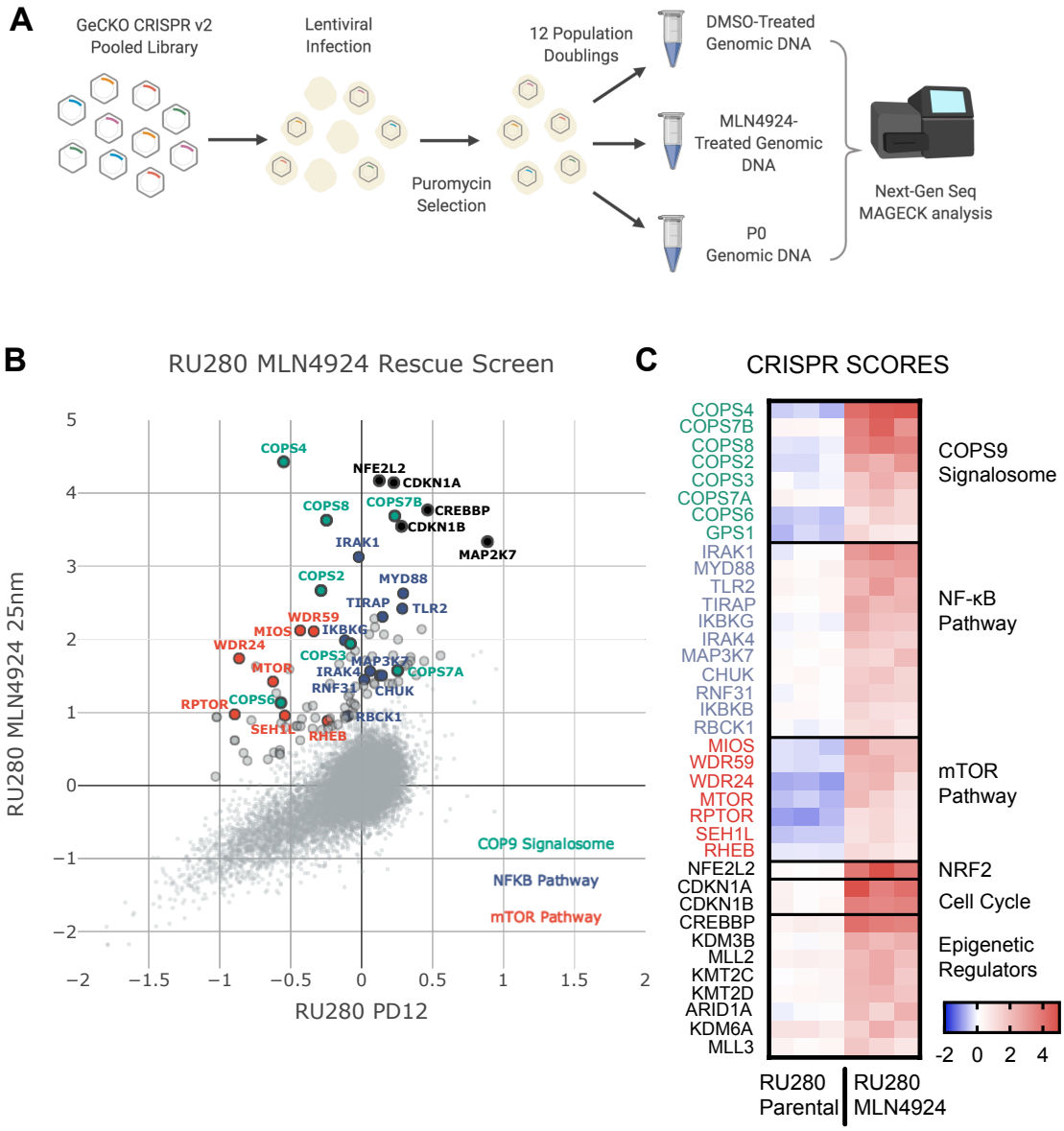

Figure 6

Whole genome CRISPR Suppressor Screen of MLN4924-treated RU280 cells identifies the NF- κB and mTOR pathways as potential mechanisms of sensitivity and resistance

A. Flowchart of the CRISPR/Cas9 inactivation screen conducted using the Gecko v2 lentiviral human library (131,867 total guides, 6 guides per gene). Cells were infected at approximately .3 MOI and to ensure 500 fold sequencing coverage.

B. X,Y plot of average CRISPR scores for the RU280 MLN4924 25nM and RU280 population doubling 12 (PD12) DMSO data sets.

C. Heat map of top enrichment CRISPR scores organized by pathways of 3 RU280 PD12 replicates and 3 RU280 MLN4924 25nM replicates.

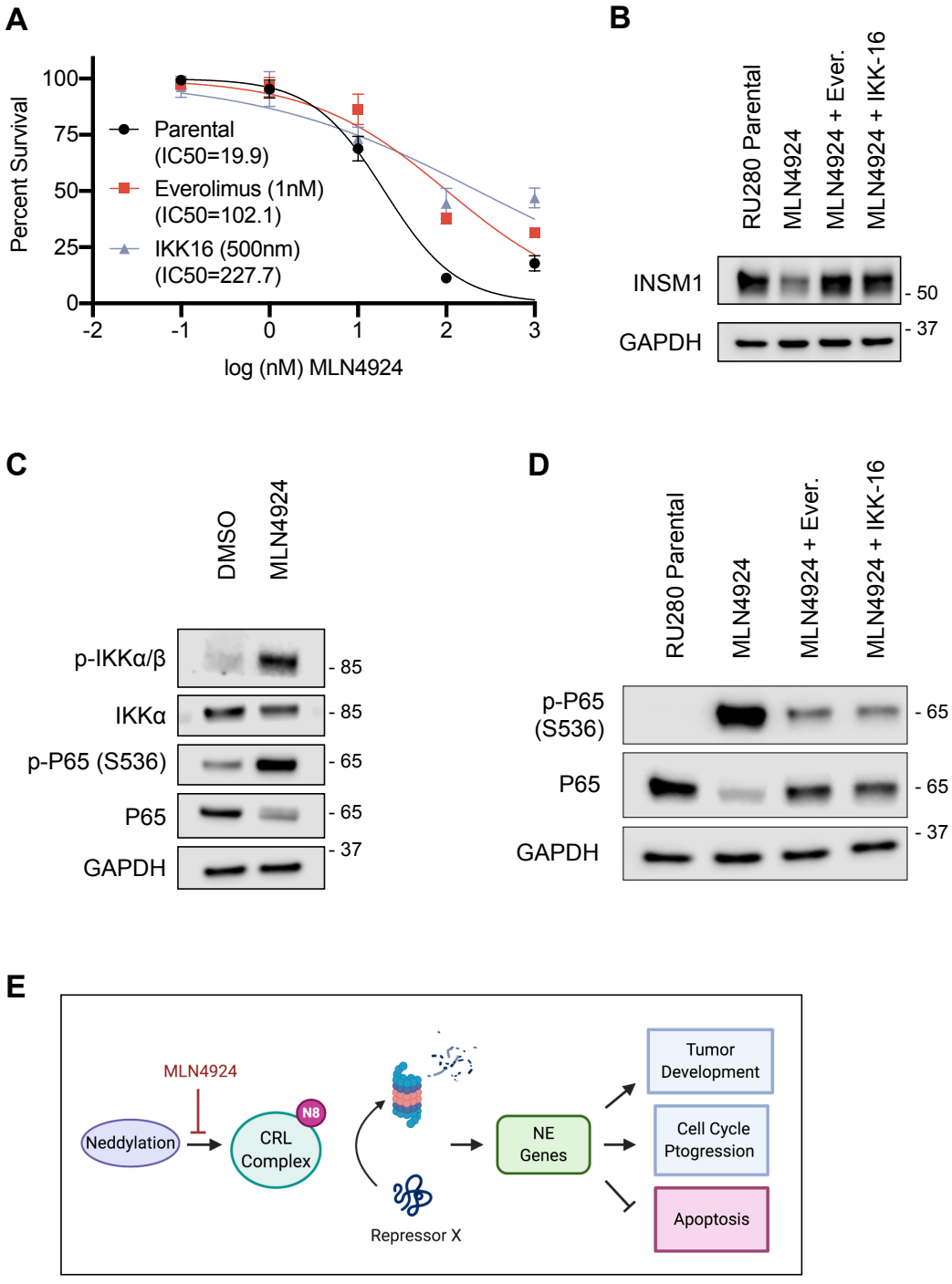
A
Percent Survival
100
75
50
25
0
-2
-1
0
1
2
3
log (nM) MLN4924
Parental
(IC50=19.9)
Everolimus (1nM)
(IC50=102.1)
IKK16 (500nm)
(IC50=227.7)
B
RU280 Parental
MLN4924
MLN4924 + Ever.
MLN4924 + IKK-16
INSM1
GAPDH
- 50
- 37
C
DMSO
MLN4924
p-IKKα/β
IKKα
p-P65 (S536)
P65
GAPDH
- 85
- 85
- 65
- 65
- 37
D
RU280 Parental
MLN4924
MLN4924 + Ever.
MLN4924 + IKK-16
p-P65
(S536)
P65
GAPDH
- 65
- 65
- 37
E
MLN4924
Neddylation
CRL
Complex
N8
Repressor X
NE
Genes
Tumor
Development
Cell Cycle
Ptogression
Apoptosis

Figure 7

Abrogation of the NF-κB and mTOR pathway provides resistance to the effects of MLN4924 on SCLC

A. IC50 results of 72 hour treatment with MLN4924 of RU280 parental, 1 nM Everolimus, or 500 nM IKK-16. Cells were treated with DMSO, Everolimus, or IKK-16 for 24 hours prior to start of IC50 assay.

B. Western blot analysis of INSM1 for RU280 parental, 25 nm MLN4924, 1 nM Everolimus plus 25 nM MLN4924, or 500 nM IKK-16 plus 25 nM MLN4924 cell lines. Cells were treated with Everolimus or IKK-16 for 24 hours prior to addition of MLN4924. Samples were collected after 96 hours of MLN4924 co-treatment.

C. Western blot analysis of NF-κB members in RU280 ex vivo cells treated with 100 nM treated for 48 hours.

D. Western blot analysis for the NF-κB transcription factor p65. Samples were prepared as in **(B).**

E. Proposed model of neddylation regulation of neuroendocrine signature, proliferation and apoptosis in SCLC.

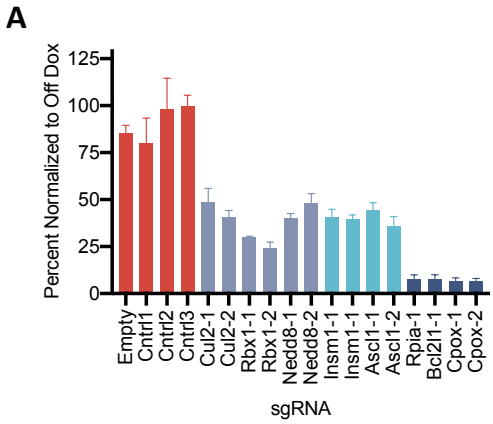

Figure S1

Validation of select sgRNAs

A. Validation of individual guides from our RP mSCLC data set using the G6263 mSCLC line. Bar amplitude represents percentage of on-dox condition cells to the off-dox condition cells at day 10. Samples were supplemented with 1 ug/mL doxycycline every other day. Readout was determined using CellTiterGlo.

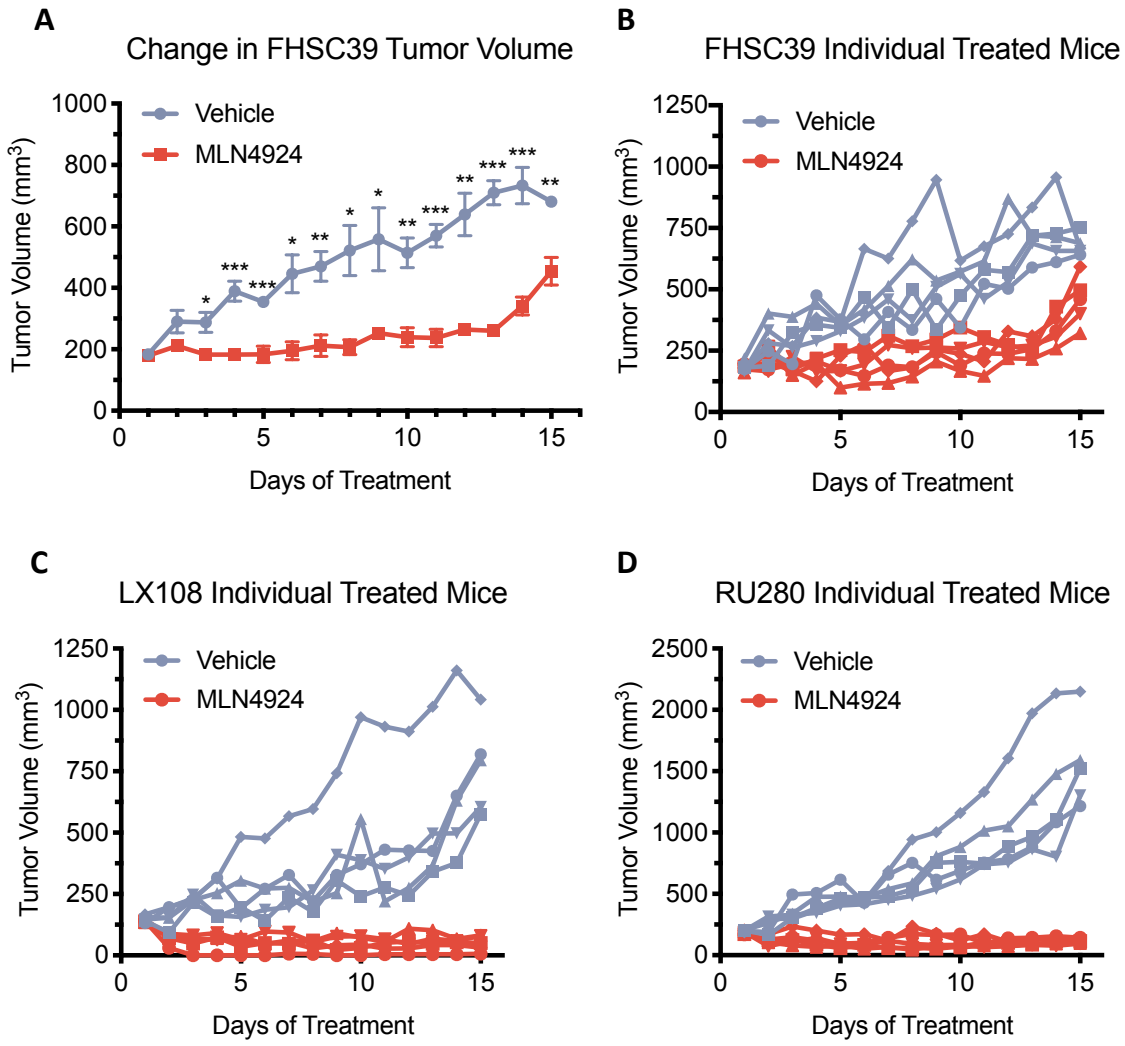

Figure S2

MLN4924 treatment of a non-sensitive PDX model in vivo:

A. Tumor growth inhibition curves of 5 vehicle (HPBCD) and 5 MLN4924 (60 mg/kg, 7dpw) treated FHSC39 PDX flank tumors over 15 days. * Indicates $p < .05$, ** indicates $p < .01$, *** indicates $p < .001$.

B-D. Tumor growth curves of individual mice treated with MLN4924 or vehicle in the FHSC39 (**B**), LX108 (**C**), and RU280 (**D**) PDX models.

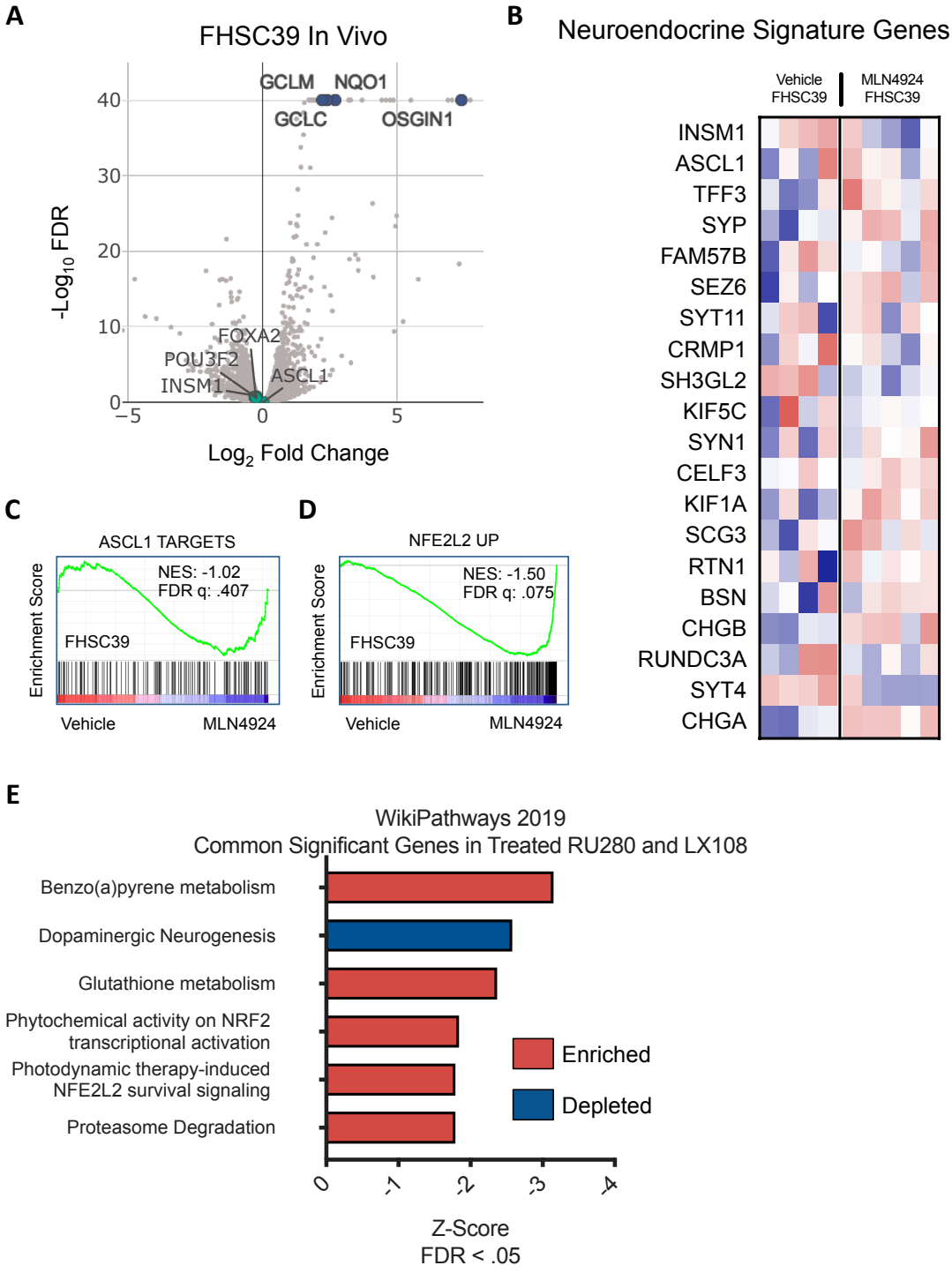
A
FHSC39 In Vivo
GCLM
NQO1
GCLC
OSGIN1
FOXA2
POU3F2
INSM1
ASCL1
-Log10 FDR
Log2 Fold Change
B
Neuroendocrine Signature Genes
Vehicle FHSC39
MLN4924 FHSC39
INSM1
ASCL1
TFF3
SYP
FAM57B
SEZ6
SYT11
CRMP1
SH3GL2
KIF5C
SYN1
CELF3
KIF1A
SCG3
RTN1
BSN
CHGB
RUNDC3A
SYT4
CHGA
C
ASCL1 TARGETS
NES: -1.02
FDR q: .407
FHSC39
Enrichment Score
Vehicle
MLN4924
D
NFE2L2 UP
NES: -1.50
FDR q: .075
FHSC39
Enrichment Score
Vehicle
MLN4924
E
WikiPathways 2019
Common Significant Genes in Treated RU280 and LX108
Benzo(a)pyrene metabolism
Dopaminergic Neurogenesis
Glutathione metabolism
Phytochemical activity on NRF2 transcriptional activation
Photodynamic therapy-induced NFE2L2 survival signaling
Proteasome Degradation
Enriched
Depleted
Z-Score
FDR < .05

Figure S3

Transcriptional analysis of MLN4924-treated tumors in SCLC

A. Volcano plot of EdgeR analysis results from RNA-seq performed on 5 MLN4924 treated and 4 Vehicle (HPBCD) treated FHSC39 PDX SCLC tumors. Green markers indicate NE genes and blue dots indicate NRF2 targets.

B. Heat map of expressed neuroendocrine signature genes of treated FHSC39 in vivo PDX models compared to vehicle controls. Color indicates z-score for within 4x5 comparison.

C. Gene set enrichment analysis plots for treated FHSC39 tumors using list of identified direct targets of ASCL1 in SCLC.

D. Gene set enrichment analysis plots for treated FHSC39 tumors using list of NRF2 targets.

E. Enrichr pathway analysis of common genes significantly downregulated or upregulated in treated LX108 and RU280 tumors. Pathways displayed have an FDR <.05 using the WikiPathways 2019 database.

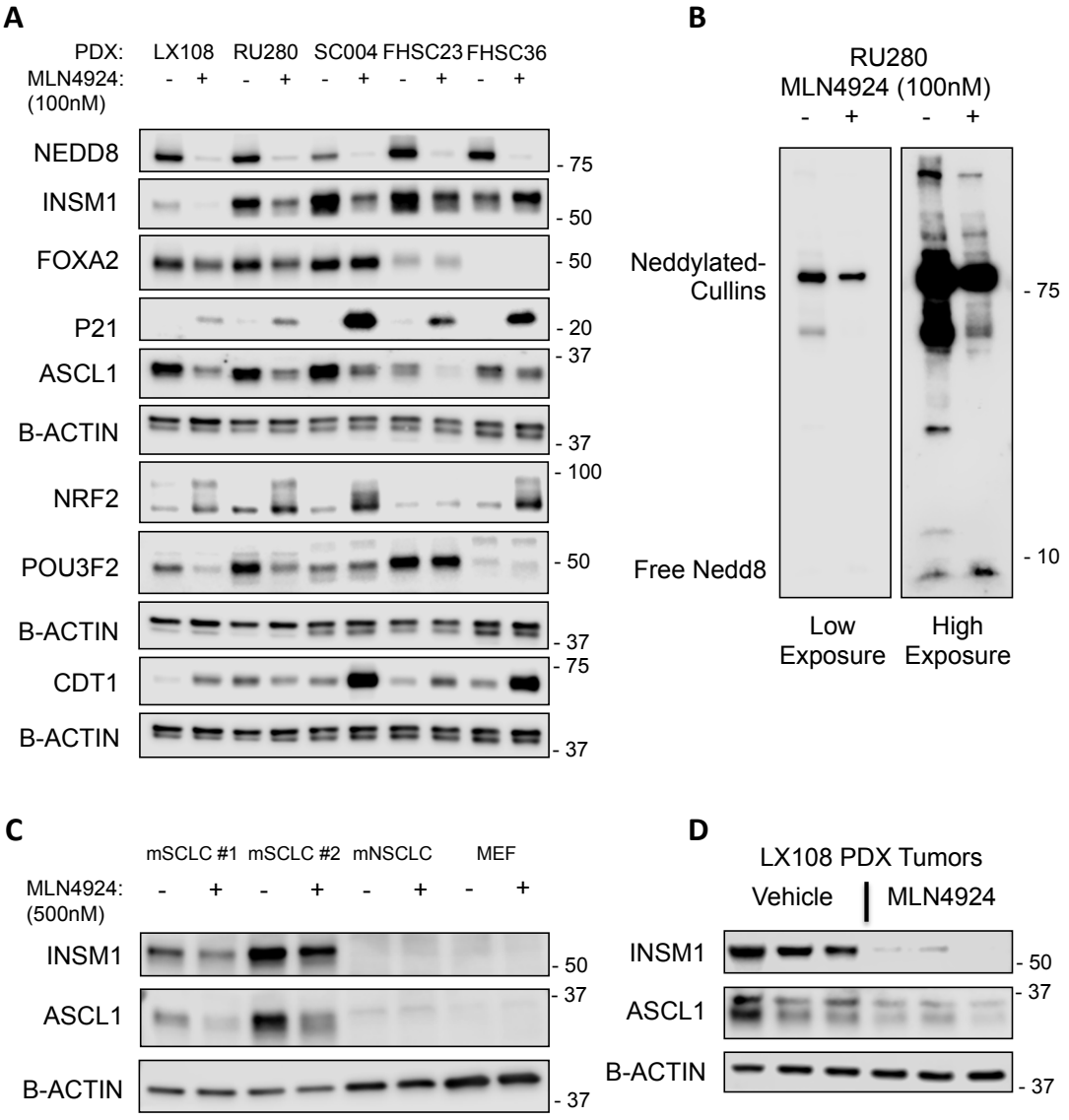

Figure S4

MLN4924 downregulates neuroendocrine genes in SCLC

A. Western blot of MLN4924-treated SCLC PDX models. Cells were treated for 48 hours with DMSO or 100 nM of MLN4924.

B. Western blot of anti-NEDD8 for the sensitive PDX model RU280. Cells were treated with DMSO or 100 nM of MLN4924 for 48 hours.

C. Western blot of treated mSCLC (G6263 and G6337 lines), mNSCLC (2C), and MEF (E50) cells. Cells were treated with DMSO or 500 nM of MLN4924 for 48 hours.

D. Western blot of extracted LX108 PDX model flank tumors treated with vehicle or MLN4924 over 15 days.

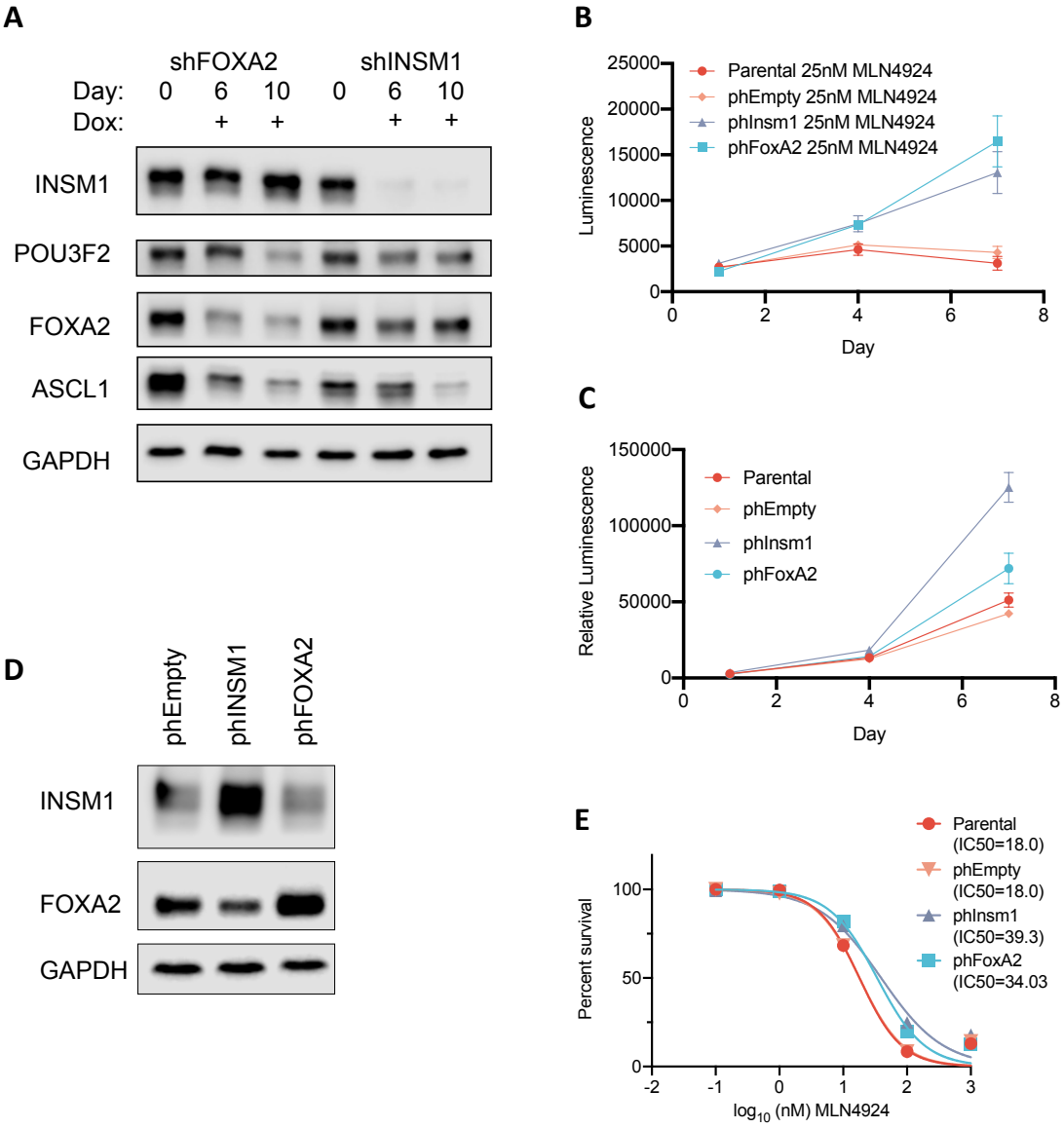

Figure S5

Genetic perturbation of the neddylation pathway downregulates neuroendocrine genes in SCLC

A. Western blot of lentiviral infected inducible hairpins for FOXA2 and INSM1 in the PDX SCLC model RU280. Samples were supplemented with 1 ug/mL doxycycline and collected at day 0, 6, and 10.

B-C. Proliferation results of RU280 parental , empty vector (phEmpty), INSM1 (phINSM1), or FOXA2 (phFOXA2) overexpression lines. Cells were supplemented with either 25 nM of MLN4924 (**B**) or DMSO (**C**). Cell viability was assayed on day 1, 4, and 7. Readout was determined by CellTiter Glo.

D. Western blot of RU280 cells constitutively overexpressing empty vector (phEmpty), INSM1 (phINSM1), or FOXA2 (phFOXA2).

E. IC50 results of 72 hour treatment with MLN4924 of RU280 parental, phEmpty, phFOXA2, or phINSM1 overexpression cells.

A

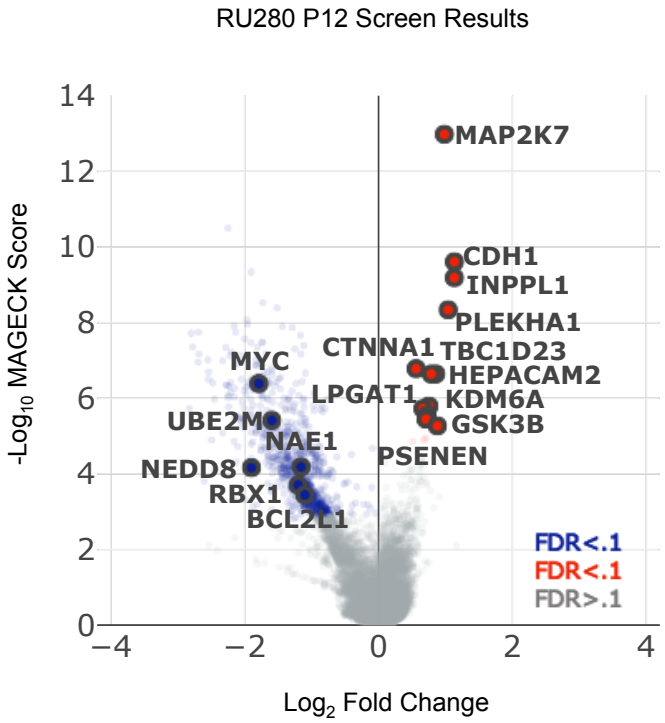

B

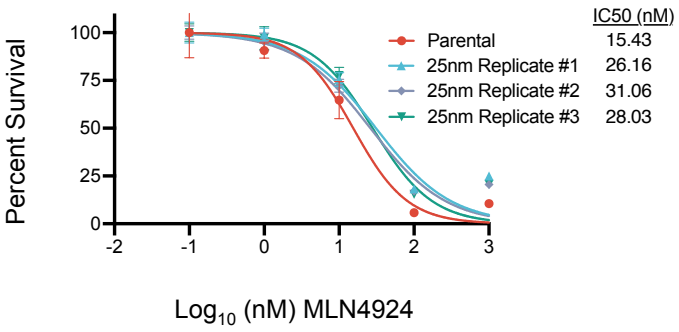

Figure S6

A. Volcano plots of MAGeCK analysis results from 3 screened RU280 replicates treated with DMSO and collected after 12 population doublings.

B. IC50 results of 72 hour treatment with MLN4924 for each of the 3 polyclonal RU280 25 nM MLN4924 screen replicates after conclusion of CRISPR/Cas9 screen.

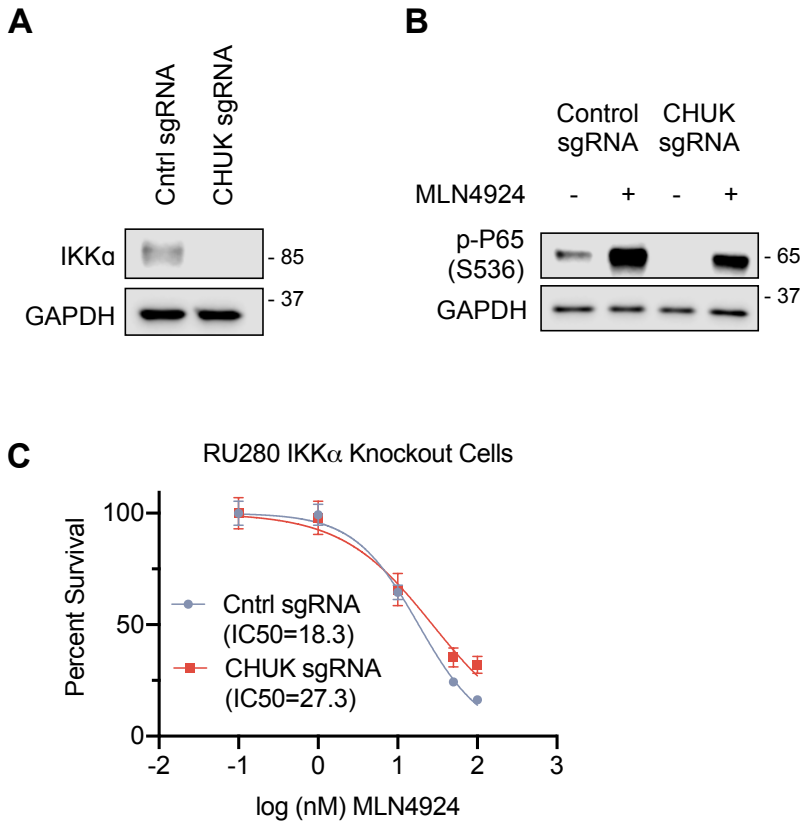

Figure S7

Genetic perturbation of the NF-κB pathway provides resistance to the effects of MLN4924 on SCLC

A. Western blot validation of IKKalpha knockout cells in the RU280 cell line.

B Western blot analysis of phospho-P65 levels in RU280 ex vivo cells infected with a control sgRNA or CHUK sgRNA. Cells were treated with DMSO or 25 nM MLN4924 for 96 hours.

C. IC50 results of 72 hour treatment with MLN4924 of RU280 Control sgRNA and CHUK sgRNA cells.

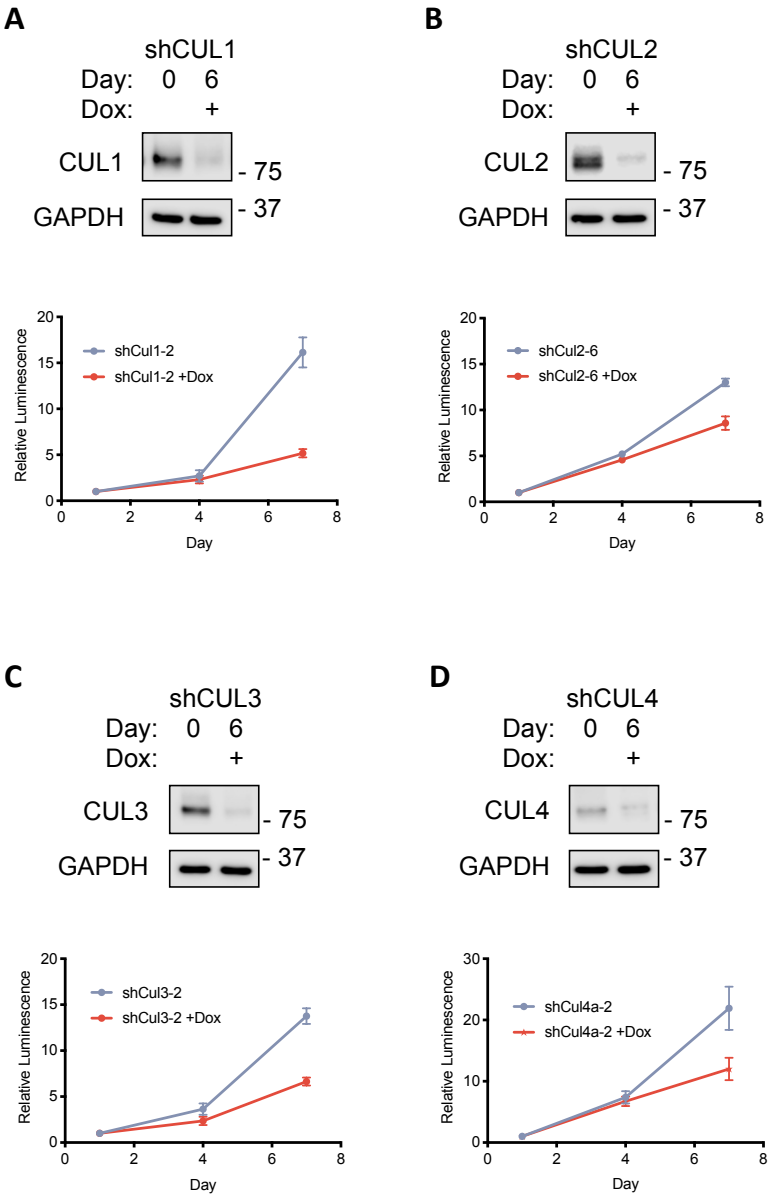

Additional Figure S8

Knockdown of Cullin genes in SCLC

A-D. Western blot of lentiviral infected inducible hairpins for Cullin family members in the PDX SCLC model RU280. Samples were supplemented with 1 ug/mL doxycycline and collected at day 0 and day 6. Corresponding proliferation assay results comparing on-dox and off-dox RU280 shCUL1 (**A**), shCUL2 (**B**), shCUL3 (**C**), or shCUL4 (**D**) knockdown cell lines. Samples were assayed at day 1, 4, and 7 with readout determined by CellTiter Glo.

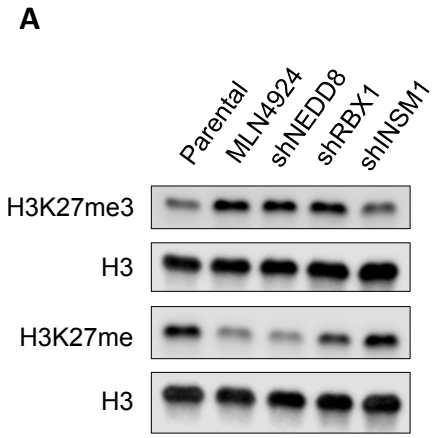

Additional Figure S9

Changes in H3K27me3 in neddylation-inhibited SCLC

A. Western blot of histone extracts for RU280 knockdown cells. Samples for parental, MLN4924, shNEDD8, shRBX1, and shINSM1 RU280 cells. MLN4924 was added at 25 nM for 96 hours. Knockdown cells were supplemented with 1 ug/mL doxycycline and collected at day 6.

Chapter 2: Effects of Neddylation Inhibition in SCLC

2.1 The Role of CRL Complexes in SCLC

Neddylation largely promotes the activation of Cullin-RING complexes. Once activated, these complexes facilitate the ubiquitin-mediated degradation of target proteins (Chiba and Tanaka, 2004). In accessing potential mechanisms, we had hoped to identify relevant overabundant target proteins by characterizing treated tumors and cells for protein expression levels of canonical CRL substrates, but we were unable to tie the presence of any one substrate to our exceptional responding PDX models. Despite those results, this section will focus on individual CRL complexes, their targets, and their potential involvement in our observed MLN4924-mediated phenotype. The canonical CRL1 complex comprises CUL1, either one of the E3 RING enzymes, an adaptor protein named SKP1, and a receptor protein from the F-box family (Jin et al., 2004). We note that one important receptor protein, SKP2, has been implicated in the tumorigenesis of SCLC, but did not become depleted in our screens (Yokoi et al., 2003). Interestingly, two of the most studied substrates are p21 and p27 (Chen et al., 2008); proteins for which we observed increased expression throughout most of our sensitive and resistant PDX models. Inactivation of these cell cycle regulators did cause enrichment in our suppressor screen, but further investigation is warranted to determine if their expression is selectively functionally relevant. Next, the canonical CRL2 complex consists of CUL2, RBX1, Elongin B, Elongin C, and the receptor protein VHL (Zhao et al., 2014). Despite the high significance of CUL2, ELOB, and ELOC in our screen results, VHL was not identified as significantly depleted. We are still interrogating other CUL2 adaptors for their functional effects. As CRL2 substrates have not been well

studied beyond HIF1alpha (Ivan et al., 2001), it is possible that an undetermined receptor and substrate provide functional relevance in SCLC.

Canonically, the CRL3 complex is formed from CUL3, RBX1, and a substrate receptor protein from the BTB (Bric-a-brac, Tramtrack, Broad-complex domain) protein family (Chen et al., 2015b). Numerous studies involving CRL3 focus on the BTB protein member KEAP1, its substrate NRF2, and their role in regulating antioxidants and oxidative stress (Chen et al., 2015b). The CRL3 complex functions as a tumor suppressor in numerous tumor types, including KEAP1 mutant NSCLC (Singh et al., 2006). NRF2 scores highly in our suppressor screen, and is transcriptionally active in both our MLN4924-sensitivie and resistant PDX models. Similar to the status of p21 and p27, further investigation is warranted to determine if NRF2 expression is functionally relevant in only our sensitive models. Next, CUL4 has two isoforms that compose CRL4A and CRL4B. The two CRL4 complexes contain DDB1 and a DCAF family member protein (Zhao et al., 2014). The most well studied CRL4-target protein, CDT1, can cause DNA re-replication when not properly degraded (Lin et al., 2010). CDT1 protein levels do not consistently increase in our sensitive models and CDT1 fails to enrich in our suppressor screen. CRL4 complex members also do not become significantly depleted in our inactivation screen. Lastly, the CRL5 complex most commonly uses the RBX2 E3 ubiquitin ligase and the BC Box adaptor proteins, but can also associate with RBX1 (Heuze et al., 2005), (Kamura et al., 2001), (Wei and Sun, 2010). The receptor proteins of the CRL5 complex have not been as well characterized as other CRL complexes. Studies have focused on the suppressor of cytokine signaling

(SOCS) adaptor proteins and the complex's ability to promote degradation of Src (Laszlo and Cooper, 2009), (Pan et al., 2011). Our screen results indicate that CRL5 is an unlikely contributor to the observed MLN4924 phenotype.

2.2 Inactivation of the COPS9 Signalosome Suppresses the Effects of MLN4924 in SCLC

To ascertain potential mechanisms of sensitivity and resistance in SCLC for MLN4924, we performed a suppressor screen with the MLN4924-sensitive PDX model RU280 using the genome-wide CRISPR/Cas9 GeCKO v2 library. This screen looked for genes that promoted survival concurrent with inhibition of the neddylation pathway. We identified numerous intriguing genes and pathways in our results. The enrichment results included the COPS9 Signalosome (CSN). This multiunit complex's main function is to deneddylate substrates, most notably cullin-RING ubiquitin ligases (Lyapina et al., 2001), (Petroski and Deshaies, 2005). The signalosome comprises the 8 subunits of COPS1, COPS2, COPS3, COPS4, COPS5, COPS6, COPS7, and COPS8 (Henke et al., 1999), (Glickman et al., 1998) (See Figure B). COPS7 has functionally redundant isoforms COPS7A and COPS7B that typically act in a cell-specific manner (Olma et al., 2009). Our data shows a stronger enrichment for COPS7B, suggesting a potential SCLC specificity for that isoform. We postulate that the knockout of these CSN genes prevent the proper localization and function of the complex, preventing CRL complexes and other neddylated proteins from becoming deneddylated, essentially freezing them in an active state. This theory can be tested through analysis of neddylated protein levels upon inactivation of CSN members.

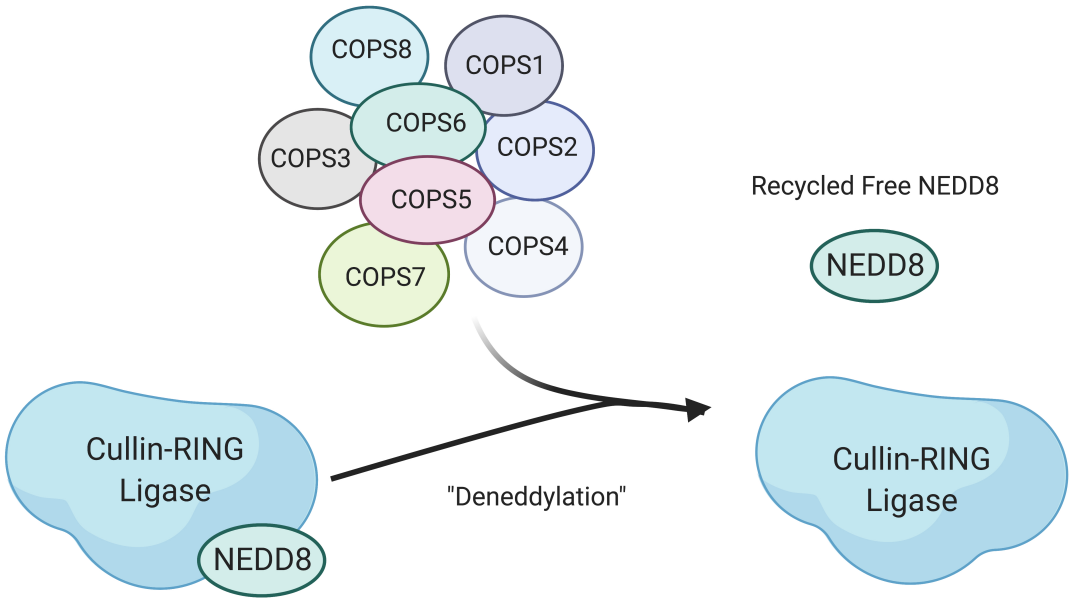

Figure B: COPS9 Signalosome

2.3 Inactivation of the mTOR Pathway Suppresses the Effects of MLN4924 in SCLC

We identified numerous genes in the mTOR pathway as enriched in our suppressor screen replicates treated with MLN4924. Our results point to inactivation of the mTOR pathway mitigating the effects of neddylation inhibition in SCLC. Tumors with inactivating mutations in mTOR could provide a resistance mechanism to MLN4924 therapy. The mechanistic target of rapamycin (mTOR) pathway regulates anabolic processes like protein synthesis, metabolism, growth and proliferation (Inoki et al., 2005). The pathway is activated in response to signaling cascades caused by amino

acids, metabolites, as well as oxygen and energy levels (Kim and Guan, 2019). The mechanism in how mTOR inhibition functionally provides resistance to MLN4924 is unclear. One potential mechanism is that the accumulation of proteins due to neddylation inhibition can be mitigated by interruption of mTOR-regulated protein synthesis. In our suppressor screen results the mTORC1 members RPTOR, RHEB and mTOR show sgRNA enrichment in the MLN4924-treated cells (See Figure C). The mTOCR1 complex's major function is to promote protein translation through the phosphorylation of S6K and 4E-BP1 and the suppression of autophagy (Burnett et al., 1998), (Hay and Sonenberg, 2004), (Ganley et al., 2009), (Hosokawa et al., 2009). Interestingly, knockout of these genes, in addition to other mTORC1 related genes, are highly detrimental to the growth of untreated RU280 cells and suggest an obligate inhibition of neddylation for mTOR inactivation to be beneficial. Additional suppressor screen hits that show sgRNA enrichment in MLN4924 treated cells include MIOS, WDR59, WDR24, and SEH1L. These genes make up the GATOR2 complex, which functions to inhibit the GATOR1 complex, itself an inhibitor of mTORC1 (Bar-Peled et al., 2013), (Panchaud et al., 2013). Several studies focusing on variant SCLC have looked into the therapeutic role of mTOR inhibition (Huang et al., 2018a), (Chalishazar et al., 2019). These studies focus on mTOR inhibition as a therapeutic approach instead of the pro-survival phenotype we see in our treated cells. While mTOR has numerous crossplay interactions with other pathways, most notably the NF-KB pathway, we have yet to ascertain if there is a resistance mechanism specific to the inhibition of mTOR's downstream signaling. Future work will focus on characterizing this pathway using genetic and pharmacological approaches.

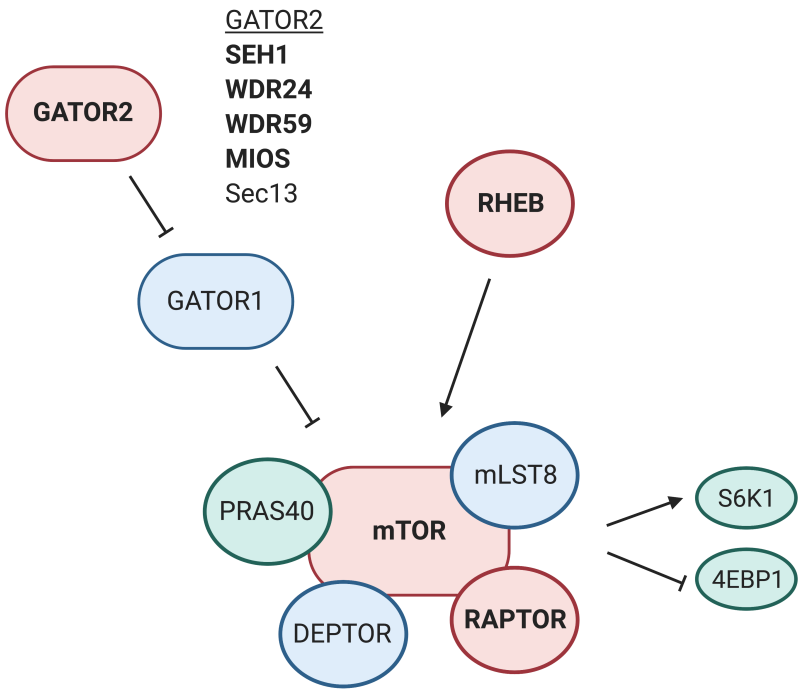

Figure C: mTOR Pathway

2.4 Inactivation of the NF-κB Pathway Suppresses the Effects of MLN4924 in SCLC

The NF-κB pathway is intertwined in nearly all cells types and is critical for immunity, growth, autophagy, and apoptosis (Karin and Greten, 2005). Downstream signaling is promoted by a family of NF-κB DNA-binding factors consisting of 5 differing dimers of RelA (p65), RelB, c-Rel, NFKB1, and NFKB2 (Karin, 2006),(Perkins, 2012). The inhibitors of NF-κB, named IKB proteins, sequester the dimers in the cytoplasm and prevent their nuclear translocation and function (Hayden and Ghosh, 2012), (Hinz et al., 2012). IKB proteins are targeted for degradation, which allows the activation and

translocation of the dimer. The inhibitory IKB proteins are phosphorylated by an IKB kinase, which targets the protein for degradation (Karin and Delhase, 2000). Our suppressor screen results show enrichment for genes (CHUK, IKBKB, IKBKG) that encode the IKK complex proteins (See Figure D). IKKalpha and IKKbeta function as the catalytic enzymes in the IKK complex while IKKgamma provides regulation and is required for the IKK complex activation of NF-κB (DiDonato et al., 1997), (Mercurio et al., 1997), (Zandi et al., 1997), (Yamaoka et al., 1998). Upstream of the IKK complex is the TAK1 kinase encoded by MAP3K7, a gene found enriched in our screen (Vidal et al., 2001), (Silverman et al., 2003). Interestingly, TAK1 and the IKK kinases can stimulate multiple enzyme cascades, for instance IKKbeta is known to phosphorylate TSC1 and activate downstream mTOR signaling (Lee et al., 2007). Upstream of TAK1 in the NF-κB pathway are a variety of ligands, adaptors, and kinases. Genes like IRAK1, IRAK4, TLR2, and MYD88 are all enriched in our suppressor screen.

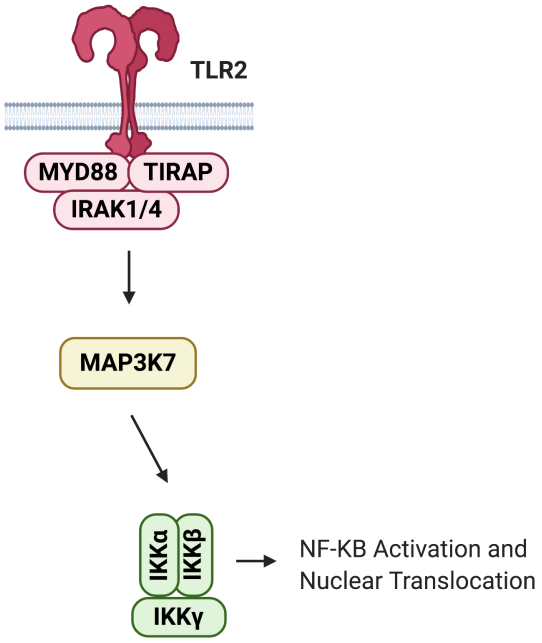

Figure D: NF-κB Pathway

We observed activation of the NF-κB pathway upon MLN4924 treatment in SCLC. Increased levels of phosphorylated IKK complex members implied downstream activation of NF-κB dimers. Indeed, we observed increased levels of phosphorylated p65 upon MLN4924 treatment, which also suggested activation of the NF-κB dimer. However, MLN4924 is known to inhibit the degradation of IKB through multiple CRL-dependent mechanisms, which potentially sequesters p65 despite its phosphorylation status (Milhollen et al., 2010), (Schweitzer et al., 2016), (Read et al., 2000). Investigation into the cellular localization of phosphorylated p65 is ongoing. We have yet to determine specific transcriptional consequences tied to p65 phosphorylation and further investigation is required. One potential mechanism could be through p65's interaction with an additional gene identified in our screen, CREBBP. This HAT-domain

containing enzyme becomes phosphorylated by IKK and can then acetylate p65, which causes binding specificity and activity changes for p65's transcriptional role (Hoberg et al., 2006), (Huang et al., 2007). Determination of whether the reduction in activated p65 is directly responsibly for MLN4924 resistance is still ongoing. Notably, activation of the canonical NF-κB pathway typically promotes cell survival and thus its role in MLN4924-treated SCLC may be incredibly unique. The search for a potential NF-κB mechanism that interacts with the regulation of NE genes is continuing.

2.5 The Histone Mark H3K27me3 in Neddylation-Inhibited SCLC

Histone modifications are a critical function for the epigenetic regulation of transcription in the cell (Bonasio et al., 2010). Histone tails undergo post-translational modifications (PTM) that can include phosphorylation, acetylation, ubiquitination, and methylation (Bannister and Kouzarides, 2011). Changes in histone PTMs can alter the chromatin structure and the expression of genes (Schuettengruber et al., 2017). One set of factors that modulates the chromatin structure through the silencing of genes is the polycomb complex family (Schuettengruber et al., 2017). The polycomb recessive complex PRC2 is comprised of the histone methyltransferase EZH2, EED, and SUZ12 (Kirmizis et al., 2004). This multiprotein complex represses transcription by promoting the trimethylation of histone H3 K27 (Bracken et al., 2006). EZH2 expression is connected with the maintenance of cell fates (Bracken and Helin, 2009), (Margueron and Reinberg, 2011) and has an oncogenic role in tumors including SCLC (Sato et al., 2013), (Coe et al., 2013). While pharmacological inhibition of EZH2 has shown some promise in reducing

SCLC growth (Sato et al., 2013), (Poirier et al., 2015), the identities of PRC2-repressed genes and their roles in SCLC are not well elucidated.

To potentially identify a broader mechanistic explanation for the downregulation of the NE signature upon neddylation inhibition, we looked at global histone post-translational modification differences. We performed histone extraction on untreated RU280 PDX cells, cells treated with MLN4924, and cells with knockdowns of NEDD8, RBX1, or INSM1. We looked at the levels of H3K27me3, a mark indicating transcriptionally repression, and the H3K27me1 mark that correlates with active transcription. Treatment of RU280 cells with MLN4924 results in an increased level of the repressive H3K27me3 mark (See Additional Fig. 9A). The H3K27me1 mark also decreases in expression level. These results suggest a global downregulation in active transcription upon inhibition of neddylation. Cells harboring knockdowns of NEDD8 or RBX1 replicate the effects of the small molecule. Both shNEDD8 and shRBX1 cells increased global levels of H3K27me3 comparably to MLN4924-treated cells. A control cell line featuring the knockdown of the NE transcription factor INSM1 resulted in no expression changes in histone marks compared with the untreated RU280 PDX cell line. In summation, we show a dramatic response in the methylation levels of H3K27 upon treatment of the RU280 PPDX model with MLN4924. The functional consequence of increased H3K27me3 levels has yet to be determined in the context of neddylation inhibition. If this epigenetic change is functionally consequential it would diverge from the current understanding of EZH2-promoted methylation as pro-oncogenic in SCLC. (See Chapter 4 for potential future experiments)

Chapter 3: Identification of Genes and Pathways as Therapeutic Targets in SCLC Through Use of CRISPR/Cas9 Screens

3.1 CRISPR SCLC Screens in the Literature

In the last two years, several studies sought to identify potential novel therapies for SCLC by way of screening technologies. A recent report from Huang et al. used a pooled sgRNA library targeting transcription factors to test a sampling of human SCLC cell lines (Huang et al., 2018b). Their system setup precluded screening of high-grade NE tumors expressing high ASCL1 levels and thus focused on variant SCLC cell lines. This screen identified a new novel variant SCLC subtype featuring expression of the POU2F3 gene, ultimately classified as SCLC-P. Expression of this gene denotes a subtype with a tuft cell lineage. This NE-low subtype expresses higher levels of TRPM5, SOX9, GFI1B, CHAT, ASCL2, and AVIL than other subtypes (SCLC-A and SCLC-N). Huang et al. also identified SOX4, NEUROD1, E2F3, and OTX2 as SCLC-specific dependencies. The authors note that these additional genes were already associated with SCLC (Cooper et al., 2006), (Parisi et al., 2007), (Castillo et al., 2012), (Osborne et al., 2013), (Christensen et al., 2014). In our mSCLC screen data set the mouse orthologs of the genes identified by Huang et al. are not significantly depleted, indicating the difference between their screened variant lines and the high-grade NE lines screened in our data. Additionally, a reported screen from Li et al. focused on autochthonous $Rb1^{lox/lox}$, $Trp53^{lox/lox}$ SCLC cell lines using a smaller, focused sgRNA library. The screen described the pyrimidine synthesis pathway as a SCLC specific-dependency (Li et al., 2019). Specifically, the Dhodh gene, a member of the pyrimidine metabolism pathway, was the top depleted gene. They contended that tumor types

other than SCLC could compensate for the inability to synthesize the pyrimidine base. In addition to the Dhodh gene, they also identified other pyrimidine synthesis pathway genes including Umps and Cad. Of the three 3 genes discussed in the Li et al. report, Cad was the sole gene found significant in our data set. Lastly, an additional report used a genome-wide sgRNA library to screen a single $Rb1^{lox/lox}$, $Trp53^{lox/lox}$, Mycl OE cell line (Nagel et al., 2019). This screen identified and focused on ATR and CHK1 as SCLC-specific targets. Nagel et al. showed etoposide and cisplatin treatment synergized with the inhibition of ATR or CHK1. We also identified these DDR pathway members as potential therapeutic targets in our mSCLC screen (See Chapter 3.2, Figure 1, and Supplementary Tables). Since Nagel and authors' whole genome screen focused on a single $Rb1^{lox/lox}$, $Trp53^{lox/lox}$, Mycl line, we believe our comprehensive screen of 5 mSCLC cell lines originating from Rb/p53 GEMMs lacking constitutive Mycl overexpression provides a distinct and more comprehensive data set. Our use of 5 independent cell lines isolated from separate mice increases the analysis power of our screen data.

3.2 Known SCLC Therapeutic Targets Identified in our CRISPR Screen

We performed whole genome CRISPR Cas9 inactivation screens on murine Rb/p53 deleted SCLC lines in an effort to identify new therapeutic targets for SCLC. We were encouraged to see orthologs of known candidate SCLC targets LMYC, ATR, CHEK1, and BCL2L1 due to their previous implications as SCLC targets. Inactivation of LMYC in the Rb/p53 SCLC mouse model decreases tumor burden and progression, but direct pharmacological targeting of LMYC remains remote (Kim et al., 2016). We also

identified the pro-survival BCL-2 family member BCL2L1 (BCLxL) in our screen. The anti-apoptotic BCL2 family members function by binding and sequestering pro-apoptotic proteins and preventing cell death (Chen et al., 2005). We identified the pro-apoptotic gene BCL2L11 as a potential SCLC tumor suppressor in our mSCLC screen. Another promising therapeutic area for SCLC involves targeting of the DNA damage response (DDR) pathway. Proteins in this pathway include ATR, CHEK1, PARP and WEE1 (Foy et al., 2017). Mouse orthologs of ATR and CHEK1 significantly become depleted in our screen. Many of these proteins are highly expressed in SCLC samples and inhibitors show promising results in preclinical studies (Byers et al., 2012), (Cardnell et al., 2013), (Sen et al., 2017a), (Sen et al., 2017b), (Doerr et al., 2017). The presence of these genes in our screen functioned as a validation to our approach and gave confidence for interrogations of identified novel targets.

3.3 The Purine Synthesis Pathway in SCLC

Consistent with recent screens in SCLC (Li et al., 2019; Nagel et al., 2019), we identified preferential sensitivities for knockout of metabolic pathways in SCLC compared with our MEF control. Recent work has highlighted the effects of inosine monophosphate dehydrogenase (IMPDH) inhibition in subsets of SCLC (Huang et al., 2018a), suggesting a potential therapeutic role for not only IMPDH, but for other enzymes involved in the purine synthesis pathway. Interestingly, this work correlated sensitivity to IMPDH inhibitors with lower expression levels of ASCL1 in human SCLC cell lines. In our mouse screen data, with cell lines featuring expression of ASCL1, we observed a significant depletion of the IMPDH2 gene, while inactivation of IMPDH1 had

no effect. While the determination of whether ASCL1-high cells are preferentially sensitive to IMPDH2 loss remains unclear, our results do suggest a significance for purine synthesis in SCLC. Purines are one of the cell's most abundant metabolite as they are critical for synthesis, energy, survival, and proliferation of the cell (Pedley and Benkovic, 2017). Unsurprisingly, cancer cells hold increased energy and synthesis demands, which require purine metabolites (Vander Heiden and DeBerardinis, 2017), (Vernieri et al., 2016). Cells obtain purine through either the salvage or de novo synthesis pathways. The salvage pathway, essentially the recovery of purines from used metabolites, is used under basal conditions in the cell (Henderson and Khoo, 1965), (Murray, 1971). Proliferating cells and tumor cells, with larger demands for purines, shift production to the energy intensive de novo synthesis pathway. This pathway uses 6 enzymes encoded by GART, PAICS, ATIC, PPAT, PFAS, and ADSL and to synthesize the metabolite IMP (See Figure E). At this point the two pathways converge and make use of the IMPDH isoforms discussed previously (Pedley and Benkovic, 2017). In our murine screen data, each one of these 6 genes in the de novo pathway holds a negative log fold change. More specifically, the mouse orthologs for PAICS, PPAT, PFAS, and ADSL significantly become depleted in our CRISPR inactivation screen, with ADSL and PAICS being among the top 25 hits. These 6 enzymes form the purinosome, a macromolecule complex that facilitates the efficiency of purine synthesis (An et al., 2008), (Zhao et al., 2015), (Pedley and Benkovic, 2018). Targeting the purinosome in SCLC may become a therapeutic option as work progresses on potential specific inhibitors of this complex (Spurr et al., 2012).

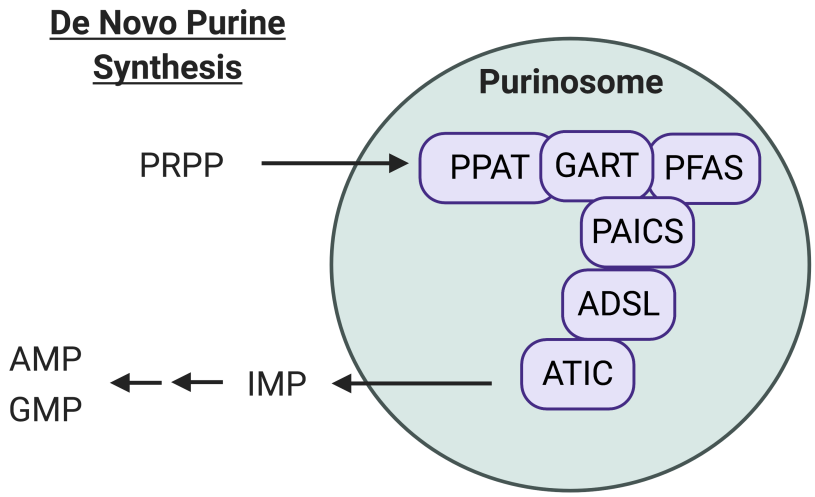

Figure E: Purine Synthesis Pathway

3.4 The Heme Synthesis Pathway in SCLC

Overactive and aberrant metabolism has long been a known distinguishing marker of cancer. Heme, an essential molecule best known for its prosthetic role in enzymes that transport oxygen, is also critical for functions including energy metabolism, drug metabolism, and a number of other cellular processes. (Padmanaban et al., 1989), (Sassa and Nagai, 1996), (Ponka, 1999). Additionally, heme is imperative for the development and differentiation of erythroid lineage cells, liver cells, and nervous system cells (Smith et al., 2011), (Padmanaban et al., 1989), (Sassa and Nagai, 1996), (Ponka, 1999). Heme disregulation has been observed in several tumor types including NSCLC (Sohoni et al., 2019), (Hooda et al., 2013). Potentially, targeting the eight

enzymes and precursors of the heme synthesis pathway may be a therapeutic strategy in tumor types with heightened heme reliance. In the results of our whole-genome inactivation screen, we identified many genes encoding enzymes in heme synthesis. One of the strongest hits in our screen, Cpox, encodes a mitochondrial enzyme, which modifies a side chain of the heme precursor (Yoshinaga and Sano, 1980). Furthermore, Hmbs, Alad, and Fech significantly become depleted in our mSCLC data compared with the MEF controls, suggesting a particular sensitivity to heme biosynthesis inhibition in our mouse SCLC lines (See Figure F). The heme pathway is unlikely to be an actionable therapeutic target but the mechanisms in which make heme an essential metabolite in SCLC could bring critical information to the SCLC field. Further investigation is needed to determine the role of heme in the development and maintenance of SCLC.

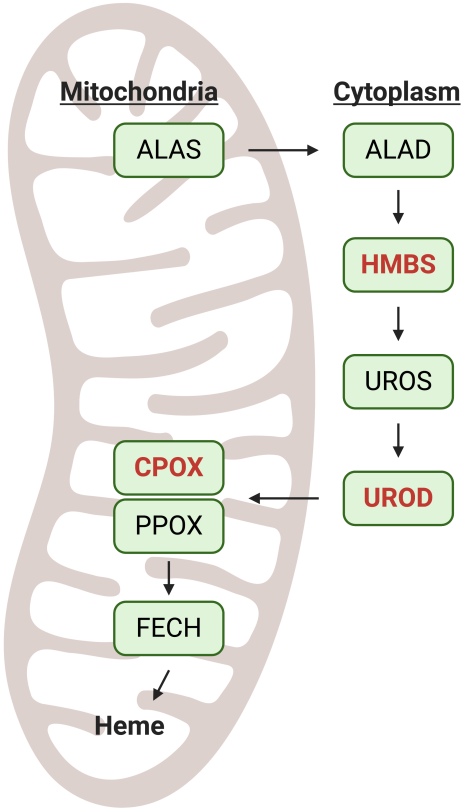

Figure F: Heme Synthesis Pathway

3.5 The Arginine Methyltransferase PRMT5 as a SCLC Target

An emerging target in many tumor types is the family of protein arginine methyltransferases, a set of enzymes that, similarly to how lysine is post-translationally modified, affixes methyl groups to the arginine residue of both histone and non-histone proteins. PRMT5 is a type II arginine methyltransferase that catalyzes the symmetrical addition of methyl groups to lysines of target histones or proteins (Bedford and Clarke, 2009). PRMT5 has been implicated as an oncogene in numerous cancer types including lung cancers, breast cancers, and liver cancers. (Gu et al., 2012), (Yang et al.,

2015), (Zhang et al., 2015). Not only did Prmt5 score highly in our screen, its methylosome complex partner, Wdr77 (Friesen et al., 2002), becomes significantly depleted in our SCLC lines. WDR77 encodes the novel WD repeat protein MEP50, which binds with PRMT5 to form the methylosome and can functionally regulate gene expression through targeting of histones, transcription factors, and chromatin regulators (Karkhanis et al., 2011). Novel inhibitors of PRMT5 are being tested in clinical trials for their effectiveness against numerous cancer types (Chan-Penebre et al., 2015) and our screen data suggests that PRMT5 inhibition may be therapeutically actionable in SCLC.

Chapter 4: Future Directions

To elucidate exact mechanisms of SCLC sensitivity to MLN4924, future work will need to ultimately tie the transcriptional repression of neuroendocrine genes to one or more of the functional changes we observed upon treatment. A more comprehensive perturbation of NE genes could elucidate which NE genes are most important in each SCLC PDX model. Assays that include combinational overexpression or knockdown of multiple NE genes could provide additional information. Epigenetically, we would like to determine precise changes in H3K27me3 mark levels for specific loci through ChIP-seq applications. These experiments will correlate the changes in histones marks with the changes we observed in our RNA-seq results. While the increased prevalence of H3K27me3 in SCLC cell lines is connected with an oncogenic role, neddylation may shield specific genes from transcriptional repression. Inhibiting neddylation may lead to increased global transcriptional repression that includes critical NE genes like INSM1 and ASCL1. ChIP-seq experiments for H3K27me1, H3K27me3, and NF-κB transcription

factors may further elucidate SCLC's sensitivity to inhibiting the neddylation pathway. Additional characterization of the mTOR and NF-κB pathways would help clarify their role in the MLN4924-induced phenotype. We would like to determine the functional consequences of mTOR and NF-κB activation in SCLC. To supplement our Everolimus and IKK-16 results, additional experiments will determine if activation of the mTOR or NF-κB pathway can recapitulate the functional effects of neddylation perturbation and specifically lead to neuroendocrine gene repression. We also hope to understand if mTOR or NF-κB inactivation can mitigate the apoptotic or proliferative effects of MLN4924. Further, a long-term goal would be to identify relevant substrate targets of CRL complexes in sensitive SCLC models . Potentially, quantitative whole proteome analysis could be employed to identify proteins regulated by neddylation relevant in SCLC. Lastly, identifying a precise predictor of MLN4924 sensitivity beyond general subtype (SCLC-A) would enable better patient outcomes if this therapy were to advance clinically. Experimentally, this could be achieved through a similar CRISPR screening approach on a SCLC-A model that is less sensitive to the neddylation inhibitor. These experiments could also provide a route for sensitizing non-responsive SCLC tumors to MLN4924.

Chapter 5: References for Chapters 1-4

An, S., Kumar, R., Sheets, E.D., and Benkovic, S.J. (2008). Reversible compartmentalization of de novo purine biosynthetic complexes in living cells. Science *320*, 103-106.

Anders, S., Pyl, P.T., and Huber, W. (2015). HTSeq--a Python framework to work with high-throughput sequencing data. Bioinformatics *31*, 166-169.

Augert, A., Eastwood, E., Ibrahim, A.H., Wu, N., Grunblatt, E., Basom, R., Liggitt, D., Eaton, K.D., Martins, R., Poirier, J.T.*, et al.* (2019). Targeting NOTCH activation in small cell lung cancer through LSD1 inhibition. Sci Signal *12*.

Augert, A., Zhang, Q., Bates, B., Cui, M., Wang, X., Wildey, G., Dowlati, A., and MacPherson, D. (2017). Small Cell Lung Cancer Exhibits Frequent Inactivating Mutations in the Histone Methyltransferase KMT2D/MLL2: CALGB 151111 (Alliance). J Thorac Oncol *12*, 704-713.

Bannister, A.J., and Kouzarides, T. (2011). Regulation of chromatin by histone modifications. Cell Res *21*, 381-395.

Bar-Peled, L., Chantranupong, L., Cherniack, A.D., Chen, W.W., Ottina, K.A., Grabiner, B.C., Spear, E.D., Carter, S.L., Meyerson, M., and Sabatini, D.M. (2013). A Tumor suppressor complex with GAP activity for the Rag GTPases that signal amino acid sufficiency to mTORC1. Science *340*, 1100-1106.

Bedford, M.T., and Clarke, S.G. (2009). Protein arginine methylation in mammals: who, what, and why. Mol Cell *33*, 1-13.

Bhatia, S., Pavlick, A.C., Boasberg, P., Thompson, J.A., Mulligan, G., Pickard, M.D., Faessel, H., Dezube, B.J., and Hamid, O. (2016). A phase I study of the investigational NEDD8-activating enzyme inhibitor pevonedistat (TAK-924/MLN4924) in patients with metastatic melanoma. Invest New Drugs *34*, 439-449.

Bonasio, R., Tu, S., and Reinberg, D. (2010). Molecular signals of epigenetic states. Science *330*, 612-616.

Borges, M., Linnoila, R.I., van de Velde, H.J., Chen, H., Nelkin, B.D., Mabry, M., Baylin, S.B., and Ball, D.W. (1997). An achaete-scute homologue essential for neuroendocrine differentiation in the lung. Nature *386*, 852-855.

Borromeo, M.D., Savage, T.K., Kollipara, R.K., He, M., Augustyn, A., Osborne, J.K., Girard, L., Minna, J.D., Gazdar, A.F., Cobb, M.H.*, et al.* (2016). ASCL1 and NEUROD1 Reveal Heterogeneity in Pulmonary Neuroendocrine Tumors and Regulate Distinct Genetic Programs. Cell Rep *16*, 1259-1272.

Bracken, A.P., Dietrich, N., Pasini, D., Hansen, K.H., and Helin, K. (2006). Genome-wide mapping of Polycomb target genes unravels their roles in cell fate transitions. Genes Dev *20*, 1123-1136.

Bracken, A.P., and Helin, K. (2009). Polycomb group proteins: navigators of lineage pathways led astray in cancer. Nat Rev Cancer *9*, 773-784.

Brownell, J.E., Sintchak, M.D., Gavin, J.M., Liao, H., Bruzzese, F.J., Bump, N.J., Soucy, T.A., Milhollen, M.A., Yang, X., Burkhardt, A.L.*, et al.* (2010). Substrate-assisted inhibition of ubiquitin-like protein-activating enzymes: the NEDD8 E1 inhibitor MLN4924 forms a NEDD8-AMP mimetic in situ. Mol Cell *37*, 102-111.

Bunn, P.A., Jr., Minna, J.D., Augustyn, A., Gazdar, A.F., Ouadah, Y., Krasnow, M.A., Berns, A., Brambilla, E., Rekhtman, N., Massion, P.P.*, et al.* (2016). Small Cell Lung Cancer: Can Recent Advances in Biology and Molecular Biology Be Translated into Improved Outcomes? J Thorac Oncol *11*, 453-474.

Burnett, P.E., Barrow, R.K., Cohen, N.A., Snyder, S.H., and Sabatini, D.M. (1998). RAFT1 phosphorylation of the translational regulators p70 S6 kinase and 4E-BP1. Proc Natl Acad Sci U S A *95*, 1432-1437.

Byers, L.A., and Rudin, C.M. (2015). Small cell lung cancer: where do we go from here? Cancer *121*, 664-672.

Byers, L.A., Wang, J., Nilsson, M.B., Fujimoto, J., Saintigny, P., Yordy, J., Giri, U., Peyton, M., Fan, Y.H., Diao, L.*, et al.* (2012). Proteomic profiling identifies dysregulated pathways in small cell lung cancer and novel therapeutic targets including PARP1. Cancer Discov *2*, 798-811.

Calbo, J., Meuwissen, R., van Montfort, E., van Tellingen, O., and Berns, A. (2005). Genotype-phenotype relationships in a mouse model for human small-cell lung cancer. Cold Spring Harb Symp Quant Biol *70*, 225-232.

Cardnell, R.J., Feng, Y., Diao, L., Fan, Y.H., Masrorpour, F., Wang, J., Shen, Y., Mills, G.B., Minna, J.D., Heymach, J.V.*, et al.* (2013). Proteomic markers of DNA repair and PI3K pathway activation predict response to the PARP inhibitor BMN 673 in small cell lung cancer. Clin Cancer Res *19*, 6322-6328.

Castillo, S.D., Matheu, A., Mariani, N., Carretero, J., Lopez-Rios, F., Lovell-Badge, R., and Sanchez-Cespedes, M. (2012). Novel transcriptional targets of the SRY-HMG box transcription factor SOX4 link its expression to the development of small cell lung cancer. Cancer Res *72*, 176-186.

Chalishazar, M.D., Wait, S.J., Huang, F., Ireland, A.S., Mukhopadhyay, A., Lee, Y., Schuman, S.S., Guthrie, M.R., Berrett, K.C., Vahrenkamp, J.M.*, et al.* (2019). MYC-Driven Small-Cell Lung Cancer is Metabolically Distinct and Vulnerable to Arginine Depletion. Clin Cancer Res *25*, 5107-5121.

Chan-Penebre, E., Kuplast, K.G., Majer, C.R., Boriack-Sjodin, P.A., Wigle, T.J., Johnston, L.D., Rioux, N., Munchhof, M.J., Jin, L., Jacques, S.L.*, et al.* (2015). A selective inhibitor of PRMT5 with in vivo and in vitro potency in MCL models. Nat Chem Biol *11*, 432-437.

Chen, L., Willis, S.N., Wei, A., Smith, B.J., Fletcher, J.I., Hinds, M.G., Colman, P.M., Day, C.L., Adams, J.M., and Huang, D.C. (2005). Differential targeting of prosurvival Bcl-2 proteins by their BH3-only ligands allows complementary apoptotic function. Mol Cell *17*, 393-403.

Chen, Q., Xie, W., Kuhn, D.J., Voorhees, P.M., Lopez-Girona, A., Mendy, D., Corral, L.G., Krenitsky, V.P., Xu, W., Moutouh-de Parseval, L.*, et al.* (2008). Targeting the p27 E3 ligase SCF(Skp2) results in p27- and Skp2-mediated cell-cycle arrest and activation of autophagy. Blood *111*, 4690-4699.

Chen, S., Sanjana, N.E., Zheng, K., Shalem, O., Lee, K., Shi, X., Scott, D.A., Song, J., Pan, J.Q., Weissleder, R.*, et al.* (2015a). Genome-wide CRISPR screen in a mouse model of tumor growth and metastasis. Cell *160*, 1246-1260.

Chen, Y., McPhie, D.L., Hirschberg, J., and Neve, R.L. (2000). The amyloid precursor protein-binding protein APP-BP1 drives the cell cycle through the S-M checkpoint and causes apoptosis in neurons. J Biol Chem *275*, 8929-8935.

Chen, Z., Sui, J., Zhang, F., and Zhang, C. (2015b). Cullin family proteins and tumorigenesis: genetic association and molecular mechanisms. J Cancer *6*, 233-242.

Chiba, T., and Tanaka, K. (2004). Cullin-based ubiquitin ligase and its control by NEDD8-conjugating system. Curr Protein Pept Sci *5*, 177-184.

Christensen, C.L., Kwiatkowski, N., Abraham, B.J., Carretero, J., Al-Shahrour, F., Zhang, T., Chipumuro, E., Herter-Sprie, G.S., Akbay, E.A., Altabef, A.*, et al.* (2014). Targeting transcriptional addictions in small cell lung cancer with a covalent CDK7 inhibitor. Cancer Cell *26*, 909-922.

Coe, B.P., Thu, K.L., Aviel-Ronen, S., Vucic, E.A., Gazdar, A.F., Lam, S., Tsao, M.S., and Lam, W.L. (2013). Genomic deregulation of the E2F/Rb pathway leads to activation of the oncogene EZH2 in small cell lung cancer. PLoS One *8*, e71670.

Cooper, C.S., Nicholson, A.G., Foster, C., Dodson, A., Edwards, S., Fletcher, A., Roe, T., Clark, J., Joshi, A., Norman, A.*, et al.* (2006). Nuclear overexpression of the E2F3 transcription factor in human lung cancer. Lung Cancer *54*, 155-162.

Daniel, V.C., Marchionni, L., Hierman, J.S., Rhodes, J.T., Devereux, W.L., Rudin, C.M., Yung, R., Parmigiani, G., Dorsch, M., Peacock, C.D.*, et al.* (2009). A primary xenograft model of small-cell lung cancer reveals irreversible changes in gene expression imposed by culture in vitro. Cancer Res *69*, 3364-3373.

DiDonato, J.A., Hayakawa, M., Rothwarf, D.M., Zandi, E., and Karin, M. (1997). A cytokine-responsive IkappaB kinase that activates the transcription factor NF-kappaB. Nature *388*, 548-554.

Doerr, F., George, J., Schmitt, A., Beleggia, F., Rehkamper, T., Hermann, S., Walter, V., Weber, J.P., Thomas, R.K., Wittersheim, M.*, et al.* (2017). Targeting a non-oncogene addiction to the ATR/CHK1 axis for the treatment of small cell lung cancer. Sci Rep *7*, 15511.

Foy, V., Schenk, M.W., Baker, K., Gomes, F., Lallo, A., Frese, K.K., Forster, M., Dive, C., and Blackhall, F. (2017). Targeting DNA damage in SCLC. Lung Cancer *114*, 12-22.

Friesen, W.J., Wyce, A., Paushkin, S., Abel, L., Rappsilber, J., Mann, M., and Dreyfuss, G. (2002). A novel WD repeat protein component of the methylosome binds Sm proteins. J Biol Chem *277*, 8243-8247.

Fujino, K., Motooka, Y., Hassan, W.A., Ali Abdalla, M.O., Sato, Y., Kudoh, S., Hasegawa, K., Niimori-Kita, K., Kobayashi, H., Kubota, I.*, et al.* (2015). Insulinoma-Associated Protein 1 Is a Crucial Regulator of Neuroendocrine Differentiation in Lung Cancer. Am J Pathol *185*, 3164-3177.

Gandhi, L., Camidge, D.R., Ribeiro de Oliveira, M., Bonomi, P., Gandara, D., Khaira, D., Hann, C.L., McKeegan, E.M., Litvinovich, E., Hemken, P.M.*, et al.* (2011). Phase I study of Navitoclax (ABT-263), a novel Bcl-2 family inhibitor, in patients with small-cell lung cancer and other solid tumors. J Clin Oncol *29*, 909-916.

Ganley, I.G., Lam du, H., Wang, J., Ding, X., Chen, S., and Jiang, X. (2009). ULK1.ATG13.FIP200 complex mediates mTOR signaling and is essential for autophagy. J Biol Chem *284*, 12297-12305.

George, J., Lim, J.S., Jang, S.J., Cun, Y., Ozretic, L., Kong, G., Leenders, F., Lu, X., Fernandez-Cuesta, L., Bosco, G.*, et al.* (2015). Comprehensive genomic profiles of small cell lung cancer. Nature *524*, 47-53.

Glickman, M.H., Rubin, D.M., Coux, O., Wefes, I., Pfeifer, G., Cjeka, Z., Baumeister, W., Fried, V.A., and Finley, D. (1998). A subcomplex of the proteasome regulatory particle required for ubiquitin-conjugate degradation and related to the COP9-signalosome and eIF3. Cell *94*, 615-623.

Gong, L., and Yeh, E.T. (1999). Identification of the activating and conjugating enzymes of the NEDD8 conjugation pathway. J Biol Chem *274*, 12036-12042.

Gu, Z., Gao, S., Zhang, F., Wang, Z., Ma, W., Davis, R.E., and Wang, Z. (2012). Protein arginine methyltransferase 5 is essential for growth of lung cancer cells. Biochem J *446*, 235-241.

Hay, N., and Sonenberg, N. (2004). Upstream and downstream of mTOR. Genes Dev *18*, 1926-1945.

Hayden, M.S., and Ghosh, S. (2012). NF-kappaB, the first quarter-century: remarkable progress and outstanding questions. Genes Dev *26*, 203-234.

Henderson, J.F., and Khoo, K.Y. (1965). On the Mechanism of Feedback Inhibition of Purine Biosynthesis De Novo in Ehrlich Ascites Tumor Cells in Vitro. J Biol Chem *240*, 3104-3109.

Henke, W., Ferrell, K., Bech-Otschir, D., Seeger, M., Schade, R., Jungblut, P., Naumann, M., and Dubiel, W. (1999). Comparison of human COP9 signalsome and 26S proteasome lid'. Mol Biol Rep *26*, 29-34.

Heuze, M.L., Guibal, F.C., Banks, C.A., Conaway, J.W., Conaway, R.C., Cayre, Y.E., Benecke, A., and Lutz, P.G. (2005). ASB2 is an Elongin BC-interacting protein that can assemble with Cullin 5 and Rbx1 to reconstitute an E3 ubiquitin ligase complex. J Biol Chem *280*, 5468-5474.

Hinz, M., Arslan, S.C., and Scheidereit, C. (2012). It takes two to tango: IkappaBs, the multifunctional partners of NF-kappaB. Immunol Rev *246*, 59-76.

Hoberg, J.E., Popko, A.E., Ramsey, C.S., and Mayo, M.W. (2006). IkappaB kinase alpha-mediated derepression of SMRT potentiates acetylation of RelA/p65 by p300. Mol Cell Biol *26*, 457-471.

Hodgkinson, C.L., Morrow, C.J., Li, Y., Metcalf, R.L., Rothwell, D.G., Trapani, F., Polanski, R., Burt, D.J., Simpson, K.L., Morris, K.*, et al.* (2014). Tumorigenicity and genetic profiling of circulating tumor cells in small-cell lung cancer. Nat Med *20*, 897-903.

Hooda, J., Cadinu, D., Alam, M.M., Shah, A., Cao, T.M., Sullivan, L.A., Brekken, R., and Zhang, L. (2013). Enhanced heme function and mitochondrial respiration promote the progression of lung cancer cells. PLoS One *8*, e63402.

Horn, L., Mansfield, A.S., Szczesna, A., Havel, L., Krzakowski, M., Hochmair, M.J., Huemer, F., Losonczy, G., Johnson, M.L., Nishio, M.*, et al.* (2018). First-Line Atezolizumab plus Chemotherapy in Extensive-Stage Small-Cell Lung Cancer. N Engl J Med *379*, 2220-2229.

Hosokawa, N., Hara, T., Kaizuka, T., Kishi, C., Takamura, A., Miura, Y., Iemura, S., Natsume, T., Takehana, K., Yamada, N.*, et al.* (2009). Nutrient-dependent mTORC1 association with the ULK1-Atg13-FIP200 complex required for autophagy. Mol Biol Cell *20*, 1981-1991.

Huang, D.T., Ayrault, O., Hunt, H.W., Taherbhoy, A.M., Duda, D.M., Scott, D.C., Borg, L.A., Neale, G., Murray, P.J., Roussel, M.F.*, et al.* (2009). E2-RING expansion of the NEDD8 cascade confers specificity to cullin modification. Mol Cell *33*, 483-495.

Huang, F., Ni, M., Chalishazar, M.D., Huffman, K.E., Kim, J., Cai, L., Shi, X., Cai, F., Zacharias, L.G., Ireland, A.S.*, et al.* (2018a). Inosine Monophosphate Dehydrogenase Dependence in a Subset of Small Cell Lung Cancers. Cell Metab *28*, 369-382 e365.

Huang, W.C., Ju, T.K., Hung, M.C., and Chen, C.C. (2007). Phosphorylation of CBP by IKKalpha promotes cell growth by switching the binding preference of CBP from p53 to NF-kappaB. Mol Cell *26*, 75-87.

Huang, Y.H., Klingbeil, O., He, X.Y., Wu, X.S., Arun, G., Lu, B., Somerville, T.D.D., Milazzo, J.P., Wilkinson, J.E., Demerdash, O.E.*, et al.* (2018b). POU2F3 is a master regulator of a tuft cell-like variant of small cell lung cancer. Genes Dev *32*, 915-928.

Inoki, K., Ouyang, H., Li, Y., and Guan, K.L. (2005). Signaling by target of rapamycin proteins in cell growth control. Microbiol Mol Biol Rev *69*, 79-100.

Ito, T., Udaka, N., Yazawa, T., Okudela, K., Hayashi, H., Sudo, T., Guillemot, F., Kageyama, R., and Kitamura, H. (2000). Basic helix-loop-helix transcription factors regulate the neuroendocrine differentiation of fetal mouse pulmonary epithelium. Development *127*, 3913-3921.

Ivan, M., Kondo, K., Yang, H., Kim, W., Valiando, J., Ohh, M., Salic, A., Asara, J.M., Lane, W.S., and Kaelin, W.G., Jr. (2001). HIFalpha targeted for VHL-mediated destruction by proline hydroxylation: implications for O2 sensing. Science *292*, 464-468.

Jia, D., Augert, A., Kim, D.W., Eastwood, E., Wu, N., Ibrahim, A.H., Kim, K.B., Dunn, C.T., Pillai, S.P.S., Gazdar, A.F.*, et al.* (2018). Crebbp Loss Drives Small Cell Lung Cancer and Increases Sensitivity to HDAC Inhibition. Cancer Discov *8*, 1422-1437.

Jia, S., Wildner, H., and Birchmeier, C. (2015). Insm1 controls the differentiation of pulmonary neuroendocrine cells by repressing Hes1. Dev Biol *408*, 90-98.

Jin, J., Cardozo, T., Lovering, R.C., Elledge, S.J., Pagano, M., and Harper, J.W. (2004). Systematic analysis and nomenclature of mammalian F-box proteins. Genes Dev *18*, 2573-2580.

Kamitani, T., Kito, K., Nguyen, H.P., and Yeh, E.T. (1997). Characterization of NEDD8, a developmentally down-regulated ubiquitin-like protein. J Biol Chem *272*, 28557-28562.

Kamura, T., Burian, D., Yan, Q., Schmidt, S.L., Lane, W.S., Querido, E., Branton, P.E., Shilatifard, A., Conaway, R.C., and Conaway, J.W. (2001). Muf1, a novel Elongin BC-interacting leucine-rich repeat protein that can assemble with Cul5 and Rbx1 to reconstitute a ubiquitin ligase. J Biol Chem *276*, 29748-29753.

Kamura, T., Conrad, M.N., Yan, Q., Conaway, R.C., and Conaway, J.W. (1999). The Rbx1 subunit of SCF and VHL E3 ubiquitin ligase activates Rub1 modification of cullins Cdc53 and Cul2. Genes Dev *13*, 2928-2933.

Karin, M. (2006). Nuclear factor-kappaB in cancer development and progression. Nature *441*, 431-436.

Karin, M., and Delhase, M. (2000). The I kappa B kinase (IKK) and NF-kappa B: key elements of proinflammatory signalling. Semin Immunol *12*, 85-98.

Karin, M., and Greten, F.R. (2005). NF-kappaB: linking inflammation and immunity to cancer development and progression. Nat Rev Immunol *5*, 749-759.

Karkhanis, V., Hu, Y.J., Baiocchi, R.A., Imbalzano, A.N., and Sif, S. (2011). Versatility of PRMT5-induced methylation in growth control and development. Trends Biochem Sci *36*, 633-641.

Kim, D.W., Wu, N., Kim, Y.C., Cheng, P.F., Basom, R., Kim, D., Dunn, C.T., Lee, A.Y., Kim, K., Lee, C.S.*, et al.* (2016). Genetic requirement for Mycl and efficacy of RNA Pol I inhibition in mouse models of small cell lung cancer. Genes Dev *30*, 1289-1299.

Kim, J., and Guan, K.L. (2019). mTOR as a central hub of nutrient signalling and cell growth. Nat Cell Biol *21*, 63-71.

Kirmizis, A., Bartley, S.M., Kuzmichev, A., Margueron, R., Reinberg, D., Green, R., and Farnham, P.J. (2004). Silencing of human polycomb target genes is associated with methylation of histone H3 Lys 27. Genes Dev *18*, 1592-1605.

Lan, M.S., and Breslin, M.B. (2009). Structure, expression, and biological function of INSM1 transcription factor in neuroendocrine differentiation. FASEB J *23*, 2024-2033.

Laszlo, G.S., and Cooper, J.A. (2009). Restriction of Src activity by Cullin-5. Curr Biol *19*, 157-162.

Lee, D.F., Kuo, H.P., Chen, C.T., Hsu, J.M., Chou, C.K., Wei, Y., Sun, H.L., Li, L.Y., Ping, B., Huang, W.C.*, et al.* (2007). IKK beta suppression of TSC1 links inflammation and tumor angiogenesis via the mTOR pathway. Cell *130*, 440-455.

Li, L., Ng, S.R., Colon, C.I., Drapkin, B.J., Hsu, P.P., Li, Z., Nabel, C.S., Lewis, C.A., Romero, R., Mercer, K.L.*, et al.* (2019). Identification of DHODH as a therapeutic target in small cell lung cancer. Sci Transl Med *11*.

Li, W., Koster, J., Xu, H., Chen, C.H., Xiao, T., Liu, J.S., Brown, M., and Liu, X.S. (2015). Quality control, modeling, and visualization of CRISPR screens with MAGeCK-VISPR. Genome Biol *16*, 281.

Li, W., Xu, H., Xiao, T., Cong, L., Love, M.I., Zhang, F., Irizarry, R.A., Liu, J.S., Brown, M., and Liu, X.S. (2014). MAGeCK enables robust identification of essential genes from genome-scale CRISPR/Cas9 knockout screens. Genome Biol *15*, 554.

Liao, H., Liu, X.J., Blank, J.L., Bouck, D.C., Bernard, H., Garcia, K., and Lightcap, E.S. (2011). Quantitative proteomic analysis of cellular protein modulation upon inhibition of the NEDD8-activating enzyme by MLN4924. Mol Cell Proteomics *10*, M111 009183.

Lin, J.J., Milhollen, M.A., Smith, P.G., Narayanan, U., and Dutta, A. (2010). NEDD8-targeting drug MLN4924 elicits DNA rereplication by stabilizing Cdt1 in S phase, triggering checkpoint activation, apoptosis, and senescence in cancer cells. Cancer Res *70*, 10310-10320.

Lockhart, A.C., Bauer, T.M., Aggarwal, C., Lee, C.B., Harvey, R.D., Cohen, R.B., Sedarati, F., Nip, T.K., Faessel, H., Dash, A.B.*, et al.* (2019). Phase Ib study of pevonedistat, a NEDD8-activating enzyme inhibitor, in combination with docetaxel, carboplatin and paclitaxel, or gemcitabine, in patients with advanced solid tumors. Invest New Drugs *37*, 87-97.

Lyapina, S., Cope, G., Shevchenko, A., Serino, G., Tsuge, T., Zhou, C., Wolf, D.A., Wei, N., Shevchenko, A., and Deshaies, R.J. (2001). Promotion of NEDD-CUL1 conjugate cleavage by COP9 signalosome. Science *292*, 1382-1385.

Margueron, R., and Reinberg, D. (2011). The Polycomb complex PRC2 and its mark in life. Nature *469*, 343-349.

Mercurio, F., Zhu, H., Murray, B.W., Shevchenko, A., Bennett, B.L., Li, J., Young, D.B., Barbosa, M., Mann, M., Manning, A.*, et al.* (1997). IKK-1 and IKK-2: cytokine-activated IkappaB kinases essential for NF-kappaB activation. Science *278*, 860-866.

Milhollen, M.A., Narayanan, U., Soucy, T.A., Veiby, P.O., Smith, P.G., and Amidon, B. (2011). Inhibition of NEDD8-activating enzyme induces rereplication and apoptosis in human tumor cells consistent with deregulating CDT1 turnover. Cancer Res *71*, 3042-3051.

Milhollen, M.A., Traore, T., Adams-Duffy, J., Thomas, M.P., Berger, A.J., Dang, L., Dick, L.R., Garnsey, J.J., Koenig, E., Langston, S.P.*, et al.* (2010). MLN4924, a NEDD8-activating enzyme inhibitor, is active in diffuse large B-cell lymphoma models: rationale for treatment of NF-{kappa}B-dependent lymphoma. Blood *116*, 1515-1523.

Murray, A.W. (1971). The biological significance of purine salvage. Annu Rev Biochem *40*, 811-826.

Nagel, R., Avelar, A.T., Aben, N., Proost, N., van de Ven, M., van der Vliet, J., Cozijnsen, M., de Vries, H., Wessels, L.F.A., and Berns, A. (2019). Inhibition of the Replication Stress Response Is a Synthetic Vulnerability in SCLC That Acts Synergistically in Combination with Cisplatin. Mol Cancer Ther *18*, 762-770.

Olma, M.H., Roy, M., Le Bihan, T., Sumara, I., Maerki, S., Larsen, B., Quadroni, M., Peter, M., Tyers, M., and Pintard, L. (2009). An interaction network of the mammalian COP9 signalosome identifies Dda1 as a core subunit of multiple Cul4-based E3 ligases. J Cell Sci *122*, 1035-1044.

Osborne, J.K., Larsen, J.E., Shields, M.D., Gonzales, J.X., Shames, D.S., Sato, M., Kulkarni, A., Wistuba, II, Girard, L., Minna, J.D.*, et al.* (2013). NeuroD1 regulates survival and migration of neuroendocrine lung carcinomas via signaling molecules TrkB and NCAM. Proc Natl Acad Sci U S A *110*, 6524-6529.

Oser, M.G., Sabet, A.H., Gao, W., Chakraborty, A.A., Schinzel, A.C., Jennings, R.B., Fonseca, R., Bonal, D.M., Booker, M.A., Flaifel, A.*, et al.* (2019). The KDM5A/RBP2 histone demethylase represses NOTCH signaling to sustain neuroendocrine differentiation and promote small cell lung cancer tumorigenesis. Genes Dev *33*, 1718-1738.

Pacheco, J., and Bunn, P.A. (2019). Advancements in Small-cell Lung Cancer: The Changing Landscape Following IMpower-133. Clin Lung Cancer *20*, 148-160 e142.

Padmanaban, G., Venkateswar, V., and Rangarajan, P.N. (1989). Haem as a multifunctional regulator. Trends Biochem Sci *14*, 492-496.

Pan, Q., Qiao, F., Gao, C., Norman, B., Optican, L., and Zelenka, P.S. (2011). Cdk5 targets active Src for ubiquitin-dependent degradation by phosphorylating Src(S75). Cell Mol Life Sci *68*, 3425-3436.

Pan, Z.Q., Kentsis, A., Dias, D.C., Yamoah, K., and Wu, K. (2004). Nedd8 on cullin: building an expressway to protein destruction. Oncogene *23*, 1985-1997.

Panchaud, N., Peli-Gulli, M.P., and De Virgilio, C. (2013). Amino acid deprivation inhibits TORC1 through a GTPase-activating protein complex for the Rag family GTPase Gtr1. Sci Signal *6*, ra42.

Parisi, T., Yuan, T.L., Faust, A.M., Caron, A.M., Bronson, R., and Lees, J.A. (2007). Selective requirements for E2f3 in the development and tumorigenicity of Rb-deficient chimeric tissues. Mol Cell Biol *27*, 2283-2293.

Paz-Ares, L., Dvorkin, M., Chen, Y., Reinmuth, N., Hotta, K., Trukhin, D., Statsenko, G., Hochmair, M.J., Ozguroglu, M., Ji, J.H.*, et al.* (2019). Durvalumab plus platinum-etoposide versus platinum-etoposide in first-line treatment of extensive-stage small-cell lung cancer (CASPIAN): a randomised, controlled, open-label, phase 3 trial. Lancet *394*, 1929-1939.

Pedley, A.M., and Benkovic, S.J. (2017). A New View into the Regulation of Purine Metabolism: The Purinosome. Trends Biochem Sci *42*, 141-154.

Pedley, A.M., and Benkovic, S.J. (2018). Detecting Purinosome Metabolon Formation with Fluorescence Microscopy. Methods Mol Biol *1764*, 279-289.

Peifer, M., Fernandez-Cuesta, L., Sos, M.L., George, J., Seidel, D., Kasper, L.H., Plenker, D., Leenders, F., Sun, R., Zander, T.*, et al.* (2012). Integrative genome analyses identify key somatic driver mutations of small-cell lung cancer. Nat Genet *44*, 1104-1110.

Perkins, N.D. (2012). The diverse and complex roles of NF-kappaB subunits in cancer. Nat Rev Cancer *12*, 121-132.

Petroski, M.D., and Deshaies, R.J. (2005). Function and regulation of cullin-RING ubiquitin ligases. Nat Rev Mol Cell Biol *6*, 9-20.

Pietanza, M.C., Byers, L.A., Minna, J.D., and Rudin, C.M. (2015). Small cell lung cancer: will recent progress lead to improved outcomes? Clin Cancer Res *21*, 2244-2255.

Poirier, J.T., Gardner, E.E., Connis, N., Moreira, A.L., de Stanchina, E., Hann, C.L., and Rudin, C.M. (2015). DNA methylation in small cell lung cancer defines distinct disease subtypes and correlates with high expression of EZH2. Oncogene *34*, 5869-5878.

Poirier, J.T., George, J., Owonikoko, T.K., Berns, A., Brambilla, E., Byers, L.A., Carbone, D., Chen, H.J., Christensen, C.L., Dive, C.*, et al.* (2020). New Approaches to SCLC Therapy: From the Laboratory to the Clinic. J Thorac Oncol *15*, 520-540.

Ponka, P. (1999). Cell biology of heme. Am J Med Sci *318*, 241-256.

Prescott, J.A., and Cook, S.J. (2018). Targeting IKKbeta in Cancer: Challenges and Opportunities for the Therapeutic Utilisation of IKKbeta Inhibitors. Cells *7*.

Read, M.A., Brownell, J.E., Gladysheva, T.B., Hottelet, M., Parent, L.A., Coggins, M.B., Pierce, J.W., Podust, V.N., Luo, R.S., Chau, V.*, et al.* (2000). Nedd8 modification of cul-1 activates SCF(beta(TrCP))-dependent ubiquitination of IkappaBalpha. Mol Cell Biol *20*, 2326-2333.

Robinson, M.D., McCarthy, D.J., and Smyth, G.K. (2010). edgeR: a Bioconductor package for differential expression analysis of digital gene expression data. Bioinformatics *26*, 139-140.

Rossi, A., Di Maio, M., Chiodini, P., Rudd, R.M., Okamoto, H., Skarlos, D.V., Fruh, M., Qian, W., Tamura, T., Samantas, E.*, et al.* (2012). Carboplatin- or cisplatin-based chemotherapy in first-line treatment of small-cell lung cancer: the COCIS meta-analysis of individual patient data. J Clin Oncol *30*, 1692-1698.

Rudin, C.M. (2012). Vismodegib. Clin Cancer Res *18*, 3218-3222.

Rudin, C.M., Durinck, S., Stawiski, E.W., Poirier, J.T., Modrusan, Z., Shames, D.S., Bergbower, E.A., Guan, Y., Shin, J., Guillory, J.*, et al.* (2012). Comprehensive genomic analysis identifies SOX2 as a frequently amplified gene in small-cell lung cancer. Nat Genet *44*, 1111-1116.

Rudin, C.M., Poirier, J.T., Byers, L.A., Dive, C., Dowlati, A., George, J., Heymach, J.V., Johnson, J.E., Lehman, J.M., MacPherson, D.*, et al.* (2019). Molecular subtypes of small cell lung cancer: a synthesis of human and mouse model data. Nat Rev Cancer *19*, 289-297.

Sanjana, N.E., Shalem, O., and Zhang, F. (2014). Improved vectors and genome-wide libraries for CRISPR screening. Nat Methods *11*, 783-784.

Saran, U., Foti, M., and Dufour, J.F. (2015). Cellular and molecular effects of the mTOR inhibitor everolimus. Clin Sci (Lond) *129*, 895-914.

Sassa, S., and Nagai, T. (1996). The role of heme in gene expression. Int J Hematol *63*, 167-178.

Sato, T., Kaneda, A., Tsuji, S., Isagawa, T., Yamamoto, S., Fujita, T., Yamanaka, R., Tanaka, Y., Nukiwa, T., Marquez, V.E.*, et al.* (2013). PRC2 overexpression and PRC2-target gene repression relating to poorer prognosis in small cell lung cancer. Sci Rep *3*, 1911.

Schuettengruber, B., Bourbon, H.M., Di Croce, L., and Cavalli, G. (2017). Genome Regulation by Polycomb and Trithorax: 70 Years and Counting. Cell *171*, 34-57.

Schweitzer, K., Pralow, A., and Naumann, M. (2016). p97/VCP promotes Cullin-RING-ubiquitin-ligase/proteasome-dependent degradation of IkappaBalpha and the preceding liberation of RelA from ubiquitinated IkappaBalpha. J Cell Mol Med *20*, 58-70.

Sen, T., Tong, P., Diao, L., Li, L., Fan, Y., Hoff, J., Heymach, J.V., Wang, J., and Byers, L.A. (2017a). Targeting AXL and mTOR Pathway Overcomes Primary and Acquired Resistance to WEE1 Inhibition in Small-Cell Lung Cancer. Clin Cancer Res *23*, 6239-6253.

Sen, T., Tong, P., Stewart, C.A., Cristea, S., Valliani, A., Shames, D.S., Redwood, A.B., Fan, Y.H., Li, L., Glisson, B.S.*, et al.* (2017b). CHK1 Inhibition in Small-Cell Lung Cancer Produces Single-Agent Activity in Biomarker-Defined Disease Subsets and Combination Activity with Cisplatin or Olaparib. Cancer Res *77*, 3870-3884.

Shah, J.J., Jakubowiak, A.J., O'Connor, O.A., Orlowski, R.Z., Harvey, R.D., Smith, M.R., Lebovic, D., Diefenbach, C., Kelly, K., Hua, Z.*, et al.* (2016). Phase I Study of the Novel Investigational NEDD8-Activating Enzyme Inhibitor Pevonedistat (MLN4924) in Patients with Relapsed/Refractory Multiple Myeloma or Lymphoma. Clin Cancer Res *22*, 34-43.

Silverman, N., Zhou, R., Erlich, R.L., Hunter, M., Bernstein, E., Schneider, D., and Maniatis, T. (2003). Immune activation of NF-kappaB and JNK requires Drosophila TAK1. J Biol Chem *278*, 48928-48934.

Singh, A., Misra, V., Thimmulappa, R.K., Lee, H., Ames, S., Hoque, M.O., Herman, J.G., Baylin, S.B., Sidransky, D., Gabrielson, E.*, et al.* (2006). Dysfunctional KEAP1-NRF2 interaction in non-small-cell lung cancer. PLoS Med *3*, e420.

Smith, A.G., Raven, E.L., and Chernova, T. (2011). The regulatory role of heme in neurons. Metallomics *3*, 955-962.

Sohoni, S., Ghosh, P., Wang, T., Kalainayakan, S.P., Vidal, C., Dey, S., Konduri, P.C., and Zhang, L. (2019). Elevated Heme Synthesis and Uptake Underpin Intensified Oxidative Metabolism and Tumorigenic Functions in Non-Small Cell Lung Cancer Cells. Cancer Res *79*, 2511-2525.

Sos, M.L., Dietlein, F., Peifer, M., Schottle, J., Balke-Want, H., Muller, C., Koker, M., Richters, A., Heynck, S., Malchers, F.*, et al.* (2012). A framework for identification of actionable cancer genome dependencies in small cell lung cancer. Proc Natl Acad Sci U S A *109*, 17034-17039.

Soucy, T.A., Smith, P.G., Milhollen, M.A., Berger, A.J., Gavin, J.M., Adhikari, S., Brownell, J.E., Burke, K.E., Cardin, D.P., Critchley, S.*, et al.* (2009). An inhibitor of NEDD8-activating enzyme as a new approach to treat cancer. Nature *458*, 732-736.

Spurr, I.B., Birts, C.N., Cuda, F., Benkovic, S.J., Blaydes, J.P., and Tavassoli, A. (2012). Targeting tumour proliferation with a small-molecule inhibitor of AICAR transformylase homodimerization. Chembiochem *13*, 1628-1634.

Sutherland, K.D., and Berns, A. (2010). Cell of origin of lung cancer. Mol Oncol *4*, 397-403.

Sutherland, K.D., Proost, N., Brouns, I., Adriaensen, D., Song, J.Y., and Berns, A. (2011). Cell of origin of small cell lung cancer: inactivation of Trp53 and Rb1 in distinct cell types of adult mouse lung. Cancer Cell *19*, 754-764.

Swords, R.T., Kelly, K.R., Smith, P.G., Garnsey, J.J., Mahalingam, D., Medina, E., Oberheu, K., Padmanabhan, S., O'Dwyer, M., Nawrocki, S.T.*, et al.* (2010). Inhibition of NEDD8-activating enzyme: a novel approach for the treatment of acute myeloid leukemia. Blood *115*, 3796-3800.

Tong, S., Si, Y., Yu, H., Zhang, L., Xie, P., and Jiang, W. (2017). MLN4924 (Pevonedistat), a protein neddylation inhibitor, suppresses proliferation and migration of human clear cell renal cell carcinoma. Sci Rep *7*, 5599.

Trapnell, C., Hendrickson, D.G., Sauvageau, M., Goff, L., Rinn, J.L., and Pachter, L. (2013). Differential analysis of gene regulation at transcript resolution with RNA-seq. Nat Biotechnol *31*, 46-53.

Trapnell, C., and Schatz, M.C. (2009). Optimizing Data Intensive GPGPU Computations for DNA Sequence Alignment. Parallel Comput *35*, 429-440.

Vander Heiden, M.G., and DeBerardinis, R.J. (2017). Understanding the Intersections between Metabolism and Cancer Biology. Cell *168*, 657-669.

Vernieri, C., Casola, S., Foiani, M., Pietrantonio, F., de Braud, F., and Longo, V. (2016). Targeting Cancer Metabolism: Dietary and Pharmacologic Interventions. Cancer Discov *6*, 1315-1333.

Vidal, S., Khush, R.S., Leulier, F., Tzou, P., Nakamura, M., and Lemaitre, B. (2001). Mutations in the Drosophila dTAK1 gene reveal a conserved function for MAPKKKs in the control of rel/NF-kappaB-dependent innate immune responses. Genes Dev *15*, 1900-1912.

Walden, H., Podgorski, M.S., Huang, D.T., Miller, D.W., Howard, R.J., Minor, D.L., Jr., Holton, J.M., and Schulman, B.A. (2003). The structure of the APPBP1-UBA3-NEDD8-ATP complex reveals the basis for selective ubiquitin-like protein activation by an E1. Mol Cell *12*, 1427-1437.

Wang, T., Birsoy, K., Hughes, N.W., Krupczak, K.M., Post, Y., Wei, J.J., Lander, E.S., and Sabatini, D.M. (2015). Identification and characterization of essential genes in the human genome. Science *350*, 1096-1101.

Wei, D., Li, H., Yu, J., Sebolt, J.T., Zhao, L., Lawrence, T.S., Smith, P.G., Morgan, M.A., and Sun, Y. (2012). Radiosensitization of human pancreatic cancer cells by MLN4924, an investigational NEDD8-activating enzyme inhibitor. Cancer Res *72*, 282-293.

Wei, D., and Sun, Y. (2010). Small RING Finger Proteins RBX1 and RBX2 of SCF E3 Ubiquitin Ligases: The Role in Cancer and as Cancer Targets. Genes Cancer *1*, 700-707.

Wooten, D.J., Groves, S.M., Tyson, D.R., Liu, Q., Lim, J.S., Albert, R., Lopez, C.F., Sage, J., and Quaranta, V. (2019). Systems-level network modeling of Small Cell Lung Cancer subtypes identifies master regulators and destabilizers. PLoS Comput Biol *15*, e1007343.

Xirodimas, D.P. (2008). Novel substrates and functions for the ubiquitin-like molecule NEDD8. Biochem Soc Trans *36*, 802-806.

Yamaoka, S., Courtois, G., Bessia, C., Whiteside, S.T., Weil, R., Agou, F., Kirk, H.E., Kay, R.J., and Israel, A. (1998). Complementation cloning of NEMO, a component of the IkappaB kinase complex essential for NF-kappaB activation. Cell *93*, 1231-1240.

Yang, F., Wang, J., Ren, H.Y., Jin, J., Wang, A.L., Sun, L.L., Diao, K.X., Wang, E.H., and Mi, X.Y. (2015). Proliferative role of TRAF4 in breast cancer by upregulating PRMT5 nuclear expression. Tumour Biol *36*, 5901-5911.

Yokoi, S., Yasui, K., Iizasa, T., Takahashi, T., Fujisawa, T., and Inazawa, J. (2003). Down-regulation of SKP2 induces apoptosis in lung-cancer cells. Cancer Sci *94*, 344-349.

Yoshinaga, T., and Sano, S. (1980). Coproporphyrinogen oxidase. I. Purification, properties, and activation by phospholipids. J Biol Chem *255*, 4722-4726.

Zandi, E., Rothwarf, D.M., Delhase, M., Hayakawa, M., and Karin, M. (1997). The IkappaB kinase complex (IKK) contains two kinase subunits, IKKalpha and IKKbeta, necessary for IkappaB phosphorylation and NF-kappaB activation. Cell *91*, 243-252.

Zhang, B., Dong, S., Li, Z., Lu, L., Zhang, S., Chen, X., Cen, X., and Wu, Y. (2015). Targeting protein arginine methyltransferase 5 inhibits human hepatocellular carcinoma growth via the downregulation of beta-catenin. J Transl Med *13*, 349.

Zhang, W., Girard, L., Zhang, Y.A., Haruki, T., Papari-Zareei, M., Stastny, V., Ghayee, H.K., Pacak, K., Oliver, T.G., Minna, J.D.*, et al.* (2018). Small cell lung cancer tumors and preclinical models display heterogeneity of neuroendocrine phenotypes. Transl Lung Cancer Res *7*, 32-49.

Zhao, H., Chiaro, C.R., Zhang, L., Smith, P.B., Chan, C.Y., Pedley, A.M., Pugh, R.J., French, J.B., Patterson, A.D., and Benkovic, S.J. (2015). Quantitative analysis of purine nucleotides indicates that purinosomes increase de novo purine biosynthesis. J Biol Chem *290*, 6705-6713.

Zhao, Y., Morgan, M.A., and Sun, Y. (2014). Targeting Neddylation pathways to inactivate cullin-RING ligases for anticancer therapy. Antioxid Redox Signal *21*, 2383-2400.

Chapter 6: Supplementary Tables

Table 1

RP mSCLC CRISPR Screen - Top Drop Out MAGeCK Results

Gene	RP Neg Score	RP Neg FDR	RP Neg Rank	RP LFC	MEF Neg Score	MEF Neg FDR	MEF Neg Rank	MEF LFC
Psma4	0.0000	0.0005	1	-3.2849	0.0000	0.0006	3	-4.5251
Cct4	0.0000	0.0005	2	-3.8255	0.0001	0.0518	152	-2.0108
Ppp1r8	0.0000	0.0005	3	-2.4806	0.0018	0.2838	658	-1.2777
Ftsj3	0.0000	0.0005	4	-3.4011	0.0000	0.0026	17	-4.1329
Phb	0.0000	0.0005	5	-2.7048	0.0000	0.0175	55	-2.0302
Mms22l	0.0000	0.0005	6	-2.4955	0.0000	0.0228	71	-3.7519
Fnta	0.0000	0.0005	7	-3.8573	0.0000	0.0262	91	-1.9052
Prmt5	0.0000	0.0005	8	-4.0980	0.0013	0.2358	565	-1.7182
Rps15	0.0000	0.0005	9	-4.0946	0.0000	0.0314	115	-2.0504
Rpia	0.0000	0.0005	10	-4.2629	0.4909	1.0000	14511	-0.1443
Adsl	0.0000	0.0010	11	-2.8865	0.1470	1.0000	6797	-0.3335
Snrpe	0.0000	0.0010	12	-3.9123	0.0046	0.4635	1003	0.3191
Gpn3	0.0000	0.0010	13	-1.6354	0.0004	0.1243	346	-0.8947
Rpl23a	0.0000	0.0012	14	-1.7373	0.0000	0.0228	72	-1.6994
Ewsr1	0.0000	0.0012	15	-1.7032	0.0347	0.9580	2699	-0.3583
Polr3h	0.0000	0.0012	16	-4.0263	0.0002	0.0924	271	-2.9285
Tuba1b	0.0000	0.0010	17	-2.8866	0.0004	0.0871	340	-2.7851
Ddx59	0.0000	0.0012	18	-2.0827	0.0026	0.3558	762	-1.3738
Rps3	0.0000	0.0012	19	-2.8271	0.0000	0.0175	51	-2.5961
Hist1h4n	0.0000	0.0005	20	-3.8732	0.9919	1.0000	21535	2.5166
Paics	0.0000	0.0016	21	-3.3718	0.0607	1.0000	3851	-0.3889
Rpusd4	0.0000	0.0016	22	-1.5756	0.0193	0.8248	1970	-0.7413
Nhp2l1	0.0000	0.0021	23	-4.1221	0.0000	0.0324	117	-2.5479
Rpl13a	0.0000	0.0021	24	-3.6369	0.0000	0.0262	90	-3.6982
Polr2c	0.0000	0.0019	25	-2.9950	0.0175	0.7787	1888	0.1810
Kansl3	0.0000	0.0021	26	-2.4455	0.0036	0.4160	898	-1.5648
Grwd1	0.0000	0.0019	27	-2.1719	0.0002	0.0805	235	-1.3284
Flii	0.0000	0.0021	28	-2.4222	0.1843	1.0000	7907	-0.3161
Atad3a	0.0000	0.0021	29	-2.6143	0.0000	0.0270	94	-1.6730
Pet112	0.0000	0.0021	30	-2.2886	0.1083	1.0000	5649	-0.3682
Heatr3	0.0000	0.0021	31	-2.4382	0.0212	0.8488	2054	-0.5895
Cad	0.0000	0.0021	32	-3.6636	0.2389	1.0000	9429	-0.0976
Phb2	0.0000	0.0021	33	-4.5553	0.0000	0.0402	136	-2.2162
Rps15a	0.0000	0.0021	34	-2.8621	0.0000	0.0006	2	-2.7517
Upf1	0.0000	0.0022	35	-2.3252	0.0000	0.0212	69	-1.6019
Chchd4	0.0000	0.0025	36	-2.5980	0.0356	0.9644	2742	-0.4763
Pop1	0.0000	0.0025	37	-2.8208	0.0002	0.0765	219	-1.9705
Polr3k	0.0000	0.0026	38	-2.5599	0.0000	0.0035	20	-3.5574
Bcl2l1	0.0000	0.0026	39	-2.1563	0.2770	1.0000	10443	-0.3570
Naa20	0.0000	0.0026	40	-3.3359	0.0000	0.0340	124	-3.7874
Wdr77	0.0000	0.0021	41	-2.8568	0.0023	0.3046	726	-1.7481
Tcp1	0.0000	0.0027	42	-2.7453	0.0000	0.0200	64	-3.7364
Ndufs2	0.0000	0.0027	43	-2.5398	0.1818	1.0000	7837	-1.0344
Gm5796	0.0000	0.0021	44	-1.1509	0.1254	0.9682	6147	-3.0392
Hnrnpu	0.0000	0.0028	45	-2.1594	0.0408	0.9847	2981	-1.2772
Vps28	0.0000	0.0025	46	-1.5478	0.0003	0.0946	291	-1.0372
Kat8	0.0000	0.0029	47	-1.5488	0.0019	0.2944	676	-1.5577
Urod	0.0000	0.0030	48	-2.5228	0.0004	0.1264	349	-0.9487
Rpl12	0.0000	0.0030	49	-4.5646	0.0000	0.0091	31	-3.7400
Vps25	0.0000	0.0030	50	-4.4674	0.0003	0.0990	280	-4.3603

Table 1

RP mSCLC CRISPR Screen - Top Drop Out MAGeCK Results

Gene	RP Neg Score	RP Neg FDR	RP Neg Rank	RP LFC	MEF Neg Score	MEF Neg FDR	MEF Neg Rank	MEF LFC
Mrp63	0.0000	0.0030	51	-5.3585	0.0001	0.0518	153	-3.1132
Gps1	0.0000	0.0030	52	-2.6639	0.0021	0.3136	712	-0.9963
Rbbp4	0.0000	0.0031	53	-1.6348	0.0001	0.0671	189	-2.2114
Dars2	0.0000	0.0031	54	-2.9816	0.0024	0.3395	737	-1.1831
Nup43	0.0000	0.0032	55	-4.9766	0.0273	0.8993	2378	-0.9306
Mtif2	0.0000	0.0032	56	-3.6635	0.0014	0.2507	598	-1.1225
Ash2l	0.0000	0.0032	57	-3.1149	0.0534	1.0000	3523	-0.7378
Tubb5	0.0000	0.0032	58	-3.9591	0.0000	0.0321	116	-3.0895
Impdh2	0.0000	0.0032	59	-2.8465	0.0095	0.6425	1421	-0.7911
Pno1	0.0000	0.0032	60	-2.8619	0.0006	0.1617	417	-2.2935
Rps27rt	0.0000	0.0032	61	-2.7378	0.0000	0.0011	11	-2.5454
Plk4	0.0000	0.0032	62	-3.4048	0.9650	1.0000	20873	0.0873
Atp2a2	0.0000	0.0032	63	-2.4809	0.0000	0.0095	34	-3.2869
BC052040	0.0000	0.0032	64	-1.5404	0.0001	0.0541	159	-2.0102
Ndufa1	0.0000	0.0034	65	-3.0397	0.0004	0.1315	358	-1.9040
Sepsecs	0.0000	0.0034	66	-3.9856	0.0005	0.1338	367	-4.2342
Pabpn1	0.0000	0.0032	67	-4.7861	0.0000	0.0175	54	-2.7585
Nedd8	0.0000	0.0034	68	-2.7570	0.0024	0.3395	741	-2.0469
Cul2	0.0000	0.0034	69	-2.7120	0.0091	0.6307	1382	-1.7286
Mrpl4	0.0000	0.0034	70	-4.0923	0.0058	0.5245	1106	-2.5066
Dctn5	0.0000	0.0034	71	-3.2635	0.0062	0.5409	1140	-2.3796
Nol11	0.0000	0.0034	72	-2.8544	0.0010	0.2142	525	-1.3593
Snrpd1	0.0000	0.0034	73	-4.3031	0.0000	0.0402	137	-3.0857
Rpl14	0.0000	0.0034	74	-3.1446	0.0000	0.0079	27	-3.1973
Gabpb1	0.0000	0.0034	75	-1.9951	0.0066	0.5558	1165	-1.0416
Fam96b	0.0000	0.0034	77	-2.5464	0.0000	0.0291	102	-2.2719
Vwa9	0.0000	0.0034	78	-3.9601	0.0854	1.0000	4880	-0.7062
Tkt	0.0000	0.0034	79	-2.4632	0.2895	1.0000	10779	-0.4068
Rngtt	0.0000	0.0036	80	-3.4464	0.0000	0.0212	66	-3.3596
Mdn1	0.0000	0.0037	81	-2.5165	0.0001	0.0548	163	-2.6301
Dkc1	0.0000	0.0037	82	-2.3458	0.0004	0.1187	326	-1.1673
Ddx39b	0.0000	0.0037	83	-3.7145	0.0392	0.9784	2902	-0.8242
Eef2	0.0000	0.0037	84	-2.4294	0.0000	0.0006	7	-2.7121
Kti12	0.0000	0.0037	85	-2.5306	0.0049	0.4793	1022	-1.1667
Lars	0.0000	0.0037	86	-1.9703	0.1604	1.0000	7193	-0.0549
Psmb4	0.0000	0.0039	87	-3.1854	0.0000	0.0161	48	-2.6348
Polr2h	0.0000	0.0039	88	-3.6024	0.0001	0.0477	157	-2.1509
Rpl10	0.0000	0.0039	89	-2.7906	0.0002	0.0774	225	-1.9556
Espl1	0.0000	0.0039	90	-3.6544	0.0000	0.0291	105	-3.0893
Lars2	0.0000	0.0039	91	-1.4276	0.0001	0.0660	186	-1.8620
Mrps14	0.0000	0.0039	92	-2.6303	0.0077	0.5932	1269	-1.3032
Eif3f	0.0000	0.0039	93	-2.9288	0.0003	0.1115	311	-1.3406
Aldoa	0.0000	0.0039	94	-1.5341	0.0000	0.0006	4	-2.8313
Sec13	0.0000	0.0041	95	-1.0170	0.0048	0.4767	1020	-0.6790
0610010B08Rik	0.0000	0.0022	96	-2.0590	0.0014	0.1009	605	-1.5694
Rpap2	0.0000	0.0044	97	-2.4256	0.0033	0.3965	860	-2.8832
Hspa5	0.0000	0.0045	98	-3.3276	0.0000	0.0034	19	-5.9873
Mtg2	0.0000	0.0045	99	-2.8144	0.0173	0.7956	1876	-0.8140
Rpl30	0.0000	0.0045	100	-4.9854	0.0000	0.0015	15	-5.9927
Mcm3ap	0.0000	0.0045	101	-2.3214	0.0002	0.0871	259	-1.7899

Table 1

RP mSCLC CRISPR Screen - Top Drop Out MAGeCK Results

Gene	RP Neg Score	RP Neg FDR	RP Neg Rank	RP LFC	MEF Neg Score	MEF Neg FDR	MEF Neg Rank	MEF LFC
Tamm41	0.0000	0.0045	102	-3.0000	0.0020	0.3054	694	-2.8393
Wdr5	0.0000	0.0045	103	-2.3345	0.0034	0.4034	878	-1.0171
Eef1a1	0.0000	0.0050	104	-1.4767	0.0005	0.1388	379	-1.4377
Ddx10	0.0000	0.0050	105	-3.3359	0.0000	0.0071	23	-2.5601
Tars2	0.0000	0.0051	106	-1.9966	0.0454	1.0000	3187	-0.8741
Snrpa1	0.0000	0.0054	107	-2.1987	0.0003	0.1065	295	-2.7692
Cpox	0.0000	0.0054	108	-3.0990	0.5669	1.0000	15825	0.6483
Mrpl36	0.0000	0.0054	109	-1.7406	0.0021	0.3136	713	-0.9096
Nhlrc2	0.0000	0.0054	110	-1.3497	0.1222	1.0000	6052	-0.3423
Zzz3	0.0000	0.0057	111	-2.6241	0.0035	0.4110	892	-1.7727
Rps12	0.0000	0.0058	112	-4.5281	0.0021	0.3120	711	-3.0768
Eif6	0.0000	0.0058	113	-4.8691	0.0000	0.0283	99	-4.2680
Mrpl41	0.0000	0.0063	114	-1.6218	0.0009	0.1984	479	-1.1764
Rpl7	0.0000	0.0068	115	-3.1406	0.0000	0.0011	13	-3.6621
Tpt1	0.0000	0.0068	116	-4.3933	0.0002	0.0871	261	-3.2587
Gm16381	0.0000	0.0054	117	-2.7579	0.0011	0.2120	533	-2.7467
Rps17	0.0000	0.0054	118	-2.1920	0.0003	0.0921	279	-2.1681
Mrpl23	0.0000	0.0078	119	-3.0191	0.0010	0.2120	507	-1.1670
Fdx1l	0.0000	0.0080	120	-2.0796	0.0112	0.6791	1564	-0.8865
Rps13	0.0000	0.0084	121	-2.3525	0.0000	0.0158	43	-3.8660
Pstk	0.0000	0.0085	122	-2.1725	0.0000	0.0191	62	-2.3116
Irs2	0.0000	0.0085	123	-1.8764	0.0125	0.7113	1637	-0.8021
Npat	0.0000	0.0085	124	-3.0755	0.0002	0.0776	226	-1.4976
Polr2l	0.0000	0.0086	125	-3.3395	0.0000	0.0395	135	-2.2578
Sacm1l	0.0000	0.0086	126	-2.2698	0.0033	0.4011	865	-0.5146
Smc3	0.0000	0.0086	127	-1.4053	0.0003	0.1162	319	-1.1893
Uqcrb	0.0000	0.0086	128	-4.0161	0.0003	0.1081	308	-2.1262
Anapc1	0.0000	0.0086	129	-2.2523	0.0009	0.2062	494	-2.1394
Pfdn1	0.0000	0.0086	130	-1.8378	0.0000	0.0258	85	-2.0932
Rfc4	0.0000	0.0089	131	-1.6003	0.0182	0.8075	1920	-0.7556
Pes1	0.0000	0.0089	132	-1.8721	0.0001	0.0464	148	-1.8813
Psmd4	0.0000	0.0068	133	-2.1268	0.0003	0.1065	313	-1.4683
Tsr2	0.0000	0.0068	134	-2.2711	0.0013	0.2252	572	-1.1543
Rpl39	0.0000	0.0068	135	-3.7959	0.0047	0.4366	1012	-3.4099
Rpl9	0.0000	0.0089	136	-4.2389	0.0000	0.0175	53	-5.1788
Cdk1	0.0000	0.0089	137	-3.6385	0.0018	0.2933	670	-2.7661
Mrpl17	0.0000	0.0089	138	-3.7225	0.0174	0.7958	1879	-1.2367
Imp3	0.0000	0.0089	139	-3.7181	0.0005	0.1354	371	-2.4298
Cyc1	0.0000	0.0092	140	-2.9049	0.0018	0.2846	659	-1.2469
Slc7a5	0.0000	0.0092	141	-2.5717	0.7672	1.0000	18393	0.3573
Terf2	0.0000	0.0096	142	-3.5392	0.0003	0.1081	307	-1.9574
Hdac3	0.0000	0.0099	143	-3.3572	0.0007	0.1716	429	-1.2053
Thap11	0.0000	0.0099	144	-3.3304	0.0000	0.0188	60	-3.2351
Hmbs	0.0000	0.0099	145	-2.0030	0.1895	1.0000	8039	0.6416
U2af1	0.0000	0.0105	146	-4.1908	0.0330	0.9467	2625	-1.2614
Ppcs	0.0000	0.0105	147	-3.5885	0.0108	0.6742	1526	-0.9268
Mettl1	0.0000	0.0105	148	-2.0427	0.1144	1.0000	5834	-0.4349
Gtpbp4	0.0000	0.0105	149	-3.8819	0.0000	0.0006	5	-3.4494
Sfpq	0.0000	0.0108	150	-1.9954	0.0011	0.2162	526	-1.3999
Dhps	0.0000	0.0108	151	-3.8227	0.0000	0.0257	84	-4.7689

Table 1

RP mSCLC CRISPR Screen - Top Drop Out MAGeCK Results

Gene	RP Neg Score	RP Neg FDR	RP Neg Rank	RP LFC	MEF Neg Score	MEF Neg FDR	MEF Neg Rank	MEF LFC
Mrpl21	0.0000	0.0108	152	-2.4565	0.0022	0.3233	718	-1.7177
Hsd17b10	0.0000	0.0108	153	-3.9638	0.0005	0.1348	370	-2.5139
Psmd6	0.0000	0.0108	154	-2.7387	0.0000	0.0366	128	-1.2897
Znhit2	0.0000	0.0108	155	-3.4950	0.0000	0.0382	131	-4.3232
Rpl36a	0.0000	0.0108	156	-0.9533	0.0000	0.0191	61	-1.6165
Pnkp	0.0000	0.0086	157	-2.1442	0.0004	0.1110	329	-1.8572
Psmc5	0.0000	0.0111	158	-2.8065	0.0028	0.3690	781	-1.1635
Ddost	0.0000	0.0111	159	-1.8737	0.0007	0.1786	453	-1.5643
Mis18a	0.0000	0.0112	160	-3.0860	0.0374	0.9718	2819	-1.1449
Atp5h	0.0000	0.0112	161	-1.9562	0.1522	1.0000	6948	-0.4683
Rad21	0.0000	0.0112	162	-3.0997	0.0257	0.8912	2291	-1.5469
Nampt	0.0000	0.0112	163	-3.5919	0.7956	1.0000	18750	0.1356
Qrsl1	0.0000	0.0114	164	-2.8222	0.0001	0.0444	144	-1.8125
Cdc45	0.0000	0.0114	165	-2.9419	0.0000	0.0277	98	-1.9737
Slc7a6os	0.0000	0.0114	166	-1.8637	0.0004	0.1243	345	-1.7003
Gfer	0.0000	0.0114	167	-2.1652	0.0030	0.3806	814	-0.7277
Gm21637	0.0000	0.0094	168	-3.9203	0.0029	0.3081	795	-6.3473
Ppil1	0.0000	0.0114	169	-2.6158	0.0434	0.9992	3087	-1.0462
Tceb2	0.0000	0.0118	170	-2.0917	0.0002	0.0829	241	-1.3325
Bub1b	0.0000	0.0118	171	-2.9103	0.0006	0.1536	393	-3.0335
Ddx56	0.0000	0.0118	172	-2.4156	0.0000	0.0277	97	-4.5949
Rpl21	0.0000	0.0119	173	-2.3856	0.0000	0.0079	28	-6.2838
Wdr26	0.0000	0.0119	174	-2.2592	0.0172	0.7950	1871	-1.0552
Mrpl43	0.0000	0.0119	175	-3.5144	0.0001	0.0547	161	-1.9715
Cdipt	0.0000	0.0119	176	-3.5595	0.0026	0.3616	767	-1.1877
Apex2	0.0000	0.0119	177	-1.7313	0.2998	1.0000	11046	-0.1328
Ssbp1	0.0000	0.0120	178	-2.8713	0.2509	1.0000	9771	-0.2260
Nup160	0.0000	0.0124	179	-4.0019	0.0367	0.9685	2785	-1.4407
Tsen54	0.0000	0.0124	180	-4.6181	0.0039	0.4280	944	-2.0658
Ccdc130	0.0000	0.0124	181	-2.8632	0.1296	1.0000	6270	-0.4054
Crnkl1	0.0000	0.0124	182	-3.1104	0.0382	0.9774	2848	-0.5497
Tbcb	0.0000	0.0124	183	-2.6091	0.0002	0.0871	257	-2.1791
Dut	0.0000	0.0124	184	-2.4986	0.0004	0.1188	328	-2.3143
Nop58	0.0000	0.0124	185	-4.4255	0.0015	0.2616	619	-1.6436
Ints9	0.0000	0.0124	186	-2.1701	0.0000	0.0179	58	-2.5582
Wdr55	0.0000	0.0108	187	-2.6412	0.0075	0.5531	1249	-1.6144
Wdr61	0.0000	0.0130	188	-2.4267	0.0356	0.9644	2741	-0.7443
Birc6	0.0000	0.0137	189	-1.4364	0.0561	1.0000	3647	-0.3023
Rbm25	0.0000	0.0137	190	-2.0398	0.0013	0.2401	573	-0.8700
Gm5797	0.0000	0.0107	191	-2.2299	0.0076	0.5154	1266	-0.8987
Cct6a	0.0000	0.0138	192	-3.3481	0.0010	0.2122	511	-2.5926
Uspl1	0.0000	0.0144	193	-1.5355	0.0034	0.4016	868	-0.2873
Taf1c	0.0000	0.0144	194	-1.1857	0.0845	1.0000	4855	-0.4780
Cpsf3l	0.0000	0.0144	195	-2.6456	0.0061	0.5369	1134	-0.8720
Lyrm4	0.0000	0.0144	196	-2.1642	0.0023	0.3372	731	-0.9802
Rps29	0.0000	0.0144	197	-3.5027	0.0000	0.0095	35	-6.2215
Ttc27	0.0000	0.0144	198	-3.2023	0.0001	0.0613	171	-1.1206
Shfm1	0.0000	0.0118	199	-2.6144	0.0002	0.0766	240	-5.2308
Gnb2l1	0.0000	0.0147	200	-1.6870	0.0003	0.1009	288	-1.7611
Ndufaf5	0.0000	0.0147	201	-2.4693	0.0481	1.0000	3291	-0.1006

Table 1

RP mSCLC CRISPR Screen - Top Drop Out MAGeCK Results

Gene	RP Neg Score	RP Neg FDR	RP Neg Rank	RP LFC	MEF Neg Score	MEF Neg FDR	MEF Neg Rank	MEF LFC
Mthfd1	0.0000	0.0147	202	-1.6121	0.5760	1.0000	15994	0.4585
Gm2913	0.0000	0.0120	203	-2.7594	0.0004	0.0485	327	-3.2880
Vmn2r37	0.0000	0.0086	204	-0.5473	0.7471	1.0000	18120	0.5071
Rpl26	0.0000	0.0149	205	-2.1939	0.0000	0.0382	133	-4.9236
Urb1	0.0000	0.0150	206	-1.5623	0.0091	0.6310	1390	-0.3953
Hypk	0.0000	0.0151	207	-2.2322	0.0843	1.0000	4847	-0.4044
Dnm1l	0.0000	0.0124	208	-1.3534	0.0511	1.0000	3433	-0.7589
Prdx1	0.0000	0.0152	209	-2.3590	0.2655	1.0000	10125	-0.3328
Bard1	0.0000	0.0152	210	-3.1360	0.0146	0.7501	1745	-1.5678
Nop56	0.0000	0.0152	211	-1.9941	0.0000	0.0341	125	-1.6725
Med17	0.0000	0.0153	212	-2.4023	0.0015	0.2603	616	-1.8384
Yy1	0.0000	0.0153	213	-1.1491	0.0009	0.1972	474	-1.0539
Tbcd	0.0000	0.0153	214	-1.9455	0.0002	0.0855	248	-1.8602
Tsg101	0.0000	0.0153	215	-2.7728	0.0001	0.0552	164	-3.9878
Rpl17	0.0000	0.0153	216	-3.8048	0.0002	0.0822	238	-2.3265
Pwp1	0.0000	0.0158	217	-1.7726	0.1991	1.0000	8321	-0.3908
Rbx1	0.0000	0.0159	218	-2.5560	0.0129	0.7194	1664	-1.0657
Cdc16	0.0000	0.0159	219	-1.4960	0.0001	0.0643	180	-1.9674
Hnrnpk	0.0000	0.0159	220	-2.9987	0.0010	0.2139	524	-5.4759
Mrpl20	0.0000	0.0159	221	-2.6574	0.0032	0.3925	849	-1.3809
Gcsh	0.0000	0.0160	222	-1.0221	0.1129	1.0000	5779	0.2612
Krr1	0.0000	0.0164	223	-3.4573	0.0003	0.1164	322	-3.2515
Stip1	0.0000	0.0165	224	-2.9742	0.0015	0.2588	614	-1.5709
Rrp7a	0.0000	0.0165	225	-2.6954	0.0096	0.6425	1424	-1.4894
Rtcb	0.0000	0.0165	226	-2.3767	0.0035	0.4075	888	-0.8230
Las1l	0.0000	0.0165	227	-1.9716	0.0032	0.3900	844	-0.8826
Plk1	0.0000	0.0166	228	-4.4464	0.0012	0.2276	539	-2.8873
Ppan	0.0000	0.0169	229	-2.5714	0.0000	0.0262	92	-0.9949
Dclre1b	0.0000	0.0170	230	-0.9337	0.8286	1.0000	19230	0.4669
Dcaf7	0.0000	0.0171	231	-2.0702	0.0478	1.0000	3280	-0.5613
Bap1	0.0000	0.0171	232	-1.6970	0.2558	1.0000	9886	-0.2600
Narfl	0.0000	0.0172	233	-2.4251	0.0001	0.0730	214	-2.2019
Atxn10	0.0000	0.0175	234	-2.5159	0.0035	0.4067	887	-0.9783
Mcrs1	0.0000	0.0182	235	-2.0663	0.8258	1.0000	19188	0.3802
Crcp	0.0000	0.0185	236	-3.0592	0.0280	0.9088	2400	-0.3779
Mterfd2	0.0000	0.0185	237	-1.4006	0.2257	1.0000	9061	-0.1349
Amd1	0.0000	0.0187	238	-3.5430	0.2431	1.0000	9551	-0.2294
Nars2	0.0000	0.0188	239	-1.9482	0.0107	0.6742	1519	-1.0894
Vmp1	0.0000	0.0160	240	-4.1965	0.0015	0.2409	611	-3.2492
Ahctf1	0.0000	0.0188	241	-2.7862	0.0036	0.4140	897	-2.6027
Slc25a51	0.0000	0.0188	242	-3.4548	0.0566	1.0000	3668	-0.8405
Zfp207	0.0000	0.0188	243	-3.8753	0.0023	0.3287	722	-1.9238
Rtfdc1	0.0000	0.0188	244	-1.8905	0.0114	0.6838	1583	-0.1610
Nfib	0.0000	0.0161	245	-2.0769	0.1156	1.0000	5863	0.1044
Rpl7l1	0.0000	0.0188	246	-2.3416	0.0002	0.0855	246	-3.0636
Gclc	0.0000	0.0192	247	-2.1815	0.7241	1.0000	17877	0.1721
Suds3	0.0000	0.0194	248	-3.5187	0.7311	1.0000	17950	0.2350
Gm2863	0.0000	0.0112	249	-2.9955	0.9042	1.0000	20090	1.0948
Taf11	0.0000	0.0199	250	-2.2603	0.0314	0.9355	2550	-0.7841
Actr2	0.0000	0.0199	251	-3.1533	0.0009	0.2072	495	-1.8837

Table 2

RP mSCLC CRISPR Screen - Top Enrichment MAGeCK Results

Gene	RP Pos Score	RP Pos FDR	RP Pos Rank	RP LFC	MEF Pos Score	MEF Pos FDR	MEF Pos Rank	MEF LFC
Crebbp	0.0000	0.0025	1	2.5090	0.5887	1.0000	16394	-1.5393
Spink5	0.0000	0.0025	2	2.1160	0.2089	0.9999	9391	0.1925
Tada2b	0.0000	0.0327	3	1.9824	0.0181	0.8724	1654	-0.0733
Bcl2l11	0.0000	0.0327	4	2.2622	0.0700	0.9586	4615	0.6344
Olfr1459	0.0000	0.0327	5	1.4327	0.0069	0.7813	843	1.0201
Mid2	0.0000	0.0930	6	1.5626	0.0416	0.9369	3107	0.6717
Pten	0.0000	0.0975	7	2.1074	0.0000	0.0031	7	0.9720
Pcdhgc5	0.0000	0.0799	8	1.1618	0.5034	1.0000	15206	0.1717
Gm3402	0.0000	0.0799	9	1.7676	0.4241	1.0000	13812	-1.7508

Table 3
MLN4924 Suppressor Screen - Top Enriched Genes

Gene	P12 #1	P12 #2	P12 #3	Avg P12	MLN #1	MLN #2	MLN #3	Avg MLN	MLN-P12 Diff
COPS4	-0.5003	-0.4075	-0.7430	-0.5503	4.1187	4.5016	4.6482	4.4228	4.9731
NFE2L2	0.1276	0.0650	0.1787	0.1238	3.8474	4.7670	3.8858	4.1667	4.0429
CDKN1A	0.4299	0.1021	0.1471	0.2264	4.7443	3.6368	4.0349	4.1387	3.9123
COPS8	-0.2751	-0.3106	-0.1592	-0.2483	3.4625	3.8326	3.5817	3.6256	3.8739
COPS7B	0.2962	0.2600	0.1430	0.2330	3.5667	4.4080	3.0758	3.6835	3.4505
CREBBP	0.3666	0.5747	0.4538	0.4650	4.0834	3.6801	3.5321	3.7652	3.3001
CDKN1B	0.4631	0.1019	0.2774	0.2808	3.6477	3.4486	3.5282	3.5415	3.2607
IRAK1	-0.2550	0.0829	0.1084	-0.0212	2.9509	3.4332	2.9875	3.1238	3.1451
COPS2	-0.3838	-0.3713	-0.1049	-0.2867	2.6557	2.2473	3.0919	2.6650	2.9517
WDR24	-0.8362	-0.7762	-0.9800	-0.8641	1.9547	2.1752	1.0815	1.7372	2.6013
MIOS	-0.3269	-0.3790	-0.5947	-0.4335	2.6465	1.8563	1.8555	2.1194	2.5529
MAP2K7	0.8523	1.0459	0.7623	0.8868	2.9072	3.8887	3.2008	3.3322	2.4453
WDR59	-0.3152	-0.3739	-0.3237	-0.3376	2.1750	2.3164	1.8306	2.1074	2.4449
PQBP1	-0.7144	-0.9975	-0.5228	-0.7449	1.8652	1.5669	1.4455	1.6259	2.3708
MYD88	0.2701	0.1698	0.4379	0.2926	2.4564	2.6348	2.7840	2.6251	2.3325
KDM3B	0.1270	-0.0689	0.2112	0.0898	2.4730	2.0277	2.3398	2.2802	2.1904
TIRAP	0.1385	0.0563	0.2453	0.1467	2.6190	2.0577	2.2395	2.3054	2.1587
TLR2	0.3662	0.2051	0.2881	0.2865	2.1234	2.9779	2.1486	2.4166	2.1302
IKBKG	-0.1484	-0.0688	-0.1374	-0.1182	2.4144	1.8004	1.7348	1.9832	2.1014
RNASEH2B	-0.6115	-0.4187	-0.5037	-0.5113	1.6491	1.3652	1.7534	1.5892	2.1005
KHDRBS1	0.3929	-0.0296	-0.0834	0.0933	3.1423	1.2355	2.1143	2.1640	2.0707
MTOR	-0.6462	-0.4832	-0.7468	-0.6254	2.0808	1.3574	0.8249	1.4210	2.0464
COPS3	0.0998	-0.2158	-0.1231	-0.0797	1.6718	2.3479	1.7957	1.9385	2.0182
FZR1	0.3983	-0.2163	-0.0224	0.0532	1.9114	1.9180	2.3718	2.0670	2.0138
UBE2M	-1.0054	-1.1777	-0.8829	-1.0220	0.5180	1.2046	1.0861	0.9362	1.9583
KMT2C	-0.0168	0.1842	0.3049	0.1575	2.1230	2.4900	1.5758	2.0629	1.9055
ARID1A	-0.1749	-0.0544	0.0901	-0.0464	1.9747	1.2726	2.2754	1.8409	1.8873
RPTOR	-0.9420	-1.0461	-0.6961	-0.8947	0.9970	1.1729	0.7502	0.9734	1.8681
RNASEH2A	-0.6411	-0.4485	-0.7169	-0.6022	1.2705	1.1013	1.4128	1.2615	1.8637
TP73	-0.1591	0.0632	-0.1366	-0.0775	2.0148	1.7962	1.4630	1.7580	1.8355
GADD45G	-0.1184	-0.4455	0.0868	-0.1590	1.6897	2.0283	1.2613	1.6598	1.8188
KMT2D	0.1963	0.2575	0.3143	0.2560	2.0752	2.1657	1.7435	1.9948	1.7387
MLL2	0.3883	0.4711	0.4101	0.4232	2.0357	2.5005	1.8699	2.1354	1.7122
COPS6	-0.5897	-0.4914	-0.6276	-0.5696	0.8038	1.4185	1.1720	1.1315	1.7010
CSNK1A1	-0.0615	0.2326	0.0529	0.0747	2.2864	0.8956	2.1152	1.7657	1.6911
GADD45A	-0.0438	-0.0247	0.1559	0.0291	2.2082	1.7614	1.1638	1.7111	1.6820
HNRNPA2B1	-0.8882	-0.8736	-0.5701	-0.7773	0.2705	1.2573	1.1476	0.8918	1.6691
AIP	0.0063	-0.2571	-0.4184	-0.2231	1.4868	1.5084	1.1744	1.3899	1.6129
hsa-mir-718	0.4565	0.0904	0.1171	0.2214	2.3660	1.2181	1.7517	1.7786	1.5572
NAE1	-1.0376	-0.8052	-0.8418	-0.8949	1.3856	-0.1522	0.6194	0.6176	1.5125
IRAK4	-0.0752	0.1900	0.0614	0.0587	1.8584	1.5018	1.3295	1.5632	1.5045
SEH1L	-0.6154	-0.5040	-0.5058	-0.5417	0.8899	1.2185	0.7569	0.9551	1.4968
STT3A	-0.3908	-0.3132	-0.4520	-0.3854	1.7123	0.7059	0.7948	1.0710	1.4563

Table 3
MLN4924 Suppressor Screen - Top Enriched Genes

Gene	P12 #1	P12 #2	P12 #3	Avg P12	MLN #1	MLN #2	MLN #3	Avg MLN	MLN-P12 Diff
PPRC1	-0.2413	-0.3870	-0.4048	-0.3443	1.1548	1.1805	0.9360	1.0904	1.4348
RNF31	-0.1340	0.1675	0.0198	0.0178	1.6336	1.3839	1.3165	1.4447	1.4269
GPS1	-0.7438	-0.3905	-0.5661	-0.5668	1.2236	0.7206	0.6151	0.8531	1.4199
JUN	0.4666	0.3314	0.2334	0.3438	1.8108	1.9712	1.4802	1.7541	1.4103
ATXN2L	0.1160	-0.2129	-0.0315	-0.0428	1.3624	1.5432	1.1566	1.3540	1.3968
MAP3K7	0.1815	0.0015	0.1992	0.1274	1.3323	1.1893	1.9942	1.5053	1.3779
PAX5	0.3138	0.3336	0.2000	0.2824	1.3072	2.1034	1.5233	1.6446	1.3622
CHUK	0.1364	0.2599	0.0331	0.1431	1.4927	1.7369	1.2833	1.5043	1.3612
DEAF1	0.4192	0.2651	0.3444	0.3429	1.5430	1.9454	1.6185	1.7023	1.3594
SLC30A1	-0.0552	0.2247	-0.1288	0.0136	1.2257	1.6385	1.2300	1.3647	1.3512
PKNOX1	0.0254	-0.0755	-0.2017	-0.0839	1.6010	0.9738	1.1974	1.2574	1.3413
EIF4G1	-0.6733	-0.4149	-0.5216	-0.5366	0.9777	0.3462	1.0715	0.7984	1.3350
MAP3K4	-0.3870	-0.4989	-0.3814	-0.4224	1.2981	0.3907	1.0462	0.9117	1.3341
DPP9	0.2845	0.3346	0.3519	0.3237	1.7256	2.0672	1.1794	1.6574	1.3337
MIER3	0.2755	0.3208	0.3196	0.3053	2.0210	1.8020	1.0834	1.6355	1.3302
COPS7A	0.4018	0.2012	0.1566	0.2532	1.5692	1.9504	1.1941	1.5712	1.3180
CPEB4	0.1343	-0.0099	0.1371	0.0871	1.6956	0.8122	1.7013	1.4030	1.3159
NUFIP2	-0.1317	-0.1350	-0.0123	-0.0930	0.6597	1.5547	1.4418	1.2188	1.3118
PAPOLA	0.2358	-0.0613	0.0975	0.0907	1.2284	1.3920	1.5340	1.3848	1.2941
RBM47	-0.8320	-0.8545	-0.8104	-0.8323	0.7412	0.1824	0.4109	0.4448	1.2771
HNRNPD	-0.3239	-0.4419	-0.6195	-0.4618	0.4421	0.7978	1.2007	0.8135	1.2753
EIF4H	-0.5306	-0.4558	-0.3724	-0.4529	1.0055	0.6458	0.7845	0.8120	1.2649
LIN37	0.6489	0.3177	0.3542	0.4403	1.7011	1.5813	1.8210	1.7011	1.2609
RNASEH2C	-0.1602	-0.3830	-0.4390	-0.3274	1.0968	0.8477	0.8381	0.9275	1.2549
STT3B	-0.5442	-0.3983	-0.3515	-0.4313	0.9982	1.2024	0.2333	0.8113	1.2426
MPC1	0.6880	0.6151	0.3647	0.5559	2.1240	2.0772	1.1263	1.7758	1.2199
HSP90B1	0.0634	0.0215	0.0310	0.0387	1.3924	1.2707	1.0939	1.2523	1.2137
USP22	-0.0278	-0.1142	-0.0869	-0.0763	1.4869	1.2298	0.6858	1.1342	1.2105
LIN9	0.0552	0.5645	-0.0458	0.1913	1.7965	0.9677	1.4066	1.3903	1.1990
MAFG	-0.0566	-0.1677	-0.1302	-0.1182	0.9076	1.1012	1.1885	1.0658	1.1840
NCOR1	0.4426	0.0874	0.1229	0.2176	1.4380	1.5105	1.2206	1.3897	1.1721
HNRNPAB	-0.2333	-0.0599	0.1275	-0.0553	0.9466	1.1093	1.2940	1.1167	1.1719
SRM	0.3097	0.2112	0.2564	0.2591	1.4203	2.2561	0.5888	1.4217	1.1626
ELP5	-1.0120	-0.9912	-1.0870	-1.0301	-0.3147	0.2295	0.4556	0.1235	1.1535
CTU1	-0.7838	-0.8257	-0.8069	-0.8055	0.2557	0.3117	0.4490	0.3388	1.1443
SIRT1	-0.2768	-0.3203	-0.0732	-0.2235	1.1893	1.0360	0.5283	0.9179	1.1414
ELF3	0.0688	-0.1163	-0.0871	-0.0449	1.4780	0.6541	1.1439	1.0920	1.1369
RHEB	-0.2376	-0.2254	-0.2590	-0.2407	1.1656	0.8909	0.5955	0.8840	1.1247
WBP4	-0.6175	-0.1366	-0.2845	-0.3462	0.4406	0.8373	1.0530	0.7770	1.1232
PMAIP1	0.3469	0.3356	0.4710	0.3845	1.4856	1.4880	1.5467	1.5068	1.1223
CTU2	-0.6879	-0.4802	-0.6872	-0.6184	1.2434	0.0418	0.0759	0.4537	1.0721
GDAP2	-0.2965	-0.0252	-0.0387	-0.1201	1.2530	0.9550	0.6388	0.9489	1.0691
TMX1	-0.5908	-0.6428	-0.4996	-0.5777	0.2809	0.8009	0.3666	0.4828	1.0605

Table 3
MLN4924 Suppressor Screen - Top Enriched Genes

Gene	P12 #1	P12 #2	P12 #3	Avg P12	MLN #1	MLN #2	MLN #3	Avg MLN	MLN-P12 Diff
SREBF1	-0.6469	-0.0743	-0.5781	-0.4331	0.8362	0.5376	0.4846	0.6194	1.0525
RBCK1	-0.0510	-0.1758	-0.0650	-0.0973	1.0029	1.1626	0.6925	0.9527	1.0500
AHR	-0.0448	-0.1602	0.0313	-0.0579	1.0483	1.1386	0.7846	0.9905	1.0484
RFX5	-0.3111	-0.2520	-0.2759	-0.2797	0.7801	0.6826	0.8176	0.7601	1.0398
USP24	-0.2467	-0.0586	-0.0432	-0.1162	1.0011	0.9165	0.8325	0.9167	1.0329
SLC5A10	-0.1465	-0.4085	-0.0725	-0.2091	1.1885	0.7551	0.5075	0.8170	1.0262
MOCS3	-0.2841	-0.6660	-0.7871	-0.5791	0.4868	0.2980	0.5431	0.4427	1.0217
IPO11	-0.5932	-0.6341	-0.7557	-0.6610	0.1350	0.8270	0.1173	0.3598	1.0208
hsa-mir-4510	-0.3339	-0.4245	0.0484	-0.2367	0.9242	0.7599	0.6607	0.7816	1.0183
KIAA0907	-0.1775	-0.0100	0.0118	-0.0585	1.2690	1.5066	0.1034	0.9597	1.0182
ACTL8	-0.1212	-0.2263	-0.1557	-0.1677	1.4589	0.6619	0.3829	0.8346	1.0023
DYRK1A	-0.8052	-0.4190	-0.5031	-0.5758	0.7571	0.4703	0.0495	0.4256	1.0014
TCERG1	0.1201	-0.2573	-0.4244	-0.1872	1.5350	0.7395	0.1584	0.8110	0.9982
KDM6A	0.8562	0.9227	0.5803	0.7864	1.4293	2.3557	1.5507	1.7786	0.9922
HEPACAM2	0.8211	0.9632	0.7348	0.8397	2.0341	1.8011	1.6492	1.8281	0.9884
SIX1	0.1771	0.0504	-0.0799	0.0492	0.8578	1.4200	0.8152	1.0310	0.9818
DRG2	-0.0429	-0.0003	-0.1977	-0.0803	1.3064	1.2834	0.0712	0.8870	0.9673
BRAP	-0.7074	-0.4528	-0.3759	-0.5121	0.6076	0.5857	0.1545	0.4493	0.9613
MLL3	0.3814	0.1396	0.2587	0.2599	1.6865	1.1725	0.7683	1.2091	0.9492
VHL	-0.4673	-0.4771	-0.5653	-0.5032	0.6285	0.9086	-0.2067	0.4435	0.9467
OXTR	0.0484	0.1473	0.0384	0.0780	1.3412	0.4696	1.2618	1.0242	0.9462
SCAF4	-0.5808	-0.2000	-0.1574	-0.3127	0.7112	0.7499	0.4383	0.6331	0.9459
ZNF513	-0.1631	-0.0706	-0.0428	-0.0922	0.9982	0.4341	1.1257	0.8527	0.9448
ZNF729	-0.4333	-0.0994	-0.1289	-0.2205	0.3617	1.3562	0.4331	0.7170	0.9375
MPC2	0.4719	0.1507	0.0200	0.2142	1.1138	1.4563	0.8705	1.1469	0.9326
CNOT4	-0.3433	-0.3938	-0.0983	-0.2785	-0.0510	1.0769	0.9349	0.6536	0.9321
OTUD6B	-0.4572	-0.2172	-0.2272	-0.3005	0.8421	1.0964	-0.0461	0.6308	0.9313
BRD2	-0.4802	-0.4214	-0.3509	-0.4175	-0.0661	0.8056	0.7893	0.5096	0.9271
HDAC2	-0.1199	0.1233	0.0007	0.0014	0.6873	1.0368	1.0519	0.9253	0.9240
RPL36A	-0.7348	-0.8816	-0.9335	-0.8500	0.0340	0.1187	0.0692	0.0739	0.9239
NR2C2AP	-0.5258	-0.6096	-0.4923	-0.5425	0.2791	0.2833	0.5762	0.3795	0.9221
ALKBH8	-0.1830	-0.0853	-0.1338	-0.1340	0.5137	0.9465	0.8939	0.7847	0.9188
ZBTB7A	-0.0294	-0.4935	0.0119	-0.1703	0.4192	0.9179	0.8977	0.7449	0.9153
E2F1	-0.0729	-0.1792	-0.2652	-0.1725	0.4153	0.3303	1.4738	0.7398	0.9123
LCOR	-0.1359	-0.2029	-0.4448	-0.2612	0.6330	1.3021	0.0105	0.6486	0.9098
RPS6KB1	0.2988	-0.0204	-0.0101	0.0894	0.9026	1.3003	0.7913	0.9981	0.9087
MAPK13	-0.3266	-0.4190	-0.6405	-0.4620	0.6928	0.5778	0.0691	0.4465	0.9086
BAX	0.4545	0.5156	0.4134	0.4612	1.3996	0.9235	1.7724	1.3652	0.9040
LGALS9B	-0.3421	-0.3248	-0.4089	-0.3586	0.6111	0.5912	0.4314	0.5446	0.9032
RNF146	-0.1311	-0.1996	-0.5840	-0.3049	0.6682	0.5957	0.5289	0.5976	0.9025
ZC3H7A	0.0021	-0.2651	0.1261	-0.0456	0.6570	0.8717	1.0386	0.8558	0.9014
SEC14L1	-0.0830	-0.2774	-0.2888	-0.2164	0.4473	1.5021	0.1049	0.6848	0.9012
MARCKS	-0.6499	-0.3848	-0.4447	-0.4931	0.7402	0.5051	-0.0221	0.4077	0.9008

Table 3
MLN4924 Suppressor Screen - Top Enriched Genes

Gene	P12 #1	P12 #2	P12 #3	Avg P12	MLN #1	MLN #2	MLN #3	Avg MLN	MLN-P12 Diff
KLF16	0.0938	-0.1757	-0.1683	-0.0834	0.8035	1.0477	0.5945	0.8152	0.8986
hsa-mir-33b	-0.6327	-0.0283	-0.0250	-0.2287	0.9333	0.5696	0.5004	0.6678	0.8965
LAIR2	-0.0123	-0.2252	-0.0453	-0.0943	0.7512	0.9633	0.6750	0.7965	0.8908
TRPA1	-0.0965	-0.0509	0.0522	-0.0317	0.3804	1.5356	0.6508	0.8556	0.8873
TLR6	-0.2142	-0.0790	0.0920	-0.0670	0.1856	1.2988	0.9743	0.8196	0.8866
SEC31A	-0.6106	-0.4046	-0.6464	-0.5539	0.5077	0.4602	0.0170	0.3283	0.8822
SPAG7	-0.5999	-0.4673	-0.1600	-0.4091	0.7527	0.2569	0.4070	0.4722	0.8813
AGPAT1	-0.1062	0.2131	-0.1205	-0.0045	1.0612	0.0760	1.4929	0.8767	0.8812
hsa-mir-3118-3	-0.1920	0.2178	0.7589	0.2616	0.8824	1.7675	0.7759	1.1419	0.8803
CDK10	-0.1296	-0.4451	-0.4075	-0.3274	0.8971	0.4919	0.2654	0.5515	0.8789
SLC6A6	-0.4224	-0.5701	-0.4028	-0.4651	0.7559	0.1389	0.3435	0.4128	0.8779
DDX5	-0.4825	-0.4036	-0.4998	-0.4620	0.3280	0.4029	0.5028	0.4112	0.8732
PLK4	-0.4676	-0.0443	-0.2050	-0.2390	0.1987	0.0259	1.6705	0.6317	0.8707
IKBKB	0.2389	0.1990	0.0681	0.1687	1.2525	0.9529	0.9078	1.0377	0.8691
ETS2	-0.0365	-0.1082	-0.1026	-0.0825	0.8311	1.0181	0.5088	0.7860	0.8685
SYS1	-0.9020	-0.5979	-0.2852	-0.5950	0.1434	0.5639	0.1104	0.2726	0.8676
TAF4	0.2261	0.1425	0.1107	0.1598	0.6633	1.1738	1.2380	1.0250	0.8652
ATF1	-0.0746	-0.1928	0.1276	-0.0466	0.7165	1.4834	0.2482	0.8160	0.8626
DPH3	-0.7476	-0.6738	-0.4911	-0.6375	0.3554	0.4997	-0.1800	0.2250	0.8625
POGZ	-0.3853	-0.0241	-0.0834	-0.1643	0.4232	1.3836	0.2787	0.6952	0.8594